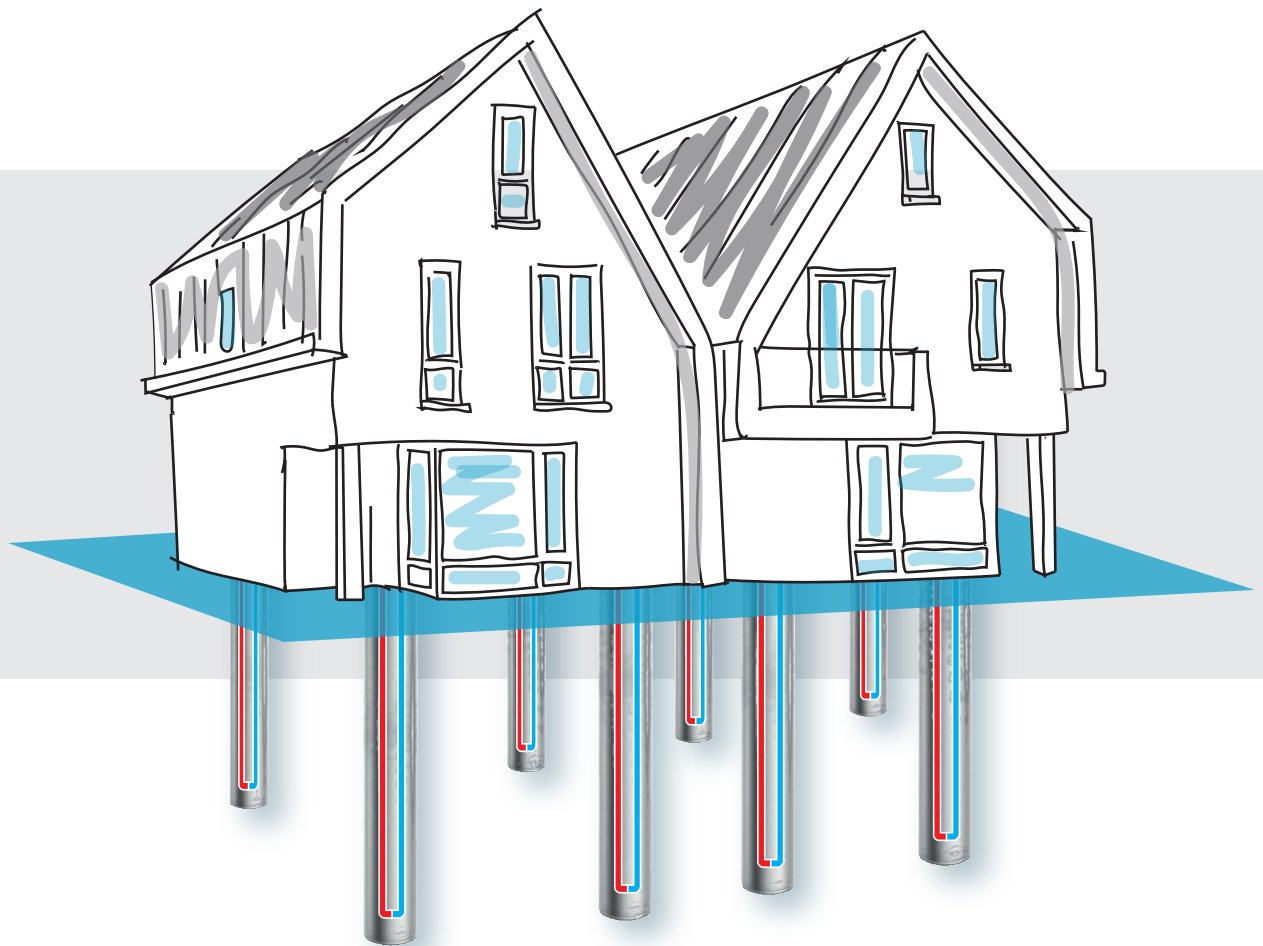


The Influence of Freezing-thawing Cycles on the Geotechnical Performance of an End-bearing Energy Pile

J. Snoeren



The influence of freezing-thawing cycles on the geotechnical performance of an end-bearing energy pile

by

J. Snoeren

to obtain the degree of Master of Science
in Applied Earth Sciences, Geo-Engineering
at the Delft University of Technology,

to be defended publicly on February 20, 2020 at 3 p.m.

Student number: 4242467
Project duration: March 1, 2019 – February 20, 2020
Thesis committee: Dr. P.J. Vardon, TU Delft, Geoscience and Engineering, (Chair)
Ir. drs. R.E.P. de Nijs, TU Delft, Geoscience and Engineering
Dr. O. Copuroglu, TU Delft, Materials, Mechanics, Management
Ir. A.A.E. van Dorst, Witteveen+Bos

An electronic version of this thesis is available at <http://repository.tudelft.nl/>.

Preface

I proudly present my master's thesis "The influence of freezing-thawing cycles on the geotechnical performance of an end-bearing energy pile". This report is a thesis at Delft University of Technology and written in cooperation with Witteveen+Bos. The report fulfills the master in Applied Earth Sciences as part of the master track Geo-Engineering at the faculty of Civil Engineering and Geosciences.

There are a number of people I would like to thank for their contribution in one way or another to this thesis. First of all my committee for their help, guidance and feedback. Renée, thank you for always being positive during the meetings, even when some results made no sense. Your advice and tips were definitely helpful. Richard, you always came up with new ideas and things I could try or people I could talk to. I am sure that I still miss certain things you have told me, but I really appreciated your way of thinking. Oğuzhan, thank you for bringing in your enthusiasm during all the meetings. The nervousity I had before a meeting totally vanished at the moments you interrupted. Phil, even with your busy agenda you were able to squeeze in a moment to go through my results and at the same time thinking out loud for solutions, thank you!

Furthermore, I want to thank the Witteveen+Bos colleagues in Amsterdam. I am happy with all the help and the interest you showed in me and my research. I always felt welcome in the office and although some of you were busy at other locations during the week, it was always 'gezellig'.

Also a special thanks to the PhD students Ali and Ivo for their support during these months. There was always a moment for coffee and at the same time for an error or one of my unclear questions. These questions were at all times answered clearly and with patience such that I could walk away with a good solution.

Last but not least, I would like to thank all my friends from study, my housemates and family for their support and positive words. It was a year in which my enthusiastic mood sometimes made place for an exhausting variant. Thank you for seeing through the setbacks and for being there during my entire study. I am really happy with all the people I met during my study in Delft and also grateful for the opportunities that came along my path. Thank you!

J. Snoeren
Delft, February 2020

Abstract

Energy piles are getting more attention for their sustainable and economic potential. The fluid pipes are integrated in the foundation piles, which makes it cost-attractive, but also relatively new to the Dutch geotechnical industry. By lowering the temperature limit of the anti-freeze fluid in the pipes the heat extraction and thereby also the necessary pile length can be optimized. However, the resulting thermal loads might influence the structural function and are therefore a main obstruction for the industry. Within this thesis three aspects of freezing-thawing of an axially compressed end-bearing energy pile are evaluated: (i) frost resistance of concrete, (ii) thermal analysis and (iii) geotechnical analysis. The objective is to work towards a conclusion on the degradation effects of freezing-thawing processes along the edge of an end-bearing energy pile and come up with practical advice for the design. The behaviour of the concrete is evaluated by literature, wherein the concrete thermal conductivity and mixture are key elements. For the thermal analysis a pile group simulation and a detailed single pile analysis is performed in Comsol Multiphysics. The soil stratigraphy is simplified and based on the Western part of the Netherlands. The input originates from the heat-cool demand of a single household related to the monthly gas usage in the Netherlands. Typical heat extraction for this specific case, i.e. long-term average amount of 7 W/m, for 7 years did not result in freezing temperatures at the edge of the most critical piles. Freezing occurred after an increased heat extraction until 10 W/m. Furthermore, the influence of daily cycles in the single pile analysis damped by the thermal resistance of the concrete pile. The geotechnical analysis is assessed in an axisymmetric model in Plaxis with and without a fully-coupled thermo-hydro-mechanical (THM) module. The first set of analyses with THM examines the influence of expansion and contraction of materials including phase changes, but without changes in soil mechanical and physical properties. Two situations are considered that are different in terms of the position of their neutral plane and negative shaft resistance. The resulting settlements can be distinguished as initial structural load and settlements due to thermal seasonal cycles, which fluctuate between 1 mm. A ratcheting behaviour was observed and resulted in a settlement of 12 and 3 mm over 5 years. However, the volumetric strain accumulation around the pile indicates unrealistic results in the THM module and conclude that the simulation of freezing-thawing cycles has to be done in a more advanced constitutive model which can capture freezing-thawing behaviour of soils. Within the second set of analyses the impact of the soil strength and stiffness due to a freezing-thawing cycle was investigated for the two situations to determine their effect on the pile behaviour in terms of load-displacement and shear distribution. The results indicate that effective cohesion is most influencing the pile behaviour and it indicates that no need exist to change the design approach of end-bearing piles as long as the potential negative shaft resistance along the pile over all layers above the bearing layer is included in the design calculation and considered fully mobilized.

Contents

Preface	iii
Abstract	v
List of Figures	ix
List of Tables	xiii
1 Introduction	1
1.1 Background	1
1.1.1 Practice	1
1.1.2 Guidelines	2
1.2 Project relevance	2
1.3 Research objective and questions	2
1.4 Thesis constraints	2
1.5 Thesis outline	3
2 Literature study	5
2.1 Principles of heat transfer	5
2.2 Freezing-thawing of soil	11
2.3 Freezing-thawing of a foundation pile	22
2.4 Freezing-thawing resistance of concrete	26
2.5 Design of pile foundations	28
2.6 Full-scale tests	35
2.7 Constitutive Modelling	38
2.8 Literature summary	41
3 Thermal Analysis	43
3.1 Analytical	43
3.2 Pile group	44
3.3 Results pile group	46
3.4 Single pile	48
3.5 Results single pile	50
3.6 Discussion	51
4 Validation and understanding THM module	53
4.1 London pile	53
4.2 Lausanne pile	55
4.3 Concluding remarks	56
5 Geotechnical THM analysis	57
5.1 Model settings	57
5.2 Results THM temperature distribution	63
5.3 Situation 1: results THM module without surcharge	64
5.4 Situation 2: results THM module with surcharge	66
5.5 Discussion	69
6 The impact of change in soil cohesion and stiffness due to freezing-thawing	71
6.1 Soil stiffness and cohesion variation	72
6.2 Situation 1: positive shaft resistance over all layers	74
6.3 Situation 2: negative shaft resistance in Holocene layers	76
6.4 Discussion	78
7 Conclusions and recommendations	81

I	Appendices	85
A	Literature	87
B	Negative skin friction Eurocode	89
C	Comsol Multiphysics	91
D	Thermo-hydro-mechanical in Plaxis	95
E	Parameters Validation	97
F	Parameters North-South metro line Amsterdam	99
G	THM analysis	103
	Bibliography	105

List of Figures

1.1	Visualization of the thesis	3
2.1	Soil temperature fluctuation	5
2.2	Ground source heat exchangers	6
2.3	Primary and secondary circuits of an energy pile system	8
2.4	Phase changes of water	9
2.5	Frost susceptibility soils	11
2.6	Two mechanisms that keep water in its unfrozen state	12
2.7	Typical soil-freezing characteristic curve	13
2.8	Influence of pressure on SFcC	13
2.9	Volumetric strain of fine grained soils after thermal cycles	14
2.10	Change of void ratio in closed system with freezing-thawing cycle	15
2.11	Void ratio after multiple freezing-thawing cycles	15
2.12	stages of soil creep	16
2.13	Uneven settlement due to thawing permafrost in Alaska	17
2.14	Hydraulic conductivity at freezing temperatures for three soil types	18
2.15	Water migration (cryosuction) in frozen fringe	18
2.16	Stress-strain curves of frozen silt under subzero temperatures	19
2.17	Long-term cohesive strength of frozen soils	19
2.18	Decrease in cohesion after certain amount of FT cycles	20
2.19	Soil stiffness of Illite clay after FT cycles	20
2.20	Mobilised shear strength for illite samples subjected to FT cycles	20
2.21	Cyclic loading of frozen silt	21
2.22	Hysteretic behaviour in the Hardening-soil small strain (HSS) model	21
2.23	Normalized shear modulus reduction curve	21
2.24	Damping ratio with cyclic shear strain	21
2.25	Restrained pile during heating and cooling	23
2.26	Restrained pile during heating and cooling plus mechanical loading	23
2.27	Ratcheting	24
2.28	Expansion of pile in free, fixed and actual condition during heating	25
2.29	Top of Pleistocene from NAP level Netherlands	28
2.30	4D/8D method	29
2.31	Values of δ	30
2.32	Neutral plane development	31
2.33	Geotechnical design process of an energy pile	32
2.34	Pile lay-out including heat transfer pipes in U-shape	33
2.35	Building supported by energy piles	33
2.36	General energy pile design approach	33
2.37	Soil profile test site Lausanne	35
2.38	Thermal load on the pile with reference temperature of 15	35
2.39	Temperature results Lausanne	36
2.40	Vertical stress within pile	36
2.41	Imposed thermal cycle London energy pile	36
2.42	Axial heating load London energy pile. OFS (Optical Fibre Sensor) and VWSG (Vibrating-Wire Strain Gauges)	37
2.43	Axial cooling load London energy pile. OFS (Optical Fibre Sensor) and VWSG (Vibrating-Wire Strain Gauges)	37
2.44	THM processes in frozen and unfrozen soils	38
2.45	Stiffness-strain soil behavior	39

2.46	Stiffness parameters of HSS in a triaxial test	39
2.47	Reduction of the secant and tangent shear modulus in HS small	40
2.48	Damping ratio with cyclic shear strain	40
2.49	Visualisation of important pile and soil characteristics during non-isothermal conditions	42
3.1	Freezing indication at the pile shaft	43
3.2	Geometry and top view Comsol pile group model	44
3.3	Simplified heat source Comsol 3D	44
3.4	Thermal top boundary condition Comsol model	45
3.5	Semidetached house	45
3.6	Monthly heat extraction based on gas demand	45
3.7	Smooth applied phase change of water	46
3.8	Average temperature at the pile edge of pile 6 in the first clay layer	47
3.9	Phase indication with cross section through piles 5, 6, 7 and 8 at day 1850	47
3.10	Temperature gradient within the fluid pipe	48
3.11	Temperature of pile edge	49
3.12	A coarse (4656 elements), normal (12669 elements), fine (106284 elements) and extremely fine (689454 elements) mesh	50
3.13	Fluid temperature difference outlet-inlet during typical heat extraction	50
3.14	Fluid inlet temperature	50
3.15	Temperature evolution at different parts of the single pile analysis during increased heat extraction	51
3.16	Temperature evolution at different parts of the single pile analysis during increased heat extraction	51
4.1	Thermal and mechanical loading scheme London pile	53
4.2	Characteristics model London energy pile	54
4.3	Results London pile	55
4.4	Thermal loading scheme Lausanne pile	55
4.5	Characteristics Lausanne energy pile	56
5.1	Modelling domain with thermal and displacement boundary conditions	58
5.2	Dilatancy cut-off in drained triaxial test	58
5.4	Heat flux boundary at edge of pile	60
5.5	Load-displacement curve situation 1 in Plaxis	61
5.6	Load-displacement curve situation 2 in Plaxis	61
5.7	Neutral plane position for situation 1 on the left and position after surface load for situation 2 on the right	62
5.8	Schematic loading-unloading-reloading behaviour of the pile due to expansion and contraction	62
5.9	Specific measurement locations in the domain	63
5.10	Year 3 of operation	63
5.11	Temperature along the shaft at measurement locations	64
5.12	Volumetric strains and ice saturation in the case without surcharge situation 1	64
5.13	Plastic points before thermal, after the first year and after the fifth year situation 1	65
5.14	Excess pore pressure along the pile shaft situation 1	65
5.15	Vertical displacement of the head and tip of the pile during 5 years of operation with neutral plane at stop situation 1	66
5.16	Shear stress along the pile situation 1	66
5.17	Volumetric strains plus ice saturation situation 2	67
5.18	Excess pore pressure in the soil along the pile shaft situation 2	67
5.19	Vertical displacement of the head and tip of the pile during 5 years of operation with neutral plane at second sand layer situation 2	68
5.20	Shear stress at the shaft of the pile situation 2	68
6.1	Plaxis approach for impact on soil strength and stiffness variation	71
6.2	Locations with manually changed sections along the shaft	72
6.3	Influence of cohesion of clay layer 1	74

6.5	Influence of stiffness of clay layer 1	75
6.7	Influence of cohesion and stiffness of clay layer 1	75
6.9	Influence of cohesion of clay layer 1	76
6.11	Influence of stiffness of clay layer 1	77
6.13	Influence of cohesion and stiffness of clay layer 1	77
6.15	Shear stress along pile in situation 2 in its thawed state	78
A.1	Frost design soil classification of U.S. Corps of Engineers	87
C.1	Temperature evolution at 1 m from pile	92
C.2	Normal and enlarged domain size pile group model	92
C.3	Sensitivity of domain size pile group model	93
C.4	10 years heat extraction	93
C.5	3D temperature evolution at t = 2560 days (7 years)	93
D.1	Load displacement curves with different temperatures at the interface	96
G.1	Temperature distribution over five years	103

List of Tables

2.1	Gas usage for mainly heating in the Netherlands	7
2.2	Thermal conductivity of mineral soils	10
2.3	Range thermal properties unfrozen soil and other components	10
2.4	b and c parameters	25
2.5	Concrete requirements freeze-thaw environments	27
2.6	Effect on thermal conductivity and frost resistance of concrete	27
2.7	Existing guideline and their freezing remarks	34
2.8	Pile characteristics Lausanne	35
2.9	Important modelling features in THM Plaxis with HSS model	39
2.10	Required soil parameters HSS model	40
2.11	Soil behaviour during freezing, thawing and multiple cycles	41
2.12	Pile behaviour during freezing, thawing and multiple cycles for a constrained pile	41
2.13	Influence of freezing and thawing on the SLS	42
3.1	Pile group parameters	46
3.2	Plastic pipe properties single pile analysis	48
3.3	Properties 35% monopropylene glycol solution at -10 °C	49
3.4	Soil properties sensitivity model	49
5.1	Thermal soil parameters asked in Plaxis	59
5.2	Thermal and hydraulic soil properties	59
5.3	Mechanical soil properties	60
5.4	Bearing capacity result in D-foundations	61
6.1	Mechanical soil parameters at freezing temperatures	73
6.2	Change in soil strength and stiffness	73
6.3	Cohesion of frozen and thawed states	74
6.4	Stiffness of frozen and thawed states	74
6.5	Pile displacement when clay 1 is affected	75
6.6	pile displacement when clay 1, clay 2 and sand 1 are affected	76
6.7	Pile displacement when clay 1 is affected	77
6.8	pile displacement when clay 1, clay 2 and sand 1 are affected	78
B.1	Negative skin friction for conceptual model	89
C.1	Input parameters temperature verification	91
E.1	Soil properties London pile model in Plaxis	97
E.2	Soil properties Lausanne pile model in Plaxis	98

Nomenclature

Abbreviations

<i>BHE</i>	Borehole Heat Exchanger
<i>FT</i>	Freezing and Thawing
<i>GSHP</i>	Ground Source Heat Pumps
<i>GWL</i>	Ground Water Level
<i>HSS</i>	Hardening Soil Small-strain
<i>LE</i>	Linear-Elastic
<i>MC</i>	Mohr-Coulomb
<i>THM</i>	Thermo-Hydro-Mechanical
<i>W/C</i>	Water-Cement



Introduction

1.1. Background

Renewable energy sources such as solar, wind and geothermal account for a small part of the global energy mix. But, they are definitely part of a growing sector in which geothermal energy can take a substantial part. Over recent years different techniques were established to extract geothermal energy from shallow to deep subsurface levels. However, shallow and deep geothermal energy structures are quite unknown in the Netherlands while there exists a major potential for this technique to help the energy transition. Shallow geothermal structures are part of a ground source heat pump (GSHP) system. Energy piles are among these thermal structures and are used for the heating and cooling of buildings. In cost perspective they are really attractive compared to the known vertical borehole heat exchanger (BHE), since the fluid pipes are integrated in the pile foundation. However, in any case the primary function of the energy pile should remain providing structural support. Besides the heat extraction, it could be used to cool buildings and anticipate on the seasonal energy demand. According to Laloui et al. (2006) this can even result in a reduction of 50% in energy usage for new buildings. Therefore, it can definitely stimulate the energy transition that currently takes place in for example the Dutch society. Before this can happen certain challenges have to be assessed. One of these is the ability of geothermal structures to match the peak heat demand during the coldest days such that an additional heat source is not necessary. This could be done by creating higher temperature gradients between the soil and the fluid pipes and allowing subzero fluid temperatures. By using this approach, the necessary pile depth could also be reduced (Eslami-nejad and Bernier, 2012). Another challenge is the unknown soil behaviour, which could effect the performance of the pile foundation. Therefore a research project at Delft University of Technology is conducted at the time of writing including numerical, laboratory and full-scale tests. The main objective here is to capture the behaviour of thermal cyclic loading and create a guideline for the Dutch construction industry. The differences with previous tests and numerical approaches in other countries are that these tests (i) will happen in soft Dutch soil layers, (ii) will go through some freezing-thawing cycles and (iii) are able to capture freezing-thawing phenomena (Arzanfudi and Al-Khoury, 2018; Golchin et al., 2019).

1.1.1. Practice

Experience from full-scale tests, numerical simulations and applications in other countries are helpful for the development of energy piles in the Netherlands. Well-known tests are performed in countries such as the UK and Austria with promising results for their specific soil conditions. Despite these tests it is still a challenge to prospect the occurring phenomena in soft (Dutch) soil conditions. Especially with its thermal loading aspect, which is one of the main challenges to overcome for the design. As result of heating and cooling an alternating effect at the soil-pile interface could develop (Amatya et al., 2012; Bourne-Webb et al., 2013). The behaviour of energy piles during cyclic loading with subzero temperatures is also of major interest to optimize the capacity of existing projects. After all, a reduction in fluid temperature might reduce the necessary pile length compared with common BHE. In Katzenbach et al. (2013) an experimental analysis on freeze-thaw performance of a BHE is performed and in Brandl (2006) a case is described in which fluid temperatures below zero occurred. In the latter case no freezing phenomena are described in the soil. However, according to Brandl (2006) and Knellwolf et al. (2011) such processes should also be avoided to prevent thaw-induced defects and changes in engineering properties of the soil.

1.1.2. Guidelines

The uncertainty of pile behaviour during thermal loading is an obstruction for contractors to apply energy piles in projects. Even though some companies are applying the technique with success, there remains a sceptical attitude towards this innovation since it could lead to extra costs, risks and it requires certain construction skills. Apart from that, there exist no detailed design method yet for (Dutch) contractors that considers the complex thermal-mechanical phenomena (Knellwolf et al., 2011). Similar manuals exist for BHE such as Geelen and Witte (2017) or a well-known German standard Sanner et al. (2013). There also exist a concise research report on energy piles in the Netherlands Geelen et al. (2003). This report discusses the energy pile projects performed in the Netherlands before 2003 as well. But among these examples no additions on practical design criteria for cyclic thermal behavior are discussed, let alone the behaviour of freezing-thawing around the pile. Instead of clear guidelines, designs are based on empirical considerations (Boënnec, 2009; Ng et al., 2014b) or some conservative safety procedures to ensure that the geotechnical functionality of the pile is not negatively affected (Boënnec, 2009; Knellwolf et al., 2011; Rotta Loria, 2018; Suryatriyastuti et al., 2014). To avoid freezing phenomena at the soil-pile interface a temperature limit is often mentioned for the fluid. This limit brings down the efficiency of the heat transfer since the lower the inlet temperature during heating mode the more efficient the operation of the GSHP system can be (Banks, 2012; Loveridge and Powrie, 2012). It is also on the safe side when considering that the concrete pile acts as a buffer, since there could be a significant temperature difference between the pipe and the pile wall (Loveridge and Powrie, 2012).

1.2. Project relevance

Unknown thermal soil behaviour remains an uncertainty in energy pile projects despite the research that has been done so far. Especially due to the combination of mechanical and thermal loading. Since during thermal variations all materials try to change shape and structure, which is definitely not in favour of a foundation. And, in the case of excessive heat extraction freeze-thaw phenomena might occur at the soil-pile interface. This can happen due to peak extraction in winter, reduced pile lengths, malfunctioning systems, competitive use with other GSHP and the change of use of a building (Sass et al., 2016)). Therefore, most guidelines recommend not to go below a certain fluid temperature. The main concerns are the deterioration of the shaft resistance, reduction of the bearing capacity and high thermal stresses within the pile. However, from a heat point of view the freezing-thawing cycles might be attractive and research has shown that the currently used temperature limits in many cases could be adopted (Loveridge and Powrie, 2012). A clear evidence on the mentioned processes except from early observations in a study of Brandl (1998) on the consequences of freezing-thawing cycles is missing. This makes the subject of this thesis, which will focus on freezing-thawing circumstances of an end-bearing energy pile and with that a clarification on the physical and mechanical soil behaviour during severe conditions.

1.3. Research objective and questions

The objective is to work towards a robust conclusion on the degradation effects of freezing-thawing along the edge of an end-bearing energy pile and propose practical additions to the design procedure if needed. The main research question is as follows:

What is the influence of freezing-thawing cycles on the geotechnical performance of an end-bearing energy pile?

To be able to answer this question, the sub questions below will be answered throughout this report.

1. What is the likelihood of freezing around an energy pile?
2. What is the influence of freezing-thawing on the concrete material?
3. How can these processes be quantified in terms of change in geotechnical pile behaviour?
4. To what range is it possible to incorporate these quantifications in the pile design approach or to give an indication for limiting situations?

1.4. Thesis constraints

This study will focus on the thermal, mechanical and water flow aspects in freezing-thawing soils, which is necessary to investigate the behaviour of an energy pile. The report describes these aspects by literature and

numerical modelling. However, due to a lack of data in this study realistic assumptions are made to analyse general situations and give qualitative conclusions. This includes a Dutch soil stratigraphy, a pile plan for a semidetached house, a monthly heat extraction based on gas demand. In spite of these assumptions, it will help the reader to understand the obstructions encountered in the design of an energy pile in potential freezing-thawing conditions.

1.5. Thesis outline

The report comprises seven chapters in total. The main structure of the report is build around three main subjects: (1) the freezing-thawing resistance of concrete, (2) the thermal analysis and (3) the geotechnical analysis. See figure 1.1 with a schematic overview. The first chapter gives a concise introduction about the subject with the project relevance and the corresponding research questions. Chapter 2 is a literature study which describes the principles of heat transfer related to geothermal energy, freezing-thawing of soils and piles, freeze-thaw resistance of concrete, pile design procedures and two full-scale tests. Furthermore, it will briefly explain constitutive modelling with the thermo-hydro-mechanical (THM) module of Plaxis. The important remarks from literature are then summarised in its latest section. Chapter 3 simulates the thermal behaviour of a pile group based on the heat demand of a single household in a simplified Dutch soil stratigraphy. The results are used for a more detailed single pile analysis. Within chapter 4 the results of two existing full-scale tests are used to validate and to understand the performance of the THM model in Plaxis. In chapter 5 the freezing indication and its corresponding extraction cycle from chapter 3 are used as an input boundary for the geotechnical analysis of a single end-bearing pile. Thereby two cases are considered in which the whole shaft contributes to the shaft friction and a case wherein the upper Holocene layers contribute to the negative shaft friction. The results and discussion is also described within this chapter. The second approach in chapter 6 changes certain soil cohesion and stiffness parameters by extra construction phases in the model. It also distinguishes between a case with totally positive shaft friction and partly negative shaft friction. The report ends with the conclusion on the thermal and the mechanical behaviour and at last the corresponding recommendations for further research in chapter 7.

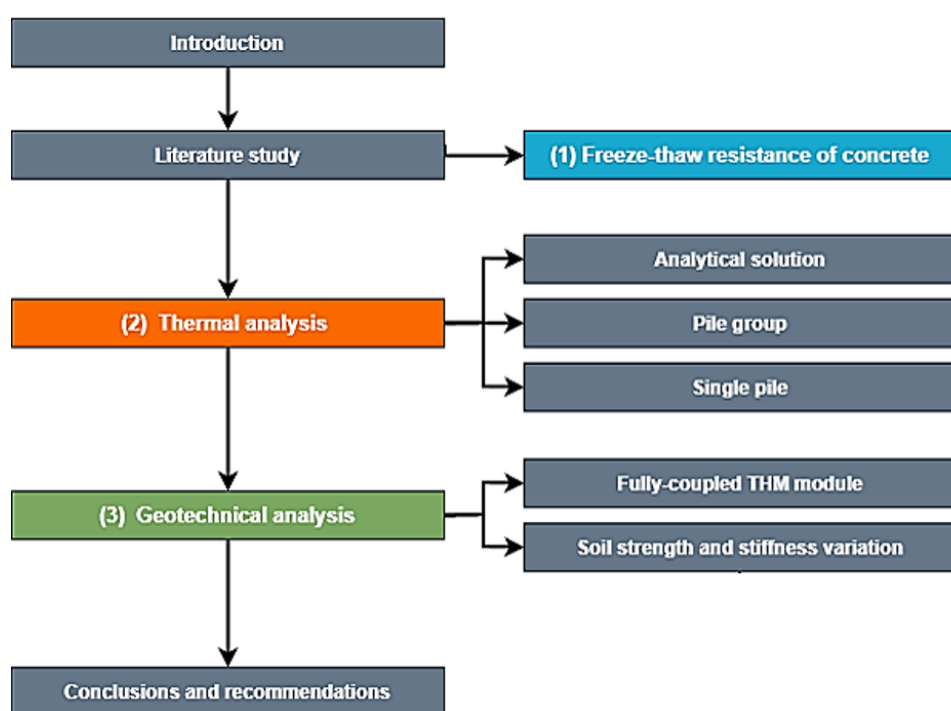


Figure 1.1: Visualization of the thesis

2

Literature study

This chapter addresses previous research on energy piles and other topics related to heat transfer in soils and constitutive modelling. For freezing and thawing a division is made in a section for soil behaviour and concrete pile behaviour. In this latter section the concrete durability in terms of frost action is also assessed. From there the design methods for a foundation pile, borehole heat exchanger and for an energy pile are elaborated in the pile design section. Hereafter two well-known full-scale tests are shortly described. The last section summarises the literature study.

2.1. Principles of heat transfer

A complex heat transfer mechanism is present in the soil that includes conduction, convection, radiation and latent heat by phase-changes (Brandl, 2006). Within this part these heat mechanisms and thermal properties of soils are elaborated and basic equations are given. Also some other factors (e.g. groundwater flow, soil moisture content and pile dimensions) that influence the performance of an energy pile will be discussed. Important decisions for the design of energy piles are based on these properties (Brandl, 2006; GSHP Association, 2012; Loveridge et al., 2013; Sani et al., 2019) and could help to determine potential freezing and thawing locations.

2.1.1. Geothermal energy

As climate change is a main topic in many parts of the world, alternative energy sources or energy saving techniques are hot topic. Geothermal energy is one of these sources and its development the last years is increasing. A division can be made by the depth from where it is extracted. At a depth between 2-4 km the term deep geothermal is used, while on the other side of the spectrum just below the subsurface it is called shallow geothermal (<200 m). The temperature at this shallow depth in most European countries varies between 10 and 15 °C, but due to seasonal and daily temperature variations this changes steadily throughout the year close to the subsurface, see figure 2.1.

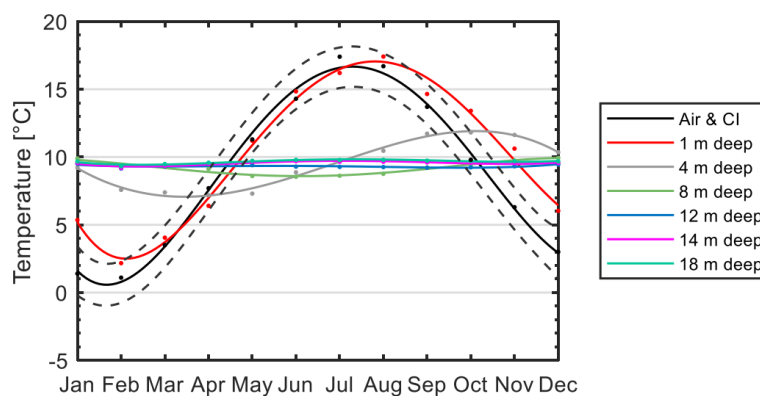


Figure 2.1: Soil temperature fluctuation with confidence interval (CI) for air temperatures (Alberdi-Pagola, 2018)

The temperature fluctuation is dependent on the specific soil thermal properties and could be simulated by periodic function in which T_{mean} is the mean annual temperature, A is the temperature amplitude and P is the time period in equation 2.1. The temperature at a certain depth z could be calculated with equation 2.2 with α as the soil thermal diffusivity (Andersland and Ladanyi, 1994).

$$T(t) = T_{mean} + A \times \sin\left(\frac{2\pi t}{P}\right) \quad (2.1)$$

$$T_{z,t} = T_{mean} + A \times \exp\left(-z\sqrt{\frac{\pi}{\alpha \times p}}\right) \times \sin\left(\frac{2 \times \pi t}{P} - z\sqrt{\frac{\pi}{\alpha \times P}}\right) \quad (2.2)$$

Many different shallow geothermal systems exist as can be seen in figure 2.2. The system is considered shallow when the upper few meters of the soil are used for space heating or cooling. Besides, a distinction can be made between an open or closed system. Two closed systems are more elaborated in this section, the vertical borehole heat exchanger and the energy pile. For a vertical borehole heat exchanger common depths are between 50 and 200 m, while for energy piles we consider the depths of foundation piles.

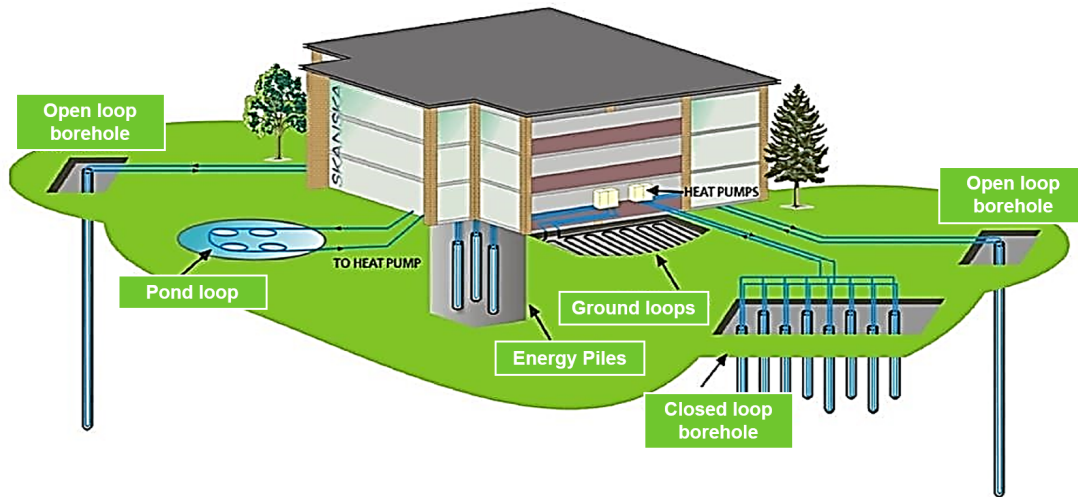


Figure 2.2: Shallow geothermal sources (Loveridge and Powrie, 2012)

Heat pump

Many different heat pumps exist and they all have their most efficient range of temperatures in which they work. It is important to distinguish the three sources of a heat pump: air, surface water and the ground. A heat pump takes care of the lift of fluid temperatures, so it is useful in for example household heating, but also for cooling by reversing the process, i.e. heating the subsoil. The heat pump contains a fluid with a very low boiling point which turns into a vapour when it is in contact with the heat from the fluid pipe. By compressing this vapour the temperature of the fluid increases sufficiently to heat up the water used in the heating network of a structure, the so-called secondary circuit. It controls a constant heat gradient among the inlet and the outlet and heat exchange values per meter of energy piles are often held between 20 and 100 W/m. The effectiveness of a heat pump is often described with the coefficient of performance (COP), which is higher when less electricity is needed for a unit of heat since it is the ratio between the energy extracted and the energy input. Common economical values of COP are above 4. The COP reduces slightly when temperature goes down. Another measurement method for its efficiency over a year is the seasonal performance factor (SPF), which is the ratio of heat energy output of a year over its used electricity.

$$COP = \frac{\text{Output heat energy after heat pump}}{\text{Input energy for operation (electricity)}} \quad (2.3)$$

The total energy extracted or injected E can be calculated by measuring the inlet and outlet temperature T of the fluid. The energy injected is calculated with equation 2.4 with Q rate of fluid flow, c_p the specific heat capacity in [$\text{kJ}/(\text{kgK})$] and t as operational time in seconds.

$$E = Q \times c_p \times (T_{in} - T_{out}) \times t \quad (2.4)$$

Sometimes a combination of energy sources is used to cover the heat demand of a structure. The so-called β -factor describes the portion of the ground source heat pump over the total heat supply. When 100% of the heat demand is supplied by the heat pump β is equal to 1.

The temperature of the liquid that is sent back into the heat pipes, exchanged its absorbed energy $P_{absorbed}$ and decreases in temperature according to equation 2.5.

$$T_{liquid,out} = T_{liquid,in} - \frac{P_{absorbed}}{Q_{pump} \times C_{fluid}} \quad (2.5)$$

2.1.2. House heat demand

To get an idea about the heat demand of some typical houses in the Netherlands and what kind of heat pumps are used, a small overview is given below in table 2.1. It is important to mention that mainly low temperature heating is possible with heat pumps, up to 35°C.

Type	Gas usage [m^3]	Energy [kWh]
Apartment	870	8961
Terraced house	1240	12772
Corner house	1480	15244
Semidetached house	1750	18025
Detached house	2300	23690

Table 2.1: Gas usage for mainly heating in the Netherlands (CBS, 2016)

The demand given in the overview is not divided equally over the year, the heating demand in the winter months lies significant higher than in the summer months as July and August. It is especially the peak demand in the coldest months that decides if a heating system can run solely on its energy piles or if it needs an extra source to meet the demand. This is often determined with the maximum capacity that the piles can extract from the subsoil. As rule of thumb the extraction limit is often taken as 50 W/m or as a limit in terms of a fluid temperature, which makes the heat pump in some cases not suitable. Another important limit is the soil thermal stability, which can be disrupted by a single system, but even faster when interaction between multiple ground source heat pump systems are considered. To get a better idea about the potential energy pile extraction during a cold winter day a short simplified derivation for a house with a heat demand of 84 kWh is done. Assume that the heat pump runs for 12 hours a day, this means that 7 kW (84/12) is asked every hour. Taking into account the limit of 50 W/m for the energy piles, a total pile length of 140 m is necessary (7000/50). The desired length of the heat pipes could be reduced by allowing higher extraction rates, i.e. lower fluid temperatures. By doing so half of the mentioned pipe length is required when 100 W/m is extracted and also peak demands could be covered in this case.

2.1.3. Soil thermal balance

Energy cannot be created or destroyed, it will follow the law of energy conservation. For a stable thermal operation within the subsoil it is of great importance that there is a balance between the input and output of energy. Any deflections could cause significant changes in temperature of the subsurface and affect the overall performance of the system. The chance of any thermal degradation around an energy structure is often low since current designs are based on the thermal capacities of the soil including certain safety boundaries. On the other hand there are enough reasons that could lead to an imbalance in long term soil temperature due to excessive heat extraction in areas with a high heat demand or due to excessive heat injection when more cooling is demanded. To prevent thermal imbalance the total system has to be in balance after 5 years and after that every 3 years at least once according to the Dutch government (Kleefkens, 2014). For potential freezing a heating season (winter) is picked where heat is absorbed from the soil.

2.1.4. Heat transfer mechanism

The total heat flow including the primary and secondary circuit is shown in figure 2.3. The paths of the primary circuit that are involved in the heat transfer in energy piles are the soil, the concrete of the pile, the pipes and the fluid within the pile. The corresponding heat transfer mechanism for these paths are thermal convection between the fluid and pipe wall, thermal conduction between concrete and soil, and the conduction in the soil itself. Convective heat transfer in the pore water could also play a role in especially coarse grained soils (Rees et al., 2000). However in reality the soil is not homogeneous and therefore properties may vary. The main driving force for energy exchange is the thermal gradient that is created between the fluid in the pipe and the soil. Besides this temperature difference the transfer is also controlled by the properties of the concrete material between the two media. The most common pile material used is concrete because of its good thermal storage capacity and heat transfer capabilities (Brandl, 2006). As the fluid flows from the inlet to the outlet it increases (heating mode) or decreases (cooling mode) in temperature.

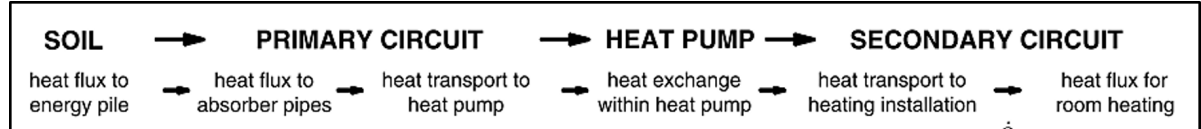


Figure 2.3: Energy pile system (Brandl, 2006)

The response of the soil due to a change in temperature requires an understanding of heat conduction, convection, heat capacity, thermal diffusivity and latent heat. These processes vary with the (un)frozen water content, degree of saturation and soil density (Andersland and Ladanyi, 1994). The reader is referred to the sections below for more information about which processes are included in the heat transfer.

Heat conduction

Heat conduction is the transfer of heat without displacement of particles. The rate of heat flow by conduction between the pile and surrounding soil is calculated according to Fourier's law and may be written as equation 2.6, where $q_{conduction}$ is the conductive heat flux and λ is the thermal conductivity of multiphase system (solid, water, gas) (Rees et al., 2000). Heat conduction is the most important mechanism that moves the heat in the soil from high to low temperature areas.

$$q_{conduction} = -\lambda \nabla T \quad (2.6)$$

Heat convection

The soil can be seen as a porous media which contains a solid material and pores filled with air or fluid that is able to flow. The movement of all particles in this fluid is seen as convection, which is a combination of heat diffusion and heat advection. Advection describes the movement of particles through the total heat flow, while advection is the movement of particles that go with the heat flow, so from higher to lower temperature or density areas. The convection process could be described by Newton's law of cooling 2.7 with h as heat transfer coefficient, T_{pile} and T_{fluid} the pile and fluid temperature (Loveridge and Powrie, 2012). The heat transfer coefficient h is dependent on fluid density, heat capacity and the flow velocity, see equation 2.8.

$$q_{convection} = h(T_{pile} - T_{fluid}) \quad (2.7)$$

$$q_{convection} = c_{fluid} \times \rho_{fluid} \times v_{fluid} \times (T - T_0) \quad (2.8)$$

Radiation

Heat radiation is the process that describes energy transfer by electromagnetic waves, so no particle movement is involved. In soils the heat transfer by radiation is often neglected. This is not the case for heat transfer at the soil surface.

Latent heat

Pore water can exist in three phases, which are the gas state (vapour), liquid state (water) and solid state (ice), see figure 2.4. When a material goes through a phase change from liquid (water) to solid (ice) latent heat

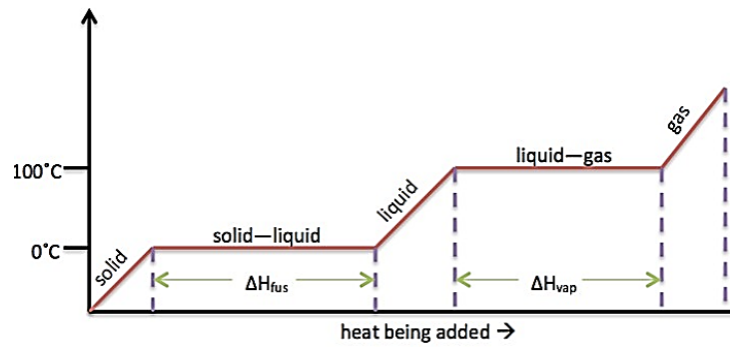


Figure 2.4: Phase changes of water

is released, this is also called the latent heat of fusion ΔH_{fus} (Andersland and Ladanyi, 1994). The thermal energy which was stored in the molecular structure is released when the material reaches the phase transition temperature, so instead of creating a temperature change, the energy changes the materials molecular structure. The latent heat of water is often quantified as 334 [kJ/kg] (Andersland and Ladanyi, 1994). For heat transfer models the contribution of vapour diffusion and latent heat due to ice forming should be considered. The total latent heat L is determined with equation 2.9 with ρ_d as dry soil density, L' as the mass latent heat $[\text{kJ/kg}]$, w the total water content and w_u the unfrozen water content (Andersland and Ladanyi, 1994). The propagation of the freezing front is mainly controlled by the latent heat during freezing (Nagare et al., 2012). Latent heat is in many models not taken into account, which results in wrong estimations of the ground temperature since latent heat slows down the decrease in the return temperature to the heat pump.

$$L = \rho_d \times L' \times \frac{w - w_u}{100} \quad (2.9)$$

2.1.5. Thermal properties

The performance and the efficiency of the heat exchange are dependent on the thermal properties of the soil described below.

Thermal conductivity

Thermal conductivity λ describes the ability of a material to conduct heat and can range from 0.2 to 5 W/mK (GSHP Association, 2012). According to Loveridge and Powrie (2012); Raouf et al. (2015) it is also the thermal conductivity of a soil that determines the heat exchange. A higher value results in a system that is more efficient. The thermal conductivity of a pile is often higher, which results in a low temperature difference between the pipe and the pile edge. Hence this is the critical case where subzero temperatures in the pipe could lead to freezing around the pile (Loveridge and Powrie, 2012). The thermal conductivity and heat capacity for a specific soil with or without ice is related to the mineralogy, salinity, dry density, pore fluid, degree of saturation, temperature, water- and ice content. Especially the degree of saturation controls the conductivity.

Three methods to determine the thermal conductivity are from Kersten (1949) in equation 2.10, from De Vries (1963) in equation 2.11 and Johansen's (1975) method, equation 2.12 and table 2.2, which gives the best results for soils in frozen and unfrozen state (Andersland and Ladanyi, 1994). Freezing increases the thermal conductivity significantly since it fills the pores with ice (Brandl, 2006), $\lambda_{water} = 0.57 \text{ W/mK}$ and $\lambda_{ice} = 2.18 \text{ W/mK}$.

$$\lambda = 0.1442[0.7 \log(w) + 0.4] \times 10^{0.6243\rho_d} \quad (2.10)$$

$$\lambda = \frac{\chi_w \lambda_w + F_a \chi_a \lambda_a + F_s \chi_s \lambda_s}{\chi_w + F_a \chi_a + F_s \chi_s} \quad (2.11)$$

$$\lambda = (\lambda_{sat} - \lambda_{dry}) k_e + \lambda_{dry} \quad (2.12)$$

	Unfrozen	Frozen
Fine grained	$K_e = \log S + 1.0$	S_r
Coarse grained	$K_e = 0.7 \log S + 1.0$	S_r

Table 2.2: Thermal conductivity of mineral soils (Andersland and Ladanyi, 1994)

Heat capacity

The total volumetric heat capacity of the soil C [$J/(m^3 K)$] according to Harris (1995) for unfrozen fully saturated soil is a summation of the capacity of the grains, the unfrozen water, ice and air present in the pores. It is the amount of heat that can be stored in a unit volume of soil per unit change in temperature. See equation 2.13 for a weighted average χ of all components with latent heat L taken into account with w_u as ratio of unfrozen water content with dry weight (Rees et al., 2000). The heat capacity of a soil depends mainly on the water content and the void ratio (Andersland and Ladanyi, 1994). Besides the volumetric variant of heat capacity, the specific heat capacity c [J/kgK] is used as well. This is the amount of heat needed to raise 1 kg of material with 1 °C. The heat capacity decreases with a lower temperature and freezing since ice has a lower capacity than water.

$$C = C_{soil}\chi_{soil} + C_{ice}\chi_{ice} + C_{water}\chi_{water} + C_{air}\chi_{air} + \frac{1}{\Delta T} \int_{T_1}^{T_2} L \frac{\partial w_u}{\partial T} dT \quad (2.13)$$

Thermal diffusivity

The thermal diffusivity D or α is a measure of how easily heat can spread through the soil mass (Sani et al., 2019) and depends on the specific heat capacity c_p , conductivity λ and the density ρ . It shows the rise in temperature that will occur due to a heat exchange, so a material with a high α will change its temperature quickly. The ice in frozen soils causes an increase in the thermal diffusivity, so a soil in thawed state changes slower in temperature than in a frozen state (Andersland and Ladanyi, 1994).

$$\alpha = \frac{\lambda}{\rho \times c} \quad (2.14)$$

Thermal properties summarized

A range of the thermal properties of all main soil components is presented in table 2.3 by Andersland and Ladanyi (1994).

Material	Heat Capacity [$kJ/(m^3 K)$]	Thermal Conductivity [$W/(mK)$]	Latent Heat [kJ/m^3]
Air	1.297	0.026	-
Water	4.16×10^3	0.56	333.5×10^3
Ice	2.20×10^3	2.21	333.5×10^3
Clay	$3.0 - 3.6 \times 10^3$	0.85 - 1.40	$1.1 - 2.5 \times 10^5$
Silty-Clay	$2.9 - 3.3 \times 10^3$	1.10 - 1.60	$1.5 - 2.0 \times 10^5$
Silt	$2.4 - 3.3 \times 10^3$	1.20 - 2.40	$0.8 - 2.0 \times 10^5$
Sand	$2.5 - 3.2 \times 10^3$	1.50 - 2.60	$0.8 - 1.7 \times 10^5$

Table 2.3: Range thermal properties unfrozen soil and other components (Andersland and Ladanyi, 1994)

2.2. Freezing-thawing of soil

The soil around an energy pile is subjected to thermal cycles during its lifetime. These variations in temperature can affect the physical, hydraulic, mechanical and dynamic properties of a soil such as the void ratio, pore water pressure, hydraulic conductivity and shear strength parameters (Andersland and Ladanyi, 1994; Steiner et al., 2018). The tests described in literature are mostly performed with positive temperatures to investigate changes on the behaviour of the soil-pile interface. These tests are used to predict mechanical behaviour and soil degradation phenomena of the soil, however the information of soil behaviour around a pile under freezing conditions is rare. Katzenbach et al. (2013) describes the damage inside the materials and the alternating contact surface between soil and the borehole wall.

Within this section the characteristics of freezing-thawing soil are elaborated such that practical problems for an energy pile can be distinguished. First of all, the properties influencing the frost susceptibility of a soil and thereby methods to describe this are evaluated. From there two separate parts go through the processes towards a frozen and thawed soil state from initiation of ice crystal nucleation to fully-frozen soil pores until thawing settlement. To be able to describe the soil changes four different subsections are presented, which elaborate on the physical, hydraulic, mechanical and dynamic behaviour.

2.2.1. Frost susceptibility

In figure 2.5 the frost susceptibility for different soils is depicted and based on three properties that are the percentage of particles smaller than 0.02 mm, soil type and a laboratory freezing test (Andersland and Ladanyi, 1994).

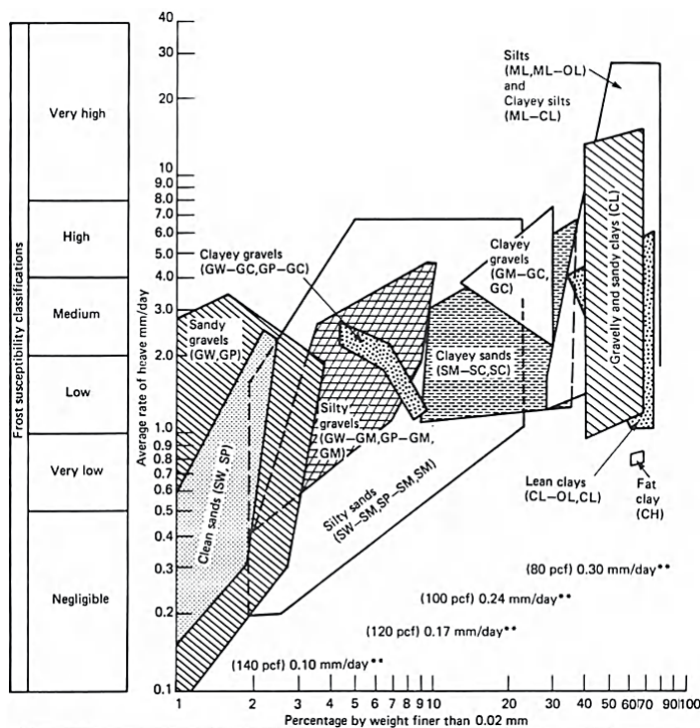


Figure 2.5: Frost susceptibility soils (Andersland and Ladanyi, 1994)

This is a first indication, but many other factors influence the freezing within a soil layer and the figure does not include the influence of an earlier experienced freezing-thawing cycle. Another classification table of the U.S. Corps of Engineers is given in Appendix A. They distinguish four frost groups. The freezing point of soils is not constant, but depends on factors summarised below. Taking into account these factors can help to predict the freezing volume and strength behaviour of a soil.

- Water content

The water content determines the amount of ice in the pores and thereby it also determines the strength properties of the soil medium. More ice will result in a stiffer soil.

- **Rate of freezing**
A low rate of freezing has a positive effect on the formation of ice lenses. It determines how uniform and fast an ice lens is formed. On the other hand a high freezing rate will lower the effect of the cryogenic process, which results in a lower pore pressure build up and a more uniform ice lens distribution (Steiner et al., 2018). For freezing around energy piles a relatively high rate is expected (Arzanfudi and Al-Khoury, 2018).
- **Groundwater flow**
Inflow of new unfrozen water will decrease the frost susceptibility around the pile.
- **Salinity**
The freezing point of water is reduced when water with a higher salinity is present. This is an advantage as freezing around the pile is undesired. In Andersland and Ladanyi (1994) a relation is given by Patterson and Smith which describes the influence of salinity on the freezing point of water.
- **Soil type**
The grain size determines the amount of unfrozen/frozen pore water when the soil is exposed to sub-zero temperatures. The common rule states that a reduction of soil particle size results in a depression of the melting point. The formation of an ice lens happens also rather in low permeable soils (Andersland and Ladanyi, 1994).
- **Stress distribution**
An increase in effective stress with depth results in a reduction of freezing phenomena (Katzenbach et al., 2013).

Melting point depression

The unfrozen water content is an important property and according to Wettlaufer and Worster (2006) there are two mechanisms which control the ice content in a soil: (i) the curvature induced premelting, also called the Gibbs-Thomson effect, and (ii) the interfacial premelting, see figure 2.6. The first mechanism is the result of surface tension and holds the grains together, the latter one occurs due to disjoining pressure and acts as a repelling force between the ice and grains. Since in soil the specific surface area (SSA) can be high and the curvature small, these processes are important in the amount of unfrozen water in the soil at freezing temperatures (Arzanfudi and Al-Khoury, 2018).

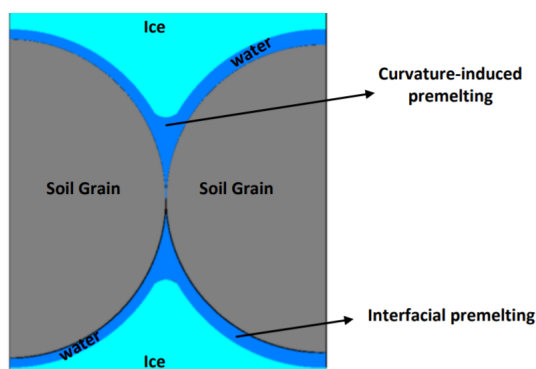


Figure 2.6: Two mechanisms that keep water in its unfrozen state (Ghoreishian Amiri et al., 2016)

More unfrozen water is expected in fine grained soils compared to coarse grained soils at temperatures below freezing point due to the low hydraulic conductivity and as result a limited water supply to the freezing area. The relationship between unfrozen water content and the freezing temperatures of the pore water for different soils is represented in a soil freezing characteristic curve (SFCC), see a typical example in figure 2.7 with different grain sizes. It can be described by using the van Genuchten en Clapeyron equation, see equation 2.15 and 2.16. With S_1 the water saturation, Ψ_m the pressure head and m , n and α are soil structure dependent parameters. The Clapeyron equation takes care of the description of the Ψ_m in terms of the phase

change to ice with L_{fus} as latent heat of fusion (334 kJ/kg) and Ψ_i as ice pressure. When considering ice pressure zero and combining the two equations, then the relationship for the SFCC curve is found.

$$S_1 = \left(\frac{1}{|\alpha \Psi_m|^n + 1} \right)^m \quad (2.15)$$

$$\Psi_m = \left(\frac{L_{fus}}{273.15 \times g} \right) \times T + \Psi_i \quad (2.16)$$

The SFCC curve can also be determined by making use of a thermo-time reflectometer, looking at the soil water characteristic curve (SWCC) described in Ren et al. (2017) and by the relation between particle size distribution described in Appendix § D.2.5 by Aukenthaler et al. (2016). The influence of the stress state is shown in figure 2.8.

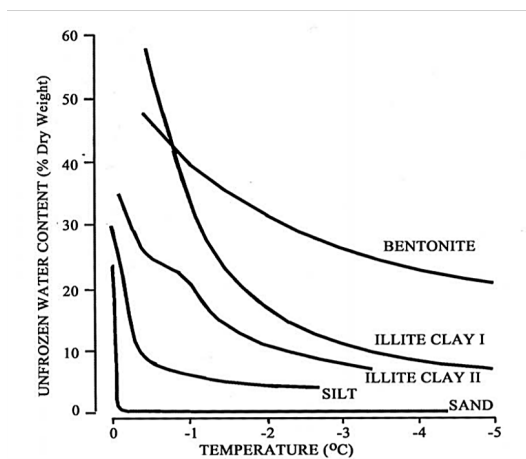


Figure 2.7: Typical SFCC (Davis, 2002)

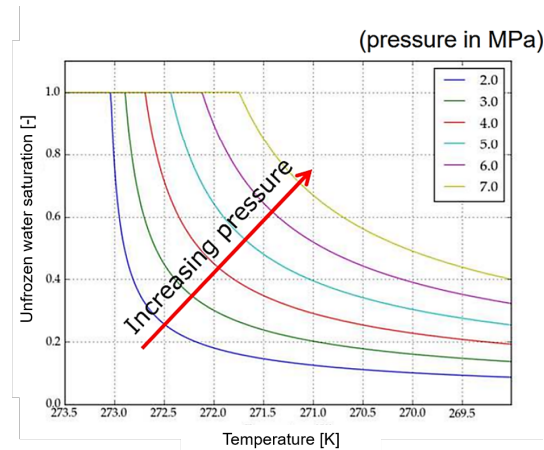


Figure 2.8: Influence of pressure on SFCC (Plaxis, 2015)

2.2.2. Freezing and thawing sequence

It is hard to compare the freezing of porous media with for example the freezing of pure water since different interactions are taking place. The process of ice forming in pores is also highly dependent on the components present in the soil. The following steps of soil freezing are considered and some processes are explained more in detail below:

1. The temperature reaches a value below the pore water freezing point such that ice crystal nucleation starts within the frozen fringe, see figure 2.15. The frozen fringe is the transition zone between the frozen and unfrozen zone, its propagation through a soil is controlled by latent heat (Nagare et al., 2012).
2. During this ice formation energy is required, the so-called latent heat of fusion. This energy slows down the cooling process.
3. Negative pore pressure develops due to water being attracted by ice, so-called cryogenic suction.
4. At lower temperatures more pore water will freeze and the unfrozen water content reduces.
5. Water expands 9% when it freezes, while the grains do not expand, this results in the expansion of pores, increase in pore pressure and potential destruction of the bonds in cohesive soils.
6. The result is a volume increase, which might result in the so-called frost heaving.

Thawing is initiated when a frozen soil heats up. It will increase the amount of unfrozen water and the strength of the soil depends on how easy the water can drain away from the frozen layer. In low permeable soils the water could cause a higher pore water pressure during the heating, which will reduce the effective stress. The following steps are considered for the thawing stage:

1. Reduction of cryogenic suction since water is not attracted anymore by the frozen fringe.
2. Water transforms back to the unfrozen state.
3. Excess pore pressure develops in low permeable soils in undrained conditions. This can also be the result of the bigger expansion coefficient of pore water than the coefficient of solid grains (Gawecka et al., 2017; Hueckel et al., 2009).
4. A reduction in effective stress and thereby a reduction in the undrained shear strength is expected (GSHP Association, 2012).
5. The dissipation of pore water can result in thermal consolidation. However this depends on the stress history of the soil.
6. Cohesive soils can loose their bonds during freezing and act remoulded when thawing starts, which is irreversible and can result in thawing settlement. Especially soils with high OCR will be affected.

2.2.3. Physical behaviour

The physical behaviour of soil during freezing-thawing cycles can be described according to their change in structure, porosity and density. These are related to the type of soil and their particle arrangement. A division in this section is made by coarse and fine grained soils.

Coarse grained

For freezing of coarse grained soils a small volume expansion can be expected during freezing. This expansion is relatively small compared with fine grained soils, but should definitely be considered when freezing occurs in a confined space such as in artificial ground freezing. A drained behaviour during freezing is often considered which prevents excess pore water pressure to build up, hence a insignificant effect by temperature variations is expected Alberdi-Pagola (2018).

Fine grained

When looking at a fine grained soil such as a clay the structure is built out of peds, i.e. aggregates of soil particles, with micropores and between the peds there are macropores. During temperature variations (irreversible) volume changes can be induced due to differences in thermal expansion/contraction coefficients, see figure 2.9 with two different alternating temperature tests without freezing.

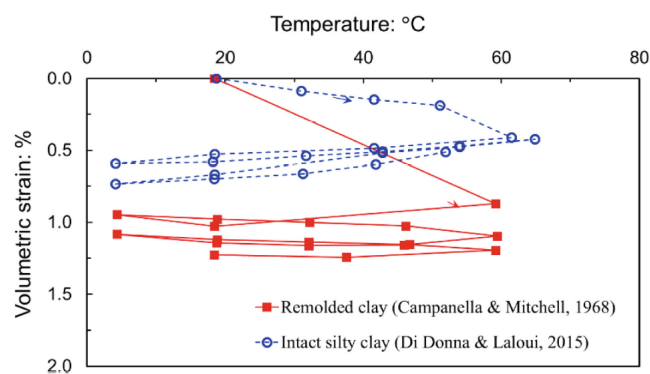


Figure 2.9: Volumetric strain of fine grained soils after thermal cycles (Ng and Zhou, 2017)

The process of freezing begins in the macropores and water is attracted from the micropores. At a specific moment ice lenses are initiated which can compress the peds and break some of the bonds that hold the peds together. When these freezing-thawing processes happen multiple times a fissured structure in clay will be visible (Steiner et al., 2018). For the thawing process of fine-grained soils processes such as thermal consolidation and dehydration have to be considered. The total freezing-thawing process depends also on the loading history of the soil (OCR) and on the earlier exposure of freeze-thaw cycles. The change is dependent on the initial structure, the moisture content, the rate of freezing and the lowest temperature (Harris, 1995). The changes in structure are described below by void ratio, strain development and creep behaviour.

Void ratio

The void ratio of a soil changes after freezing-thawing cycles according to (Qi et al., 2006). This is dependent on the overconsolidation ratio (OCR) of the soil. For normally consolidated soils the void ratio will decrease after a FT cycle (thermal contraction), while for overconsolidated soils an increase can occur (thermal expansion), see figure 2.11. Dense soils become loose and vice versa. In figure 2.10 the change in void ratio is visualized for a single freeze-thaw cycle for a fine grained soil. Different stages of the cycle are marked (Nixon and Morgenstern, 1973):

- (A) initial unfrozen state
- (B) frozen state void ratio increased due to freezing. Simultaneously, freezing water expands 9%, which is more than the expansion of solid grains.
- (C) fully thawed state with reduction in void ratio (i.e. thawed strain)
- (D) This represents the existence of negative pore pressure during thawing since this should result in an increase in effective stress.
- (E) The soil is capable to absorb the free water and results in the residual stress state with a slight increase in void ratio compared with D. Undrained situation. However the path continuous to C due to the free drainage which consolidates back to the the initial effective stress (the reloading path).

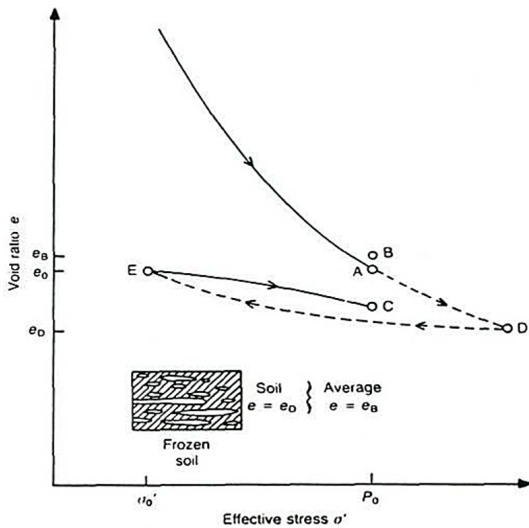


Figure 2.10: Change of void ratio in closed system with freezing thawing cycle (Nixon and Morgenstern, 1973)

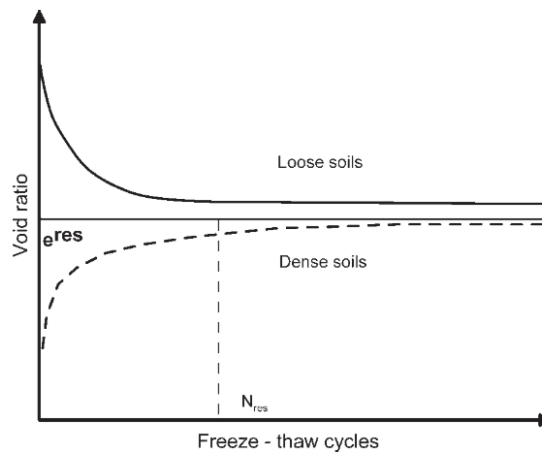


Figure 2.11: Void ratio after multiple freezing-thawing cycles (Qi et al., 2006)

Another method found to describe the behavior of frozen soils is by using the the pore ice ratio e_{ip} (Zhang and Michalowski, 2014). V_{solids} is the volume of the soil skeleton and V_{ip} describes the volume of ice present in the pores, which can be calculated from the decrease in unfrozen water from the soil freezing characteristic curve.

$$e_{ip} = V_{ip}/V_{solids} \tag{2.17}$$

$$e_{ip} = (w_0 - w) \times \frac{\rho_s}{\rho_w} \times 1.09 \tag{2.18}$$

Strain development

Equation 2.19 shows the strain development of all solid components (including ice particles) in a frozen soil. For pore water that goes through a phase change the development in strain is expressed as in equation 2.20 with β in 2.22. For gas equation 2.21 can be used with $\gamma = 1.22 \times 10^{-3}$

$$\epsilon_c = \alpha \times \delta T \quad (2.19) \quad \epsilon_{ph} = \beta \frac{\partial W_w}{\partial T} \delta T \quad (2.20) \quad \epsilon_{gas} = \gamma \times \delta T \quad (2.21)$$

$$\beta = -\frac{1}{3} \times (v_i - v_w)(1 - n) \times \rho_d \quad (2.22)$$

Creep

Deformation of a soil under constant stress is called creep and happens by the compression of the solid structure and is experienced sooner in frozen than in unfrozen soils. Creep or relaxation test are usually used to check the mechanical behaviour of frozen soils. This time-dependent behaviour is subdivided in three stages: primary (strain hardening), secondary (constant strain rate) and tertiary creep (strain softening) (Arenson et al., 2006), see figure 2.12. The curve is dependent on the stress state and the temperature of the soil (Andersland and Ladanyi, 1994). According to Andersland and Ladanyi (1994) the secondary and tertiary stage might not occur when the stress on the soil is lower than the long-term strength of frozen soil. In Abdulghader and Mohammad (2018) an experimental study was carried out on adfreeze strength and creep behavior of pile foundations in warming permafrost, which might be of value for the research on creep behaviour in frozen soils around energy piles.

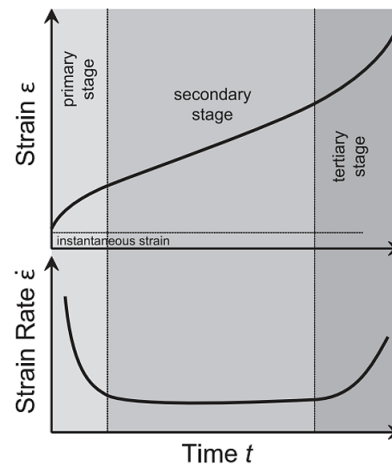


Figure 2.12: Stages of soil creep (Arenson et al., 2006)

Plastic and liquid limit

Since the viscosity of water in the pores is temperature-dependent, this has also an effect on the Atterberg limits of cohesive soils. When temperature rises water becomes less viscous and the plasticity index (PI) and liquidity index (LI) reduces (GSHP Association, 2012). In Dagesse (2015) the influence of freezing and thawing cycles of clayey soils on the Atterberg limits is investigated and concluded that there is not a clear evidence that these cycles affect the soil plasticity measured by the Atterberg limits.

2.2.4. Hydraulic behaviour

Water and soil tend to change volume when temperature changes. Water is special, since it expands during freezing (9%), but also above 4 °C. The coefficient of thermal expansion describes this behaviour for different temperatures T under constant pressure p , see equation 2.23. The coefficient of water at 0 and 10 °C is $-0.5 \times 10^{-4}/C$ and $+8.8 \times 10^{-4}/C$ respectively. In fine grained soils it is difficult for water and ice to expand, which results in a pressure build-up since the thermal expansion of the pore water is much higher than of the grains. This has an effect on the effective stress and has to be dealt with during freezing and heating of soils.

$$\beta_T = \frac{1}{V} \times \left(\frac{\partial V}{\partial T} \right)_p \quad (2.23)$$

Excess pore water pressure

Excess pore water pressures can be induced by temperature variations in the soil and this is mainly dependent on the hydraulic conductivity and the heating rate. It will happen faster in fine grained than in coarse grained soils due to the ability for the pore water to dissipate. In Ghaaowd et al. (2015) the influence of temperature variations in undrained conditions on excess pore pressure is described for thermal drain systems. Equation 2.24 by Campanella and Mitchell (1968) mentioned in Ghaaowd et al. (2015) describes the generation of excess pore water pressure with α_s , α_w and m_v the thermal volumetric expansion coefficient of solids, of water and the soil compressibility respectively. Furthermore n is the porosity of a saturated soil. Since α_w is a magnitude bigger than α_s a change in pore water pressure is expected.

$$\Delta u = \frac{n\Delta T(\alpha_s - \alpha_w)}{m_v} \quad (2.24)$$

Thaw consolidation

Thermal consolidation happens due dissipation of excess pore pressure in the soil as result of thermal expansion and contraction. A thawing soil could also induce extra settlements as result of excess pore water pressure by the attracted water during its freezing stage (Golchin et al., 2019). The total change in strain that occurs during thawing of a frozen soil exist out of strain induced due to phase change from ice to water and strain that occurs due to the compression. Since in the freezing state the ice lenses were part of the solids and the void ratio decreased, the soil skeleton has to change again during thawing to a new equilibrium (Andersland and Ladanyi, 1994). Excess water is trying to escape from the soil at a certain rate which depends on the melting of the ice and the hydraulic properties of the soil (Zhang, 2014). Due to this outflow of water, the soil starts to consolidate under the load of the soil layers above this specific layer. The overall settlement of this layer is called the thaw settlement. In Andersland and Ladanyi (1994) an equation by Croy estimates the thaw settlement based on dry soil densities in frozen and unfrozen state. A distinction in the settlement of different soft soil types can be made when looking at the over-consolidation ratio. Normally consolidated soils could have a larger settlement due to thawing than the heave induced by freezing. For over-consolidated soils, i.e. soils that experienced in the past higher loads than the loads it is experiencing now, there could still some heave be present after a thawing phase. Figure 2.13 shows an example of thawing permafrost damage.



Figure 2.13: Uneven settlement due to thawing permafrost in Alaska (by Vladimir Romanovsky)

Hydraulic conductivity

The unfrozen water content in a freezing soil decreases and thereby the permeability. This results in a reduction of the hydraulic conductivity (Andersland and Ladanyi, 1994). In coarse grained soils this reduction is larger due to faster ice formation (Burt and Williams, 1976; D’Cunha et al., 2009), see figure 2.14.

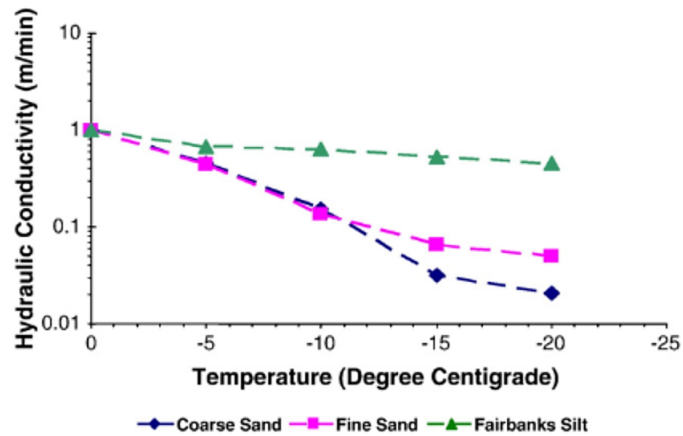


Figure 2.14: Hydraulic conductivity at freezing temperatures for three soil types (D’Cunha et al., 2009)

After thawing the permeability changes substantially. In fine grained soils the amount of microfissures and internal pore spaces increases due to expansion of frozen water (Chamberlain and Gow, 1979; Harris, 1995; Li et al., 2012). According to Harris (1995) the largest change in permeability occurs during the first freeze-thaw cycle.

Cryogenic suction

Cryogenic suction plays an important role in the initiation of an ice lens. It is defined as the pressure difference between ice, P_{ice} and unfrozen water, P_{water} (Amiri et al., 2016). It develops in response to the temperature gradient in the frozen fringe, see figure 2.15 and can be described by the Clausius-Clapeyron equation 2.25 (Ghoreishian Amiri et al., 2016). The suction S in this equation is related to the density of ice, the freezing temperature T_0 at the given pressure and the latent heat L during the phase transition from water to ice. It can be seen that a lower temperature results in a more negative pore pressure (Arzanfudi and Al-Khoury, 2018).

$$S = P_{ice} - P_{water} = -\rho_{ice} \times L \times \ln \frac{T}{T_0} \quad (2.25)$$

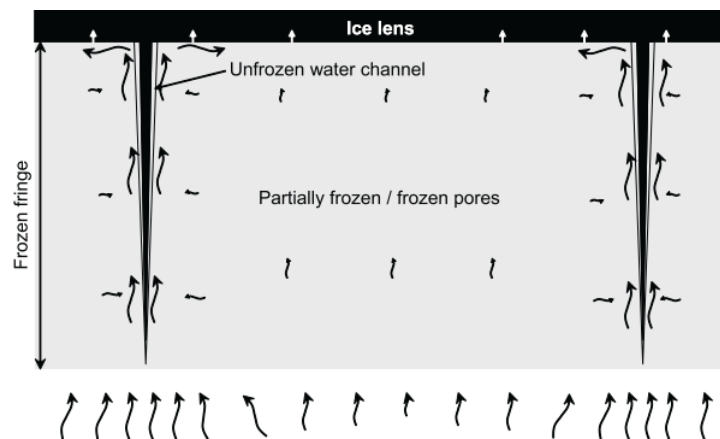


Figure 2.15: Water migration (cryosuction) in frozen fringe (Arenson et al., 2008)

2.2.5. Mechanical behaviour

Temperature and phase changes in soils often result in variations in engineering properties and soil behaviour (Chamberlain and Gow, 1979; Roman et al., 2017). The increased strength and stiffness of a frozen soil are a big advantage during the construction of certain projects, however thawing behaviour could result in strength degradation. The instantaneous increase in strength of a frozen soil is formed mainly by the cohesion of the ice matrix (Harris, 1995), because of sticky and adhesive forces. Figure 2.17 can give an indication of the

cohesion of frozen soils. For example for ice-rich varved clay, i.e. laminated sediment consisting main of clay, the cohesion can reach values of approximately 500 kPa at -4°C . Sand has a higher strength than clay in general and the lower the temperature the higher the strength. The behaviour is dominated by temperature, confining pressure, unfrozen water and creep effects. In figure 2.16 the influence of confining pressure and different freezing temperatures is visualized by Yuanming et al. (2010).

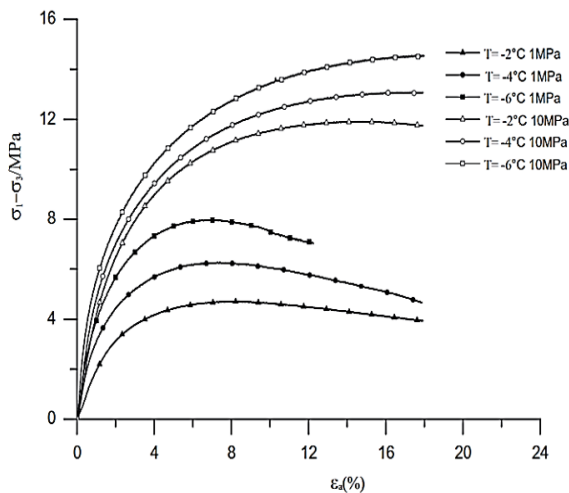


Figure 2.16: Stress-strain curves of frozen silt under subzero temperatures (Yuanming et al., 2010)

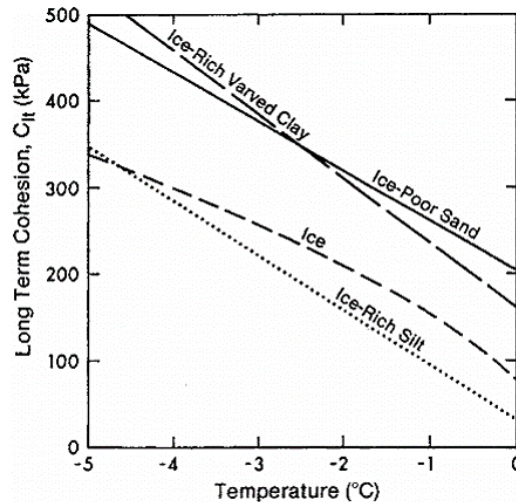


Figure 2.17: Long-term cohesive strength of frozen soils (Weaver and Morgenstern, 1981)

Whether the undrained shear strength of soils after a cycle increases or decreases depends on the overconsolidation of the clay. Harris (1995) mentions that a reduction of strength mostly takes place for cemented and overconsolidated clays. A decrease in cohesion is often mentioned in literature, while for the internal friction angle the results differ and a small increase as well as a constant value is observed.

Shear behaviour

The friction between the particles, the interlocking of particles and cohesion contribute to the shear strength. Only the solid parts can sustain shearing, so when ice is present it will contribute together with the shear strength created by the grains. The ice actually acts as a bonding agent that holds the grains together, so the presence of pore ice is the cause for the strengthening of frozen soils. In Xiao et al. (2018) the interface shear strength was investigated with a modified thermal borehole shear test. The radial displacement by expansion and contraction in combination with the temperature cycles caused a significant change in the interface shear strength. The strength of a frozen soil to withstand shear resistance can be divided into two components. One is the resistance of the frozen water content to deformation, this one is sensitive to temperature change and will be influenced when thawing occurs. The other one is the friction components of the solid grains, which is a function of the characteristics of the grains. The temperature influence for the shaft resistance is in Amatya et al. (2012) quantified during a cooling and heating phase. While Brandl (2006) states that appropriate operating conditions of energy pile installations, where the temperatures range from 5 to 20 $^{\circ}\text{C}$, hardly affect the shaft resistance of the pile. Maximum thermally-induced stress change in a pile could be an indicator for changing shear stress on the pile shaft (Bourne-Webb and Bodas Freitas, 2018). To be able to predict the mechanical behaviour after a certain amount of freezing and thawing cycles a correlation between mechanical behaviour and the amount of cycles is necessary. With this prediction the geotechnical properties of the soil model around the pile can be modified in a simulation. As mentioned earlier freezing and thawing will influence certain strength parameters and destroy the structure of soft soils. In (Li et al., 2012) a study has been conducted on the effect of freezing-thawing cycles on compacted fine grained soils. By performing laboratory test Li et al. (2012) found that the unconfined compression strength reduced by 11%, the elastic modulus by 32% and the most notable change occurred at the cohesion that decreased in some cases by 84%. Figure 2.18 depicts the decrease in cohesion found. The increase in pore pressure during expansion of water as result of freezing could lead to a reduction in effective stress. As the shear strength of a soil is dependent on the effective stress, this can result in shear failure.

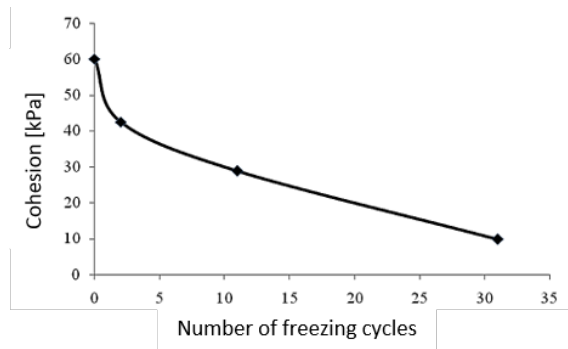


Figure 2.18: Decrease in cohesion for a compacted fine grained soil according to Li et al. (2012)

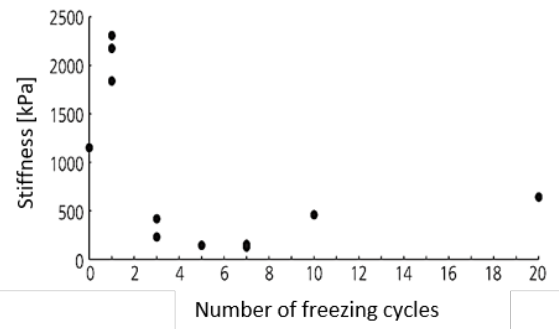


Figure 2.19: Soil stiffness of Illite clay after FT cycles (Steiner et al., 2018)

Steiner et al. (2018) also investigated the influence of FT cycles on the shear strength of a highly frost susceptible illite clay. Figure 2.20 shows the mobilised shear strength for samples subjected to FT cycles with a freezing temperature of $T = -20\text{ C}^\circ$. Steiner et al. (2018) concluded that most of the soil stiffness decreased during a change in soil structure. Alongside this conclusion most of the strain softening took place after one FT cycle and lower freezing temperatures result in larger ice lenses and weaker soils. In case of a conservative freeze-thaw design, the lowest shear strength value should be used, which in this case developed after one FT cycle.

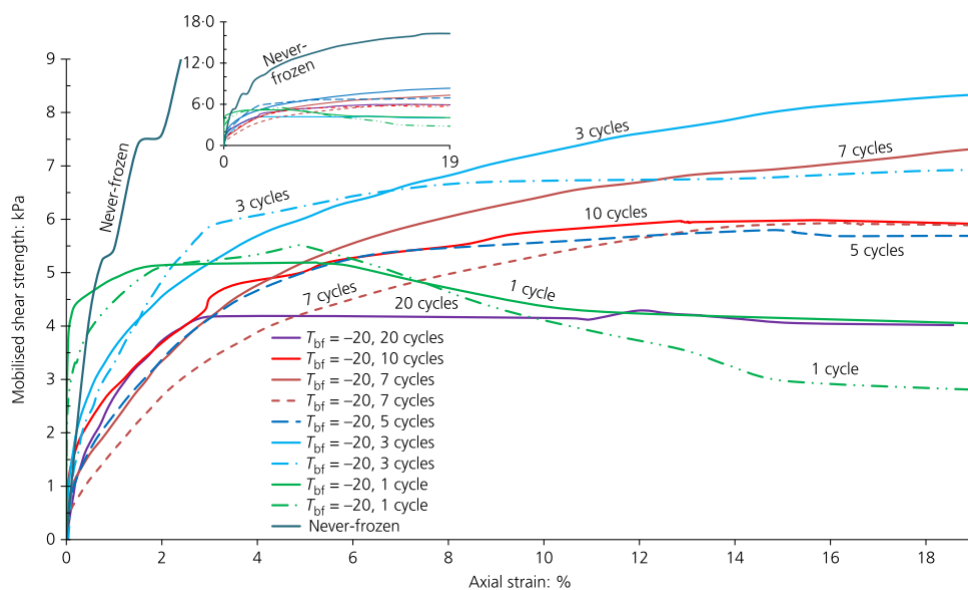


Figure 2.20: Mobilised shear strength for illite clay samples subjected to FT cycles (Steiner et al., 2018)

Stiffness

Soil stiffness is an important design property of foundations. Therefore it is necessary to understand the change in stiffness during its design life. In Steiner et al. (2018) the decrease of soil stiffness due to the damaged soil structure after subjection to freezing and thawing cycles is shown, see figure 2.19. The stiffness is influenced by parameters as void ratio, effective stress, plasticity index, OCR and also cyclic properties such as the amount of cycles and their strain amplitudes.

2.2.6. Dynamic behaviour

Soils behave as an elastoplastic material when stress is applied. During cyclic loading as with thermal cycles, the soil shows a loading-unloading-reloading behaviour as in figure 2.21. After reloading the soil has experienced some sort of permanent deformation, the plastic strain. After multiple loops the plastic strain increment decreases, this happens due to the closure of voids between the particles (Yuanming et al., 2010).

The loops are called hysteresis loops, see figure 2.22. The G_s is the secant shear modulus, which represents the average shear modulus of one complete loop. The backbone curve is another characteristic that helps to describe the loop. The backbone curve follows the path of the peaks of multiple loops and goes through the origin.

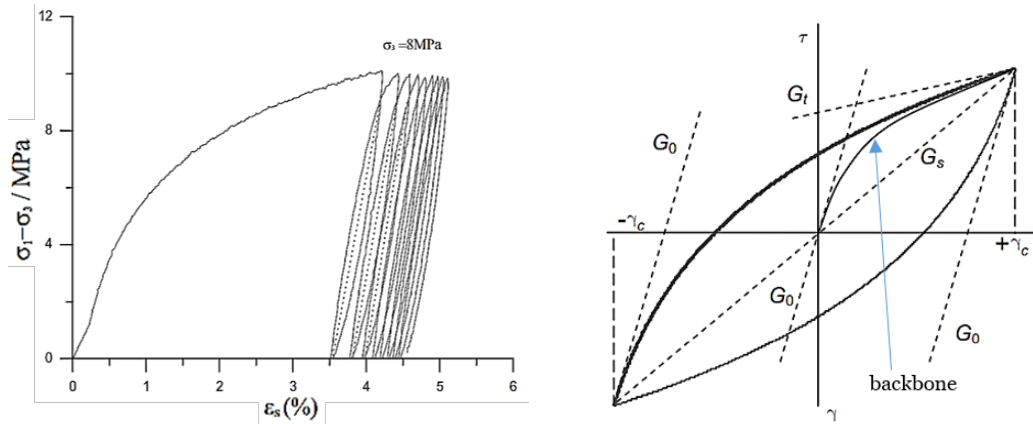


Figure 2.21: Cyclic loading of frozen silt by Yuanming et al. (2010) Figure 2.22: Hysteretic behaviour in the Hardening-soil small strain (HSS) model (Brinkgreve et al., 2007)

The secant modulus G_s follows the backbone curve and the steepest slope of the backbone curve, so the slope at very small strain and elastic part, is called the G_0 or G_{max} . There are two curves to which is often referred to when talking about cyclic behaviour of a soil and determining the backbone curve, these are the shear modulus reduction curve and the damping curve. Both are needed to predict how the soil stiffness degrades during cyclic shear straining. The shear modulus reduction curve can be determined in a shear test in which the soil stiffness decreases when the strain increases, this is mostly represented in a normalized graph with G_s/G_0 , see figure 2.23. As mentioned before, high strains are shown at the very low strains. An approximation of the curve, equation 2.26, is given in Brinkgreve et al. (2007) with the shear strength as in 2.27

$$G_s = \frac{G_0}{1 + 0.385 \frac{\gamma}{\gamma_{0.7}}} \quad (2.26)$$

$$\tau = G_s \times \gamma \quad (2.27)$$

The modulus reduction curves are mostly together with damping curves. For each cycle a damping ratio can be determined and combined they form a curve, see figure 2.48. As the strain increases, the soil loses its stiffness, becomes damaged and will have an increase in damping.

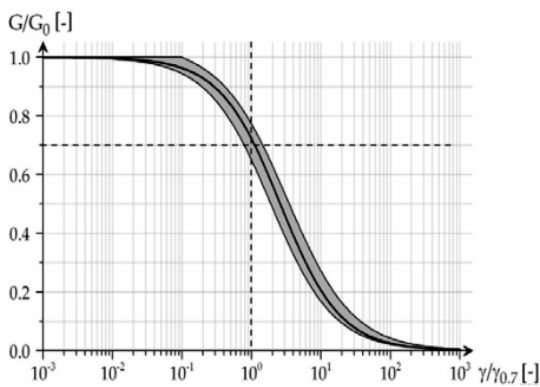


Figure 2.23: Normalized shear modulus reduction curve from (Brinkgreve et al., 2007)

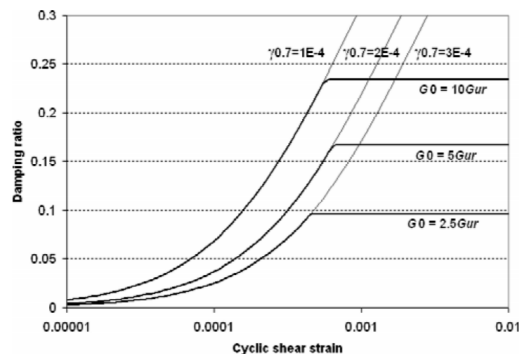


Figure 2.24: Damping ratio with cyclic shear strain (Brinkgreve et al., 2007)

2.3. Freezing-thawing of a foundation pile

Not only the soil is affected by thermal loads, but also the pile itself behaves in a different way. In this section the physical behaviour of the concrete and the mechanical behaviour of the pile is described. Also the soil-pile interface is affected and described in this section. To get a first idea of the mechanisms a freezing and a thawing stage is stepwise elaborated like in the previous section. Thereafter the mechanical and dynamic behaviour are discussed. The physical behaviour of the pile is described in the concrete durability part.

2.3.1. Freezing-thawing sequence

For the freezing stage, which means cooling of the pile, the following processes below are experienced by the concrete energy pile. Important to mention that the pile is mechanical loaded on top (fixed) by a structure and its bearing capacity is a summation of the shaft resistance in soft layers and tip resistance in a stiff sand layer. Furthermore no countermeasure are taken for frost and thaw behaviour within the concrete of the pile (e.g. air entrainment agents).

1. Thermal contraction in radial and axial direction during cooling of the concrete.
2. Lower part pile moves upward, which may result in decrease in base pressure and mobilization of negative skin friction.
3. Pile settlement occurs due to load on top.
4. Positive shaft resistance mobilized again
5. Water present within the concrete pores expand during phase change
6. More water is attracted around the pile
7. Chemical bonds in concrete might be broken

For the same conditions the thawing sequence can be described as below. The heating of the pile happens due to the stop of thermal extraction or even regeneration in warmer summer months.

1. Thermal expansion of pile in all directions, but constrained by a structural load at the top and in stiff sand layer.
2. Increase in axial stress, but very unlikely that it reaches axial strength of concrete pile.
3. Increase in base and head pressure

2.3.2. Mechanical behaviour

A well-known issue with temperature change of materials is the volume reduction and expansion that occurs. This change also develops within energy piles, since the aggregates in the concrete will cause a temperature-dependent volume change of the pile in radial and axial direction (thermal load). Three pile head conditions can be considered, there is the free head pile for piles under flexible structures, the fixed-head pile which is founded under a rigid structure and an intermediate situation (Habert et al., 2019). For the computation of the radial expansion and contraction, the diameter, the thermal expansion coefficient and the temperature difference of the pile are necessary.

When the expansion of the pile is stored as free strain ϵ_{T-free} , i.e. the pile is unrestrained (Knellwolf et al., 2011), equation 2.28 can be used with α as coefficient of thermal expansion and ΔT as change in temperature.

$$\epsilon_{T-free} = \alpha \times \Delta T \quad (2.28)$$

However, the volume change does not occur under free expansion conditions. Due to the presence of the soil around the pile, i.e. the stiff base layer and the structure on top of the pile, a thermally induced stress develops and the pile will not be able to fully expand. The strain that is observed and not transformed to a load is called the observed strain $\epsilon_{T-observed}$. The ratio between the observed and free strain is the degree of freedom n (Knellwolf et al., 2011). From this follows equation 2.29 and the difference between the free and the observed strain is called $\epsilon_{T-restrained}$. By now assuming a linear elastic behaviour of the pile, the temperature induced stress can be calculated by equation 2.30 with E_{pile} as the stiffness. The additional load on the pile is then found by multiplying the stress with the cross sectional area of the pile (Bourne-Webb et al., 2013).

$$\epsilon_{T-observed} = n \times \alpha \times \Delta T \tag{2.29}$$

$$\sigma_T = E_{pile} \times \epsilon_{T-restrained} \tag{2.30}$$

Since the pile will not be totally restrained, the expansion forces induced by heating will tend to mobilize the extra developed load in the form of shaft resistance q_{shaft} , as in figure 2.25a and 2.25b. So in case of stiffer base layer, more load is developed and less shaft resistance is mobilized.

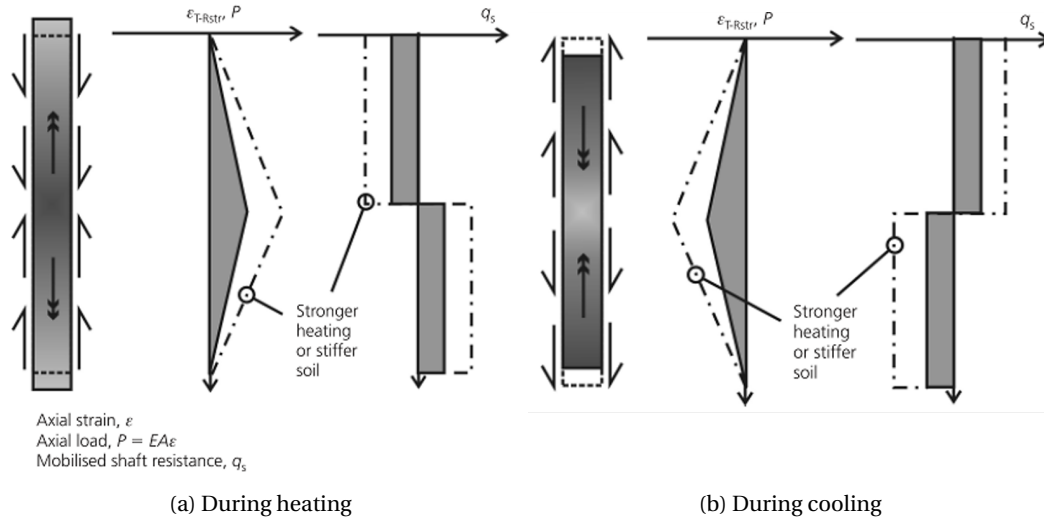


Figure 2.25: Restrainted pile during heating and cooling (Bourne-Webb et al., 2013)

The earlier analysis is without a mechanical load on top of the pile, which in a real situation needs to be included. The effects of these combined loads without restraints are depicted in figure 2.26a and 2.26b. The mechanical load on itself creates, in case of a homogeneous layer around the pile, a linear decreasing load profile from the top and a constant shaft friction along the pile.

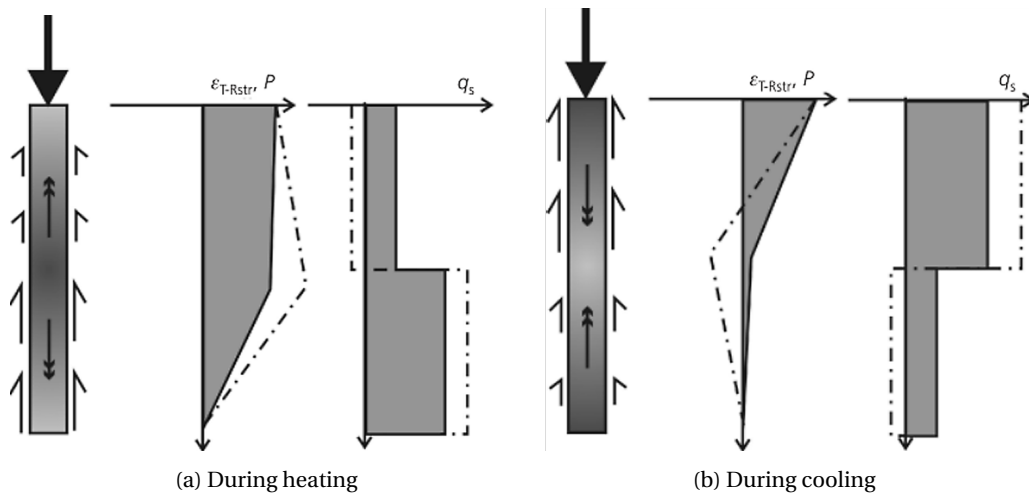


Figure 2.26: Restrainted pile during heating and cooling plus mechanical loading (Bourne-Webb et al., 2013)

2.3.3. Dynamic behaviour

During the lifetime of an energy pile it will experience multiple thermal cycles, which causes a variation in stresses in the pile and mobilized shaft resistance at the soil-pile interface. The following phenomena can be considered:

- Redistribution of axial stress in the pile

- Ratcheting

Ratcheting is displacement of the pile. Due to expansion and pile fixed at top, the pile expands downwards. Small failure in soil at the bottom can occur when this base pressure increases. A new cycle will go further through soil and whole process is repeated. After multiple cycles a substantial pile displacement can occur.

- Freeze-thaw fatigue damage in concrete

For ratcheting the steps can be as follows: (i) the pile is lifted due to contraction, (ii) load P is constant and causes the pile to settle more in the end-bearing layer, (iii) in case of frictional piles, more shaft resistance will be mobilised around the shaft, and (iv) if this process repeats as a result of expansion-contraction cycles, ratcheting takes place.

Ng et al. (2014a) observed ratcheting settlement of piles in clays and mentions that it is a main problem for the serviceability limit state (SLS) design of energy piles. In figure 2.27 the ratcheting mechanism is visualised with the shaft resistance **fully mobilised**. In the first step (a), a force F is applied that is bigger than the ultimate shaft resistance, so some extra base resistance is necessary to balance F . Due to this extra resistance, the pile will settle a little bit y_0 . In case of cooling (b), the pile will contract while no shaft resistance can be mobilised anymore above the neutral plane, while under the neutral plane the shaft resistance will be reduced. The base resistance has to increase again to compensate the loss of shaft resistance, this effect will lead to a small settlement of the pile $y_{b(b)}$. When a heating cycle follows (c) and the load F is still present, the pile will expand. This expansion reverses the shear stresses above the neutral plane and will mobilise more base resistance, resulting in even more settlement $y_{b(c)}$. After one heating/cooling cycle, another cooling phase is introduced, this leads to contraction of the pile and less mobilized base resistance. The cyclic behaviour which has led to accumulative displacement, shown in graph e as result of increasing base resistance, is called ratcheting.

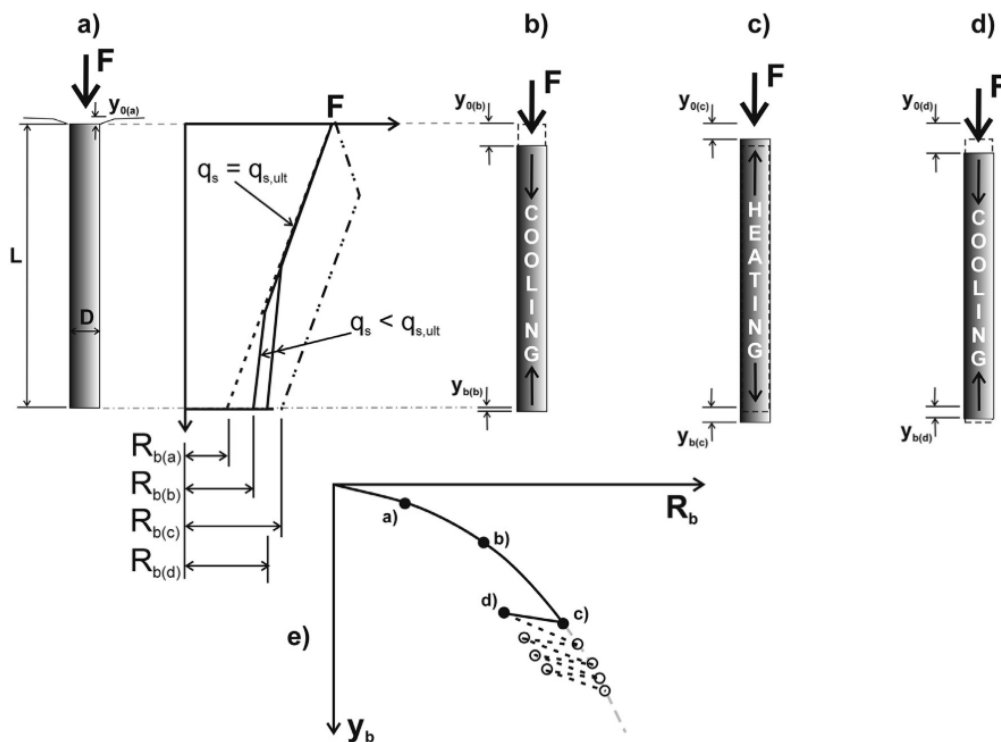


Figure 2.27: Ratcheting (Bourne-Webb and Bodas Freitas, 2018)

2.3.4. Soil-pile interface

The performance of a pile foundation is highly dependent on the properties of the interface (Li and Lu, 2011). During thermal loading a variation in radial contact pressure can develop at the interface, which could be one of the reasons of the change in shaft resistance. An experimental and numerical study was done by Olgun et al. (2014) on this phenomena. They checked if this could be the reason for the increase in pile capacity during

heating. One of the findings was an increase of less than 15 kPa in radial contact pressure, which was not significant enough to explain the increase in shaft resistance that occurs during the heating. In figure 2.28 the increase in contact pressure is depicted as elastic soil and pile, which can be represented with two springs.

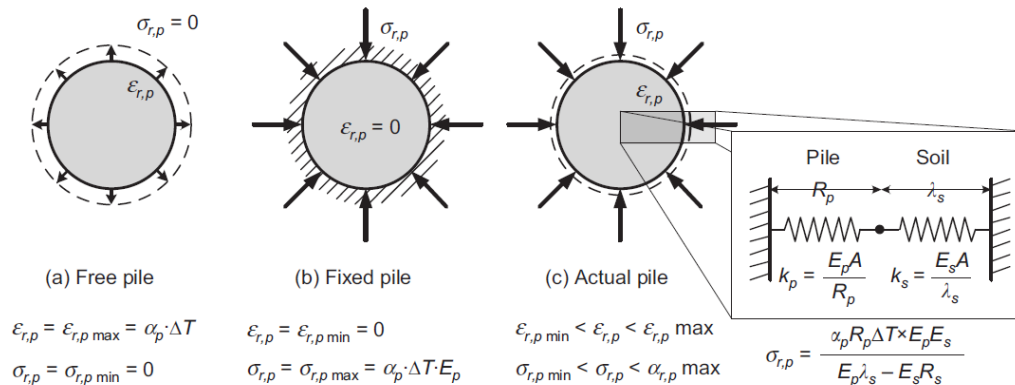


Figure 2.28: Expansion of pile in free, fixed and actual condition during heating (Olgun et al., 2014)

Adfreezing effects

Adfreezing forces can result in upward displacement of the pile foundation. This happens due to the ice formation and by water movement to the freezing area (Henry, 2000), i.e. cryosuction. Research is mainly done at permafrost areas. The adfreeze bond strength τ_a is the parameter used for the pile design in permafrost described as equation 2.31 with c_a cohesion at the interface, ϕ_a friction angle at the interface and p_n normal stress acting on the interface (Andersland and Ladanyi, 1994).

$$\tau_a = c_a + p_n \tan(\phi_a) \tag{2.31}$$

According to Andersland and Ladanyi (1994) it is difficult to predict the magnitude of these forces since it depends on many variables. An example that can help to indicate the forces F [kgf] (*kilogram × force*) on a pile is described by equation 2.32 by Dalmatov in which L [cm] is the perimeter of the pile in contact, h_α [cm] the thickness of the frozen zone, T_m [°C] the minimum soil temperature in the frozen zone and b and c are experimentally determined (Andersland and Ladanyi, 1994). Table 2.4 shows some values for b and c , but they should be used with care since these are still pile and site specific. The ice forming process will continue unless there is not enough water left in the soil, this plays a crucial role in the occurrence of frost heave (Arenson et al., 2008; Tian et al., 2014). Frost heave is dependent on the freezing rate, soil properties and the overburden pressure. A low freezing rate could cause more frost heave (Henry, 2000).

$$F = L h_\alpha (c - 0.5 b T_m) \tag{2.32}$$

Table 2.4: b and c parameters from (Morgenstern et al., 1975)

Soil type	c [kgf/cm ²]	b [kgf/cm ²]
Morane loam	0.5	0.12
Silt loam	0.4	0.10
Heavy silt loam with sand	0.4	0.16
Silty loam	0.5	0.18
Sandy loam	0.7	0.22

2.4. Freezing-thawing resistance of concrete

The strength, thermal conductivity and its resistance to frost degradation are important factors that have to be considered during the design of an energy pile. The heat transfer of a thermal concrete structure is mainly dependent on the thermal conductivity and together with the dimensions of the pile it determines the thermal resistance. The thermal conductivity of concrete ranges between 1-4 W/mk and is mostly dependent on its aggregate (GSHP Association, 2012). The strength and frost resistance of concrete depends on its mixture, i.e. aggregate, water, cement and admixtures. Research has been done on concrete exposed to severe conditions, e.g. (Copuroglu, 2006). Typical deterioration effects mentioned are surface scaling and internal cracking. Surface scaling is the loss of a surface portion of concrete and internal cracking results in more expansion cracking and decreases the mechanical properties of concrete (Copuroglu, 2006). The basic process of frost action is initiated by water present in the concrete pores that is able to expand beyond the constraints and exceeds the tensile strength of the concrete during freezing. When the pressure, generated as result of freezing, accumulates every cycle due to a higher saturation, it can cause more permanent damage on the concrete structure (Şahin et al., 2007). According to Yu et al. (2017) the water in the concrete pores freezes below a temperature of around -3°C , but this is also dependent on the solutes present.

2.4.1. Aggregates

Aggregates make around 70% of a concrete mixture and must be selected to be durable and produce consistent strength and workability. The strength is an important factor in the selection of aggregates. A well-graded aggregate increases the strength, reduces the permeability, which results in more frost resistance. Since it is the main component, the choice of aggregate type also determines the thermal conductivity.

2.4.2. Water-cement ratio

The behaviour of concrete during freezing is mainly determined by its water-cement (W/C) ratio. Its resistance to freezing increases as the ratio decreases. Since a high ratio will lead to a higher permeability and thereby an increase in capillary forces as well. This even changed the Dutch standard of concrete mixtures, wherein it was allowed to use mixtures without air entrainment agents for concrete mixtures with a water-cement ratio lower than 0.45 (Copuroglu, 2006), see XF4 table 2.5. However, it is important to bear in mind that a change in water-cement ratio also influences the final strength and workability of the concrete. A lower W/C ratio will decrease the workability and increase the final strength. It is therefore important to know how much water is present, or what W/C ratio is used in the concrete pile.

2.4.3. Admixtures

Additives such as fly ash are used to replace a certain amount of cement and also increase the concrete strength. The fine ash improves the workability of the concrete and thereby decreases the need of water for the workability. Its fine characteristic helps to reduce the permeability.

2.4.4. Air entrainment

To improve the resistance to severe conditions air entrainment admixtures are often used. Air entrainment makes the concrete more resistant to the frost damage by providing small air pores ($\approx 300\ \mu\text{m}$), which prevents that water can intrude by capillary forces. It also provides an extra space for the release of pressure during the expansion of ice. However, it also results in a decrease in density of the concrete, which reduces the thermal conductivity and the concrete strength. This reduction in strength can be counteracted by reducing the water-cement ratio.

2.4.5. Environmental classes

In NEN8005 the amount of air entrainment and other components are mentioned for concrete in different environmental classes. These four exposure classes are based on the natural occurrence of water and the amount of solutes already present. In table 2.5 the requirements for concrete exposed to freeze-thaw cycles are summarized described in NEN8005. Many available guidelines advice to use a water-cement ratio less than 0.5 for concrete exposed to freezing and thawing conditions.

- XF1, moderate water saturation without salt
- XF2, moderate water saturation with salt

- XF3, high water saturation without salt
- XF4, high water saturation with salt

Table 2.5: Concrete requirements freeze-thaw environments

Environmental class	Max water-cement factor / water-binder factor	Min cement / binder	Max grain size [mm]	Air content [% of volume]
XF1	0.55	300	-	-
			63	3.0
XF2	0.55	300	31.5	3.5
			16	4.0
			8	5.0
XF2	0.45	300	-	-
XF3	0.50	300	-	-
XF4	0.50	300	63	3.0
			31.5	3.5
			16	4.0
XF4	0.50	300	8	5.0
			-	-
XF4	0.45	320	-	-

2.4.6. Overview

The overview below summarises the effect of the concrete mixture on the design factors thermal conductivity, concrete strength and frost resistance.

	Thermal conductivity	Concrete strength	Frost resistance
Aggregate (Well-graded)	2 (limestone) - 7 W/mk (quartz)	Increase	Increase
Increase in W/C ratio	Decrease	Decrease	Decrease
Air-entrainment agent (AEA)	Decrease	Decrease	Increase
Fly ash / silica fume	Decrease	Increase	Depends on mixture

Table 2.6: Effect on thermal conductivity and frost resistance of concrete

2.4.7. Dynamic modulus of elasticity

In literature several papers exist that describe the change in concrete strength after a certain amount of freezing and thawing cycles based on the dynamic characteristics of the pile, e.g. (Li and Lu, 2011; Yu et al., 2017). In Wotherspoon et al. (2010) a test with seasonal conditions (-10°C until 23°C) is described and found that the effective stress during frozen conditions increased with 170%. An equation is proposed in (Yu et al., 2017), which describes the freeze-thaw fatigue damage of concrete after certain amount of cycles. The dynamic modulus of elasticity E_n is chosen here as damage variable, which describes the deformation resistance of the pile foundation exposed to dynamic loads. Furthermore, two environmental conditions are distinguished, a natural water environment and a saline environment. The equations below consider the natural water condition, wherein E_0 is the initial dynamic modulus of elasticity, N is the fatigue life of concrete and n is the amount of freeze-thaw cycles the concrete is exposed to. In equation 2.34 the material parameter β is introduced, this parameter relates many concrete properties (e.g. water-cement ratio, compressive strength, air content, etc.) to the frost susceptibility. The lower β , the better it is resistant to the freezing circumstances.

$$\frac{E_n}{E_0} = \frac{0.6 \log(N)}{\log(N) - 0.4 \log(N - n)} \quad (2.33) \quad \beta = \frac{0.4}{\log(N)} \quad (2.34)$$

2.5. Design of pile foundations

Foundations are constructed in various ways and exist in many types. To begin with the manufacturing of a pile foundation could take place in-situ or as precasted pile. Another difference is its loading, this could be compression, tension and/or lateral. Apart from that there are different methods of transferring a load, which could be via the shaft, tip or both. For the calculation of the bearing capacity of a pile foundation and taking into account the mechanical properties such as the cohesion and the internal friction angle, Brinch Hansen or the Koppejan method could be used in combination with cone penetration tests. Another option that results in the best prediction of the pile capacity is by making use of a test load, however this option is in most cases too expensive due to the high loads that have to be applied on the pile (Verruijt, 1990).

Piles in the Netherlands are designed according to the Dutch and European norm, NEN (2017) and Eurocode 7. The foundation types in the Netherlands differ according to the location and its geological history. In the western part of the Netherlands the bearing layer is often reached by using pile foundations, while in other parts of the Netherlands a concrete slab is mostly sufficient to transfer the loads to a bearing layer. This is also visible in figure 2.29. The stiff sand layers from Pleistocene often represent the foundation for many structures. Above these sand layers the soft Holocene layers are found, which mainly consist of marine clays with sometimes a peat layer in between. The pile length depends on the type of structure, but varies between 10 to 20 m for most constructions. Large constructions such as high buildings could even demand pile lengths of +50 m.

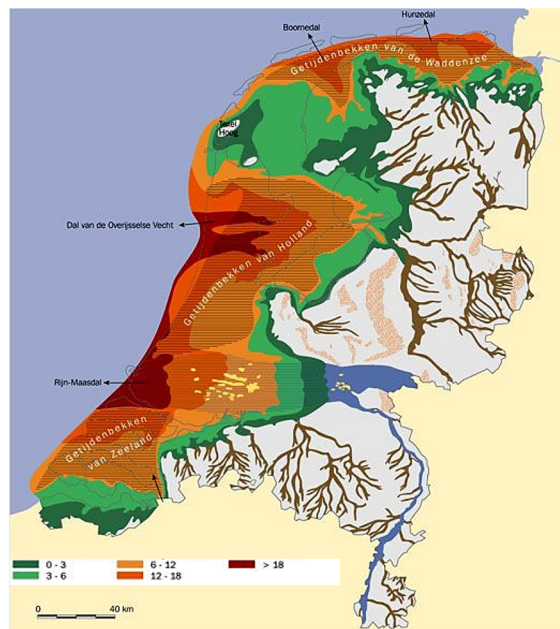


Figure 2.29: Top of Pleistocene from NAP level Netherlands (TNO, 2013)

2.5.1. Bearing capacity

In practice most formulas for bearing capacity are based on the cone penetration test (CPT), which is used as preliminary soil test for foundation design. A correlation is found between the results from a CPT test and the bearing capacity of a pile foundation. The (positive) shaft resistance (R_{shaft} in equation 2.40) and tip resistance (R_{tip} in equation 2.36) contribute both to this total bearing capacity (R_{total}) in equation 2.35). However, since there exist a positive shaft friction, the negative variant has to be considered as well. It has to be subtracted from the tip and positive shaft resistance.

$$R_{total} = R_{tip} + R_{shaft,pos} - R_{shaft,neg} \quad (2.35)$$

Tip resistance

The method used in the Netherlands for the calculation of the tip resistance is established on experience. This method is called the Koppejan method in which the parts contributing to the pile tip capacity are taken into account. Equation 2.37 represents the formula of the tip resistance $q_{tip;max}$. q_1 , q_2 and q_3 are respectively the average CPT values 4D below the tip, at 0.7 and 8D above the tip, see figure 2.30. α_p is the pile class factor, β is the factor for the shape of the foot of the pile and s takes the cross section of the foot into account, see appendix B (Mw, 2012).

$$R_{tip} = A_{tip} \times q_{tip} \quad (2.36)$$

$$q_{tip;max} = \frac{1}{2} \times \alpha_p \times \beta \times s \times \left(\frac{q_{c;1;avg} + q_{c;2;avg}}{2} + q_{c;3;avg} \right) \quad (2.37)$$

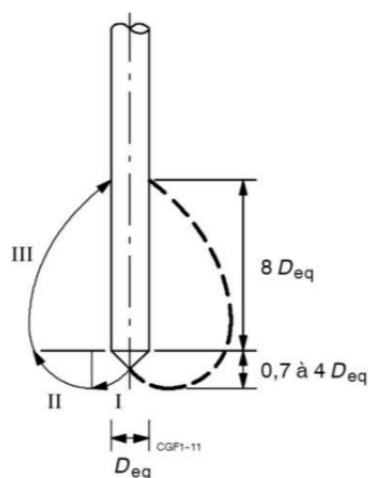


Figure 2.30: 4D/8D method

Another method mentioned earlier is the method of Brinch Hansen, which can be chosen when CPT results are not available. Brinch Hansen included the shape of the loaded area, inclination load and inclined soil surface, see equation 2.38. Furthermore, the bearing capacity coefficients N_q and N_c , which are a function of the friction angle, are also necessary. This equation can be used for the bearing capacity of the tip of a foundation pile in which ϕ and c are from the sand layer and q is the load imposed by the weight of the soft layers above. For an axial compressed pile ($i_q = i_c = 1$) equation 2.39 is used.

$$p = i_c s_c c N_c + i_q s_q q N_q + i_\gamma s_\gamma \frac{1}{2} \gamma B N_\gamma \quad (2.38)$$

$$q_{tip;max} = \sigma' \times N_q \times s_q \times i_q + \frac{1}{2} \gamma B_{ef} N_\gamma i_\gamma s_\gamma \quad (2.39)$$

Shaft resistance

The bearing capacity of a pile is also derived from the part with positive shaft resistance $p_{max;shaft;pos}$, see equation 2.40 and 2.42 with α_s as correction factor for installation type, which is different for each soil type, see NEN (2017), and q_c the cone resistance. In sand this shaft resistance comes from the friction between the pile material and the soil, while for a clay this is caused due to the adhesion between the pile material and the clay particles. For the mobilization of the shaft resistance a small slip in the order of mm is often sufficient, while the tip needs more displacement before it is mobilized (e.g. 10% of pile diameter as rule of thumb). A simple method to analyse this process is by using load-displacement curves. Another way to come up with the behaviour of a pile is by making use of the finite element method in which the pile foundation and soil

are dividing it into elements. These elements represent the soil and structural characteristics. The measured resistance is directly related to the maximum shear force along the pile. The mobilized shaft friction can then be determined by a load-settlement curve.

$$p_{max;shaft,pos} = \alpha_s \times q_c \quad (2.40)$$

There is also negative shaft resistance which is observed mainly in soft soils as a result of consolidation due to dissipation of excess pore pressure. It is considered negative since it acts in the other direction to the positive upward skin friction formed by pile settlement relative to the soil. The consolidation increases the effective stress in the soil, which results in an increase in shear stress on the pile. The negative skin friction is the most common problem in the design and construction of pile foundations in compressible soils. It could be the result of loads on the surface, lowering of groundwater level and consolidation of the soil. In case of tension piles it occurs when the surrounding soil heaves. These processes will pull on the pile wall, which causes a dragload. This dragload is increasing when the tip resistance is also increasing, since in this case the neutral plane also lies closer to the tip. The slip method is mainly used to determine this dragload, see equation 2.41, wherein $K_0 = 1 - \sin(\phi)$ and δ is equal to ϕ' for cast in-place or is equal to $0.75\phi'$ for prefab piles (NEN, 2017). In the guideline of the United States Army Corps of Engineers (USACE) the δ is also given in figure 2.31 for different pile materials. In appendix B an example calculation for the negative skin friction is performed.

$$p_{max;shaft,neg} = K_0 \times \tan\delta \times \sigma'_v \quad (2.41)$$

$$R_{shaft} = O_{pile} \times \int_L p_{max;shaft} dz \quad (2.42)$$

Pile Material	δ
Steel	0.67 ϕ to 0.83 ϕ
Concrete	0.90 ϕ to 1.0 ϕ
Timber	0.80 ϕ to 1.0 ϕ

Figure 2.31: Values of δ

Neutral point

The depth at which positive and negative shaft resistance switch is called the neutral point, see figure 5.7. At this location of the pile no relative displacements between pile and soil take place and the axial stress of the pile is at its maximum. The neutral plane in the Netherlands lies often at the boundary between the soft layers and the bearing sand layer, but its position could change. Since the pile is often embedded in the stiff sand layer no substantial displacements are normally expected that are able to move the neutral plane upwards. But when this happens it is possible that a part of the negative shaft resistance turns into additional positive shaft resistance, i.e. more shaft resistance is mobilized, which then results in a new stability equilibrium of the pile. In the calculation according to the norm NEN (2017) this does not happen since the total bearing capacity is only calculated with the shaft resistance from the bearing layer. In D-foundations the bearing capacities of piles can be calculated with different neutral planes and safety factors according NEN (2017). The behaviour of the neutral plane during thermal loading is also important to look at since expansion and contraction of the pile happens below and above this neutral location. This also counts for a degradation of the interface friction, this might change the distribution of shaft resistance along the pile as well.

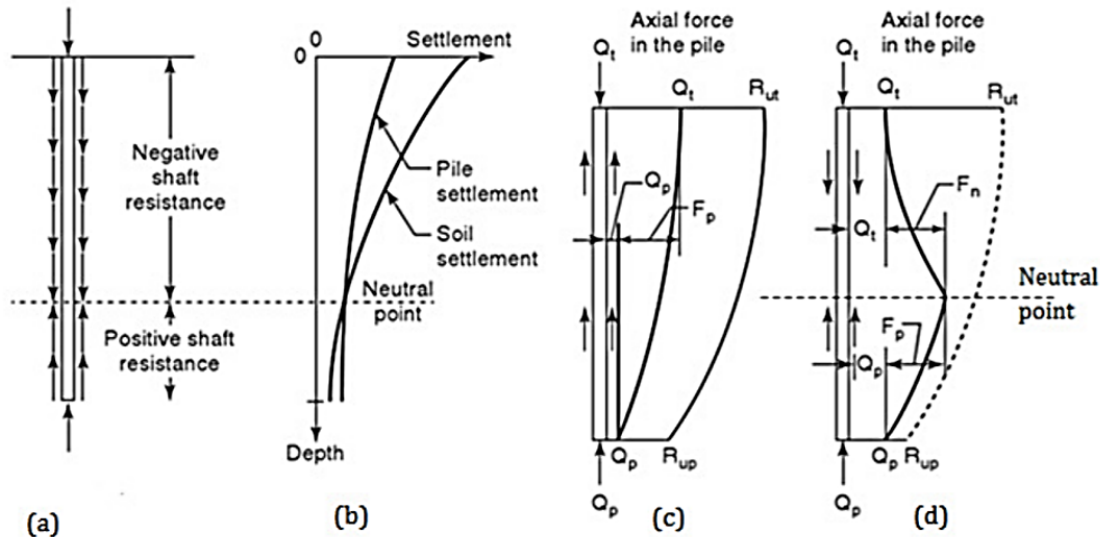


Figure 2.32: (a)Position of neutral plane, (b) settlements pile and soil, (c) No negative skin friction, (d) negative skin friction (Briaud, 2013)

Precautionary measures downdrag

In the Dutch norm (NEN, 2017) axial compressed piles are only designed on the mobilized shaft and tip resistance of the bearing sand layers, the resistance from the soft layers above these bearing layers is not included. For tension piles in (NEN, 2017) a reduction factor exist in case of flipping between tension and compression. If the load is completely flipping a reduction factor is applied. In case of small cyclic load variations a smaller reduction factor is used.

2.5.2. Static pile load tests

General behaviour of a pile is visualized with help of a load test. In a load test the settlement of a pile is observed during the application of load steps. The settlement behaviour determines the ultimate bearing capacity, which is for coarse grained soil determined at a load that causes a settlement of 10% of the diameter of the pile. For fine grained soils this is visible at the start of the non-linear part of the load-displacement curve, where plastic deformations start to occur. The settlement of a pile is a summation of the settlement in the tip and the compression of the pile. The compression of the pile depends on the average load P , the length L of the pile, the cross sectional area A_{pile} and its stiffness E_{pile} , see equation 2.43.

$$s_{top} = s_{tip} + \frac{P \times L}{A_{pile} \times E_{pile}} \tag{2.43}$$

The curve is often represented by a linear elastic perfectly plastic curve in which the first elastic part can be represented by equation 2.44 with spring constant k_p .

$$s_{tip} = \frac{P_{tip}}{k_p} \tag{2.44}$$

Within this research a single pile is used and tested under different conditions. To be able to compare the results of thermal loads on the pile a good prediction of the bearing capacity is necessary.

2.5.3. Limit state design

There are two important limit states considered in foundation design: (i) the ultimate limit state (ULS) for safety of the foundation against soil failure and (ii) serviceability limit state (SLS) for minimizing the settlements of the foundation such that there is no loss in functionality. For the ULS the resistance from the shaft and the tip must be sufficient to handle the load. The SLS checks whether the foundation has a certain safety

against excessive settlements under a predetermined load. To ensure that a pile foundation sustains a certain load, safety factors γ are used within the calculation. This is done with a safety factor over the load and a factor for the calculated resistances, see 2.45. For the resistance part it is possible to apply safety factors over the material properties instead of applying it over the total resistance.

$$\gamma \times load < \gamma \times Resistance \quad (2.45)$$

The ultimate bearing capacity for a compression pile is a combination of the tip and shaft resistance:

$$F_{r,max} = F_{r,max;tip} + F_{r,max;shaft} \quad (2.46)$$

$$F_{r,max;tip} = A_{tip} \times p_{r,max;tip} \quad (2.47) \quad F_{r,max;shaft} = O_{p;avg} \times \alpha_{shaft} \times q_c \times l \quad (2.48)$$

2.5.4. Geotechnical design process

In figure 2.33 the design process of a mechanical loaded pile is shown with some additions for a thermal-mechanical loaded (energy) pile. As mentioned earlier it is the structural behaviour of the foundation that determines the pile size, so first the pile is calculated with the ULS and the corresponding safety factors. The next step is to check the SLS of the pile, which includes also the thermal loads on the pile. Hereafter a decision is made on the dimensions.

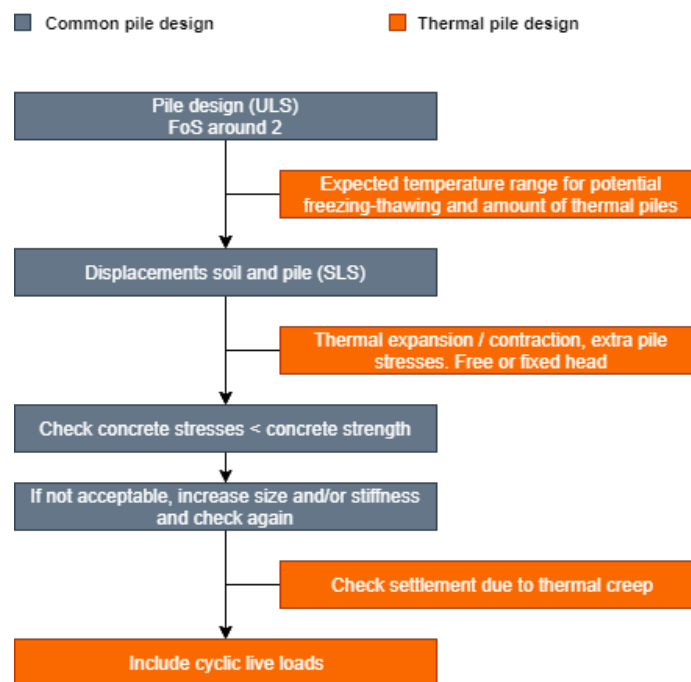


Figure 2.33: Geotechnical design process of an energy pile

2.5.5. Vertical borehole heat exchangers (BHE)

An analysis of the design standards of a borehole heat exchanger is useful for the research on energy piles. Borehole heat exchangers can be found in many places including the Netherlands. The inlet temperature and flow rate are often the main design parameters, but these also depend on the pipe-layout of the heat exchanger and on the heat demand of the structure. An example of the lay-out of a pile is depicted in figure 2.34. When embedded in concrete the pipe has often a U-shape, but there are also situations where W-shapes or multiple U-shapes are applied. The expected heating and cooling demand of a building determines how many piles are necessary, but also the depth of the piles and their configuration.

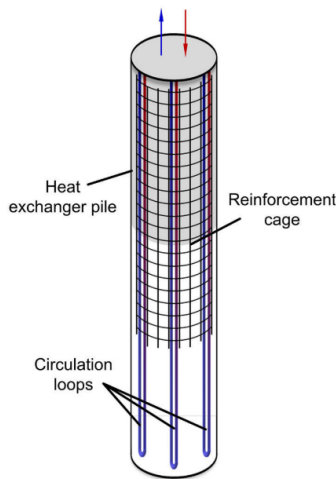


Figure 2.34: Pile lay-out including heat transfer pipes in U-shape (Olgun et al., 2015)

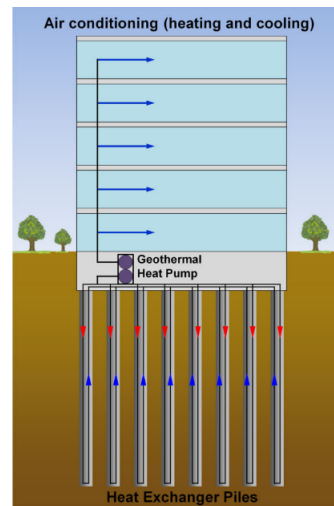


Figure 2.35: Building supported by energy piles (Olgun et al., 2015)

2.5.6. Energy piles

The system contains two parts of which one is the heating system in the building (secondary) and the other part is the pipe within the foundation pile (primary), see figure 2.35. Both parts are connected by a heat pump. The piles are either prefabricated driven piles or cast-in-place piles. The method of installation is influencing the conductivity of the soil, since for a soil displacement pile the conductivity of the soil along the pile will increase due to the densification. The depth of the energy piles is dependent on its structural function and not adjusted for its heat exchange function. Its cyclic loading is new for the industry and differs in the way that behaviour during design life should be incorporated, see figure 2.33. It demands a pile design that is capable of handling short-term and long-term temperature variation, 15-20 °C (GSHP Association, 2012). The variation in this temperature results in a change of axial stress and mobilized shaft resistance. The designer should also evaluate the live load such as freeze-thaw cycles in combination with other loads that could affect the piles capacity. Figure 2.36 shows the three designers that are responsible in the design process of an energy pile system and their responsibilities.

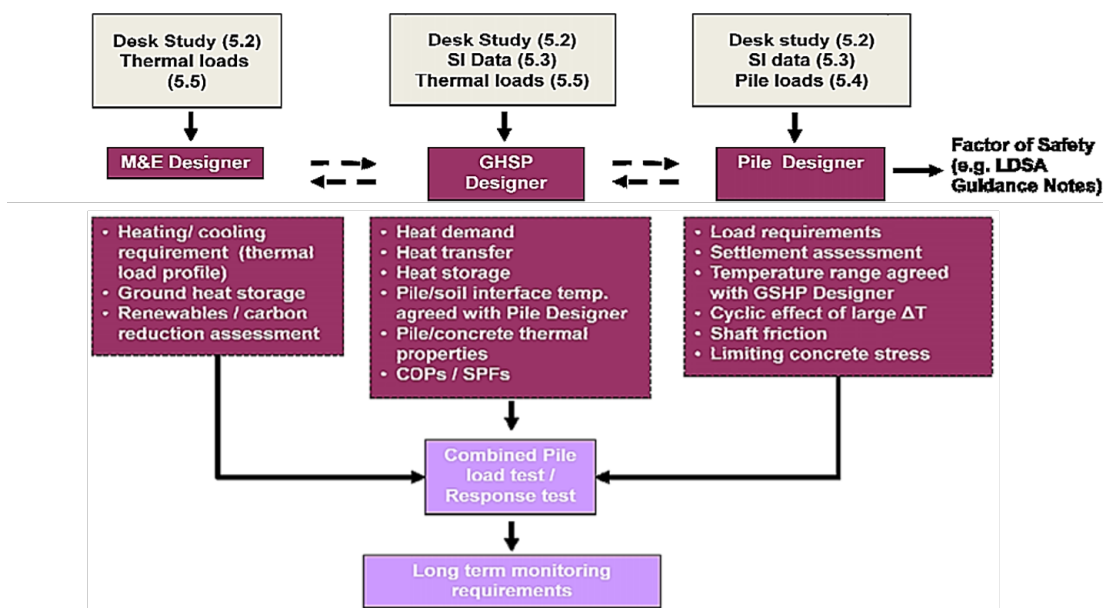


Figure 2.36: General energy pile design approach according to (GSHP Association, 2012)

Cyclic behaviour

The cyclic behaviour observed in energy piles is comparable with the behaviour of offshore structures under cyclic wave loading. The variation in axial pile loading is therefore investigated before (Sutman et al., 2019). The difference between the energy pile and a pile offshore is the deformation of the pile itself, since in offshore the pile as a whole moves, while the energy pile is cyclically loaded due to thermal expansion and contraction. Another difference is the frequency of the load, which is for energy piles daily and seasonal.

Existing guidelines

Guidelines for ground source heating systems developed already in the 80s in Austria, Germany and Switzerland (Sanner, 2017). Most consider horizontal and vertical BHE, but among those some also mention energy piles, even though the structural functionality is not assessed. It is important to bear in mind that each guideline is often meant for local climate and soil conditions. An overview of some guidelines with their important freezing remarks is shown below in table ???. Some precautionary measures mentioned are a temperature limit of the fluid, overdimensioning the piles and calculating the heat demand of a peak demand year. They are not all really cost attractive due to the extra material or loss in efficiency and they often miss a scientific basis. For more information on the development of guidelines the reader is referred to Sanner (2017).

Table 2.7: Existing guideline and their freezing remarks

Guidelines	Included	Freezing soil remarks
Netherlands		
TNO (2003)	Energy pile	$T_{fluid} > -2^{\circ}\text{C}$
ISSO-Publicatie 73 (2005)	BHE	$T_{fluid} > -3^{\circ}\text{C}$
BodemenergieNL	BHE	$T_{fluid} > -3^{\circ}\text{C}$
Germany		
VDI4640-1 (2010)	BHE	$T_{shaft} > 0^{\circ}\text{C}$
Sweden		
Normbrunn 16 (2016)	Deep BHE	Northern part Sweden $T_{fluid} < 0^{\circ}\text{C}$ allowed, rest is $T > 0^{\circ}\text{C}$
Austria		
ÖWAV RB 207 (2009)		
Spain		
UNE 100715-1 (2014)	BHE	$T_{fluid} > -2^{\circ}\text{C}$
United Kingdom		
MIS 3005 (2017)	BHE	$T_{fluid} > 0^{\circ}\text{C}$
GSHPA (2012)	BHE, Energy pile	$T_{shaft} > 0, T_{fluid} > 2$
Switzerland		
SN 546 384/6 (2010)	BHE	$T_{fluid} > 0^{\circ}\text{C}$ and $T_{shaft} > 0^{\circ}\text{C}$
USA and Canada		
NHBC (2010)	BHE	$T_{fluid} > 2^{\circ}\text{C}$
Europe		
CEN EN ISO 17628 (2015)	BHE	

2.6. Full-scale tests

The behaviour of energy piles is also studied in full-scale and laboratory environments. The tests are necessary to build confidence in the construction market, but also to allow validation for example energy pile simulations. Two well-known experimental full-scale tests are described below. The tests did not take place in soil conditions as in the Netherlands, but more in homogeneous stiff soils or piles founded on rock layers. They are used for many other projects due to the extensive data and literature that is available. The test were able capture certain phenomena related to the thermal cycles of an energy pile. The first study about the Lausanne pile considers an end-bearing pile, while the London variant is a floating pile in the stiff London clay. More information about the two famous tests is explained below.

2.6.1. Energy pile in Lausanne

At the Swiss Federal institute of Technology a full-scale experiment of an energy pile took place (Laloui et al., 2006). During this test the pile was subjected to thermal-mechanical loading. The objective of this test was to better understand the change in pile axial stress due to the thermal load applied on the pile. Several sensors measured the uplift, mobilization of the side friction and stress generated inside the pile, see figure 2.37 for soil profile and instrumentation of test pile. The tip of the pile reaches a rock layer, which makes this pile an end-bearing pile. Figure 2.38 shows the imposed cooling and heating cycle in ΔT to the pile, while a temperature of the ground of 15 °C is assumed and the mechanical load on top is constant at 1300 kN. The characteristics of the pile are mentioned in table 2.8.

Table 2.8: Pile characteristics Lausanne

	Length [m]	Diameter [mm]	Density [kg/m^3]	Stiffness E [MPa]
Pile	25.8	880	2500	29200

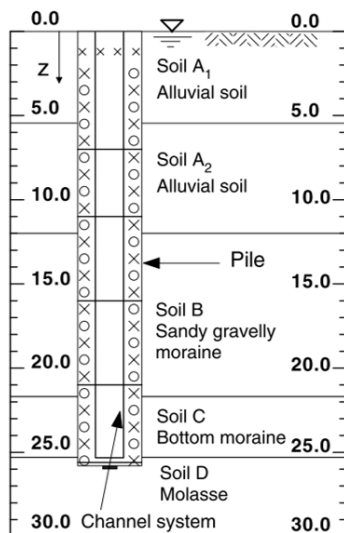


Figure 2.37: Soil profile test site Lausanne (Laloui et al., 2006)

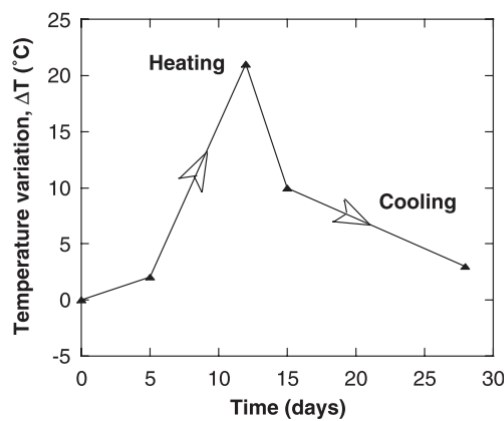


Figure 2.38: Thermal load on the pile with reference temperature of 15°C (Laloui et al., 2006)

In figure 2.39 and 2.40 the temperature after the heating-cooling cycle and the vertical stress in the pile is shown. For more test results the reader is referred to Laloui et al. (2006).

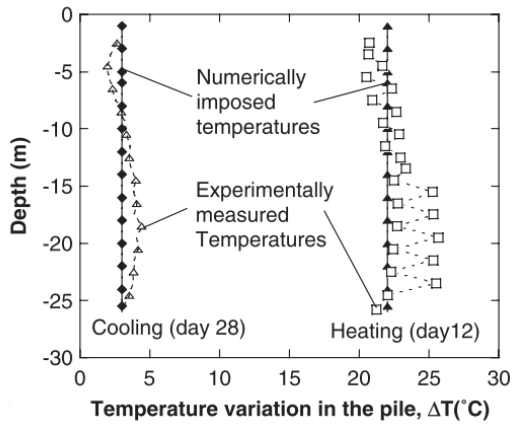


Figure 2.39: Temperature results of experimental pile Lausanne

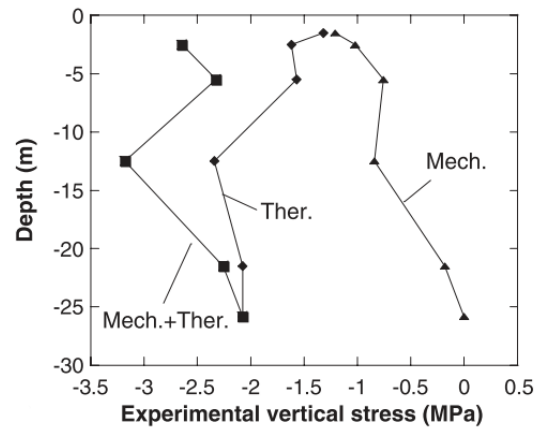


Figure 2.40: Vertical stress within pile

2.6.2. Energy pile in London

At Lambeth College in London an energy pile test is conducted over a period of seven weeks (Bourne-Webb et al., 2009). During this test the behaviour such as the concrete stress change of the pile in London stiff clay is observed. The pile obtains its bearing capacity mainly from the shaft resistance, which is different from the Lausanne pile as mentioned before. This resistance is considered high enough to handle the shear stresses mobilised at the soil-pile interface during the imposed thermal cycles, which also means that the affect on the capacity of the pile is rather low. In figure 2.41 the thermal load on the test pile is shown. The pile is also mechanical loaded with an initial loading test of 1800 kN, after which the pile is unloaded. Then during the cooling and heating cycle the pile has a constant head load of 1200 kN. Figure 2.42 and 2.43 show the axial load induced by the heating and by the cooling cycle.

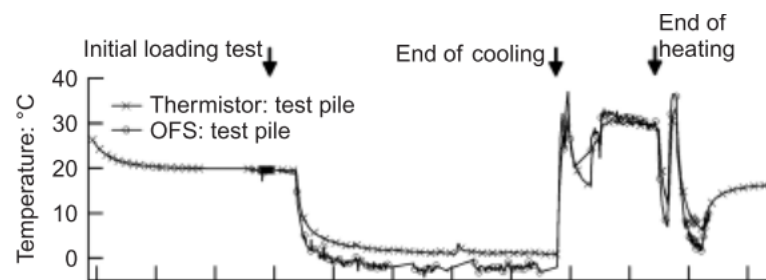


Figure 2.41: Imposed thermal cycle London energy pile

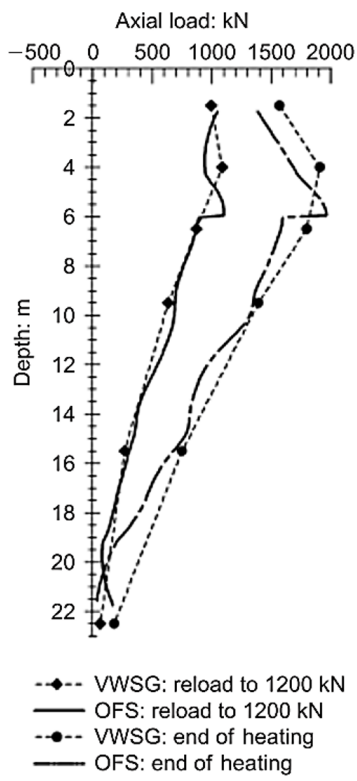


Figure 2.42: Axial heating load London energy pile. OFS (Optical Fibre Sensor) and VWSG (Vibrating-Wire Strain Gauges)

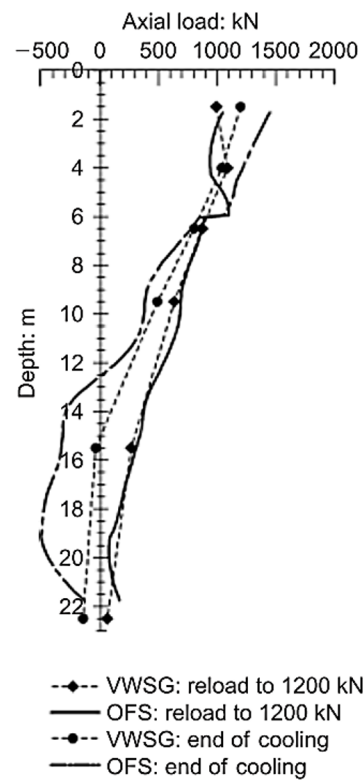


Figure 2.43: Axial cooling load London energy pile. OFS (Optical Fibre Sensor) and VWSG (Vibrating-Wire Strain Gauges)

2.7. Constitutive Modelling

Constitutive soil models aim to approximate real soil behaviour by describing the response during loading. For each situation one of the models is more appropriate than others, so their characteristics, e.g. limitations, have to be clear beforehand. An appropriate constitutive model will define at least how stresses and strains are related. This section describes the thermo-hydro-mechanical (THM) modelling of soil, particularly into the finite element program Plaxis 2D and its limitations with respect to freezing-thawing. Hereafter the Hardening Soil-Small (HSS) model is explained.

2.7.1. Thermo-Hydro-Mechanical coupling

To approach the multi-physical behaviour of soils around energy piles it is essential to use a THM model. Many interactions during thermal variations have to be considered, see figure 2.44 for an overview of phenomena when considering freezing-thawing. Many processes are influenced by each other. Examples mentioned are ice formation, latent heat, change in ice-water balance, unfrozen water in frozen soil, volume change due to ice formation and suction.

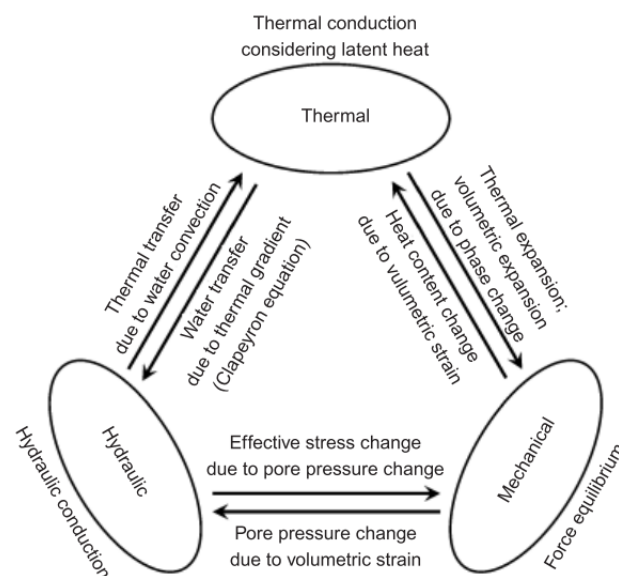


Figure 2.44: THM processes in frozen and unfrozen soils (Li et al., 2009)

The standard thermal add-on module of Plaxis without considering a constitutive model for frozen-unfrozen soil is not capable of investigating all processes. However, one important process that is captured, independent of the constitutive model, is the thermal expansion of water. The expansion is significant during phase change (Plaxis, 2015) and could result in variations in pore pressures and more plastic strains. In Aukenthaler et al. (2016) a user-defined soil model for Plaxis is introduced that is able to simulate the behaviour of frozen and unfrozen soils by including suction and temperature-dependent stiffness and strength. However, many parameters are necessary and their determination is cumbersome. So either quite a few guesses have to be made for the parameters or some processes are manually included, e.g. by extra construction phases. Table 2.9 shows the phenomena captured in the THM with a HSS model of Plaxis. In Appendix § D.2.5 an explanation is given on how some processes work in Plaxis fully-coupled THM model. About phase changing materials the Plaxis manual also warns in terms of numerical stability (Plaxis, 2019b):

"The heat transfer behaviour becomes highly nonlinear when phase change occurs. This high non-linearity may create numerical instability. To achieve convergence the number of iterations can be increased."

Table 2.9: Important modelling features in THM Plaxis with HSS model

Included in THM with HSS model	NOT included in THM with HSS model
Thermal dependent fluid and ice properties	Creep behaviour of frozen soils
Conductive and convective heat transfer	Thermal softening of soil
thermal expansion/contraction materials	Temperature dependent plastic yield functions
Latent heat	Temperature dependent expansion coefficients
SFCC curves	Cryogenic suction
Vapour diffusion (for unsaturated soils)	Adfreezing forces
Hysteresis	Change in stiffness and cohesion after cycles

2.7.2. Hardening Soil with Small-Strain

The most commonly used models are the Mohr-Coulomb (MC) and the Hardening Soil (HS) model. The MC model is often preferred for fast calculations, but it does not cover the behaviour of soils such as stress-dependent stiffness and irreversible strains during primary compression. The HS model, an elastoplastic model with isotropic hardening, takes this into account. An extension of this model, the Hardening Soil Small-Strain (HSS) model, goes even further by also considering the higher soil stiffness at very small strains, figure 2.45, and thereby also the simulation of hysteresis of soil. At very small shear strains the soil might behave as a linear elastic material and at increasing strains a non-linear decrease in stiffness is expected.

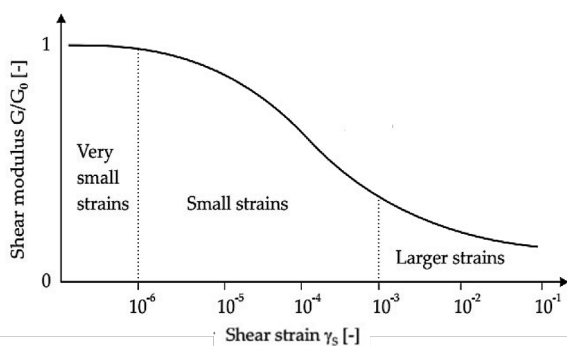


Figure 2.45: Stiffness-strain soil behavior (Skels and Bondars, 2017)

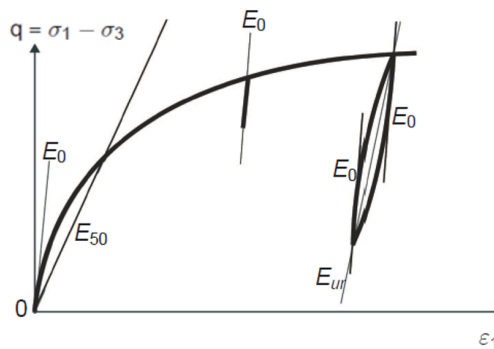


Figure 2.46: Stiffness parameters of HSS in a triaxial test (Brinkgreve et al., 2017)

Certain features in soil behaviour are important to address to simulate thermal cycles around a pile. In the first place the soil behaves in nature non-linear, which is captured by the HS model. However, due to the exposure to thermal cycles unloading-reloading behaviour is expected and the expansion coefficient are within the range of small to very small strain ranges, so the HSS model is recommended by Plaxis. One of the differences between the MC and the HSS model is the use of the parameters that describe its stiffness behaviour with secant stiffness E_{50} , tangent stiffness E_{oed} and unloading-reloading stiffness E_{ur} , see figure 2.46. Table 2.10 shows all parameters used and their derivation for in the HSS model.

Table 2.10: Required soil parameters HSS model

Parameter	Explanation	Derivation (Brinkgreve et al., 2017)
E_{oed}^{ref}	Tangent stiffness in oedometer test	$E_{oed}^{ref} = \frac{50000}{PI}$ [kPa]
E_{50}^{ref}	Secant stiffness in drained triaxial test	$E_{50}^{ref} = 2E_{oed}^{ref}$ [kPa]
E_{ur}^{ref}	Unload/reload stiffness in drained triaxial test	$E_{ur}^{ref} = 3E_{50}^{ref}$ [kPa]
G_0^{ref}	Shear modulus at very small strain range	$G_0^{ref} = (2.5 - 10) \times G_{ur}^{ref}$ or $G_0^{ref} = 33 \times \frac{(2.97-e)^2}{1+e}$ [kPa]
G_{ur}^{ref}	Unloading/reloading shear modulus	$G_{ur}^{ref} = \frac{E_{ur}^{ref}}{2(1+\nu_{ur})}$ [kPa]
ν_{ur}	Poisson's ratio for unloading/reloading	-
m	The rate of stress dependency of stiffness	0.5(sand) - 1.0(soft clay)
$\gamma_{0.7}$	Shear strain level at 72% of G_0	$(1 - 2) \times 10^{-4}$
p^{ref}	Reference stress level	Default set at 100 [kPa]

The unloading/reloading stiffness is considered elastic and for the first unloading cycle the same as the initial tangent modulus of the whole loading curve. By using a modulus reduction curve the HSS model in Plaxis is able to simulate hysteretic damping during cyclic loading, see figure 2.47 and 2.48 (Brinkgreve et al., 2007). It shows the degradation of shear stiffness with shear strain and as long as the G_{ur} is not reached during cycling the damping can increase. Higher value of cyclic shear strain is also related to a higher damping factor. However, the HSS model is not able to cover the accumulation of irreversible volumetric straining.

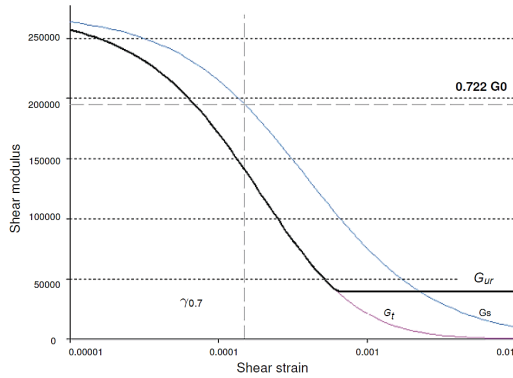


Figure 2.47: Reduction of the secant and tangent shear modulus in HS small (Brinkgreve et al., 2007)

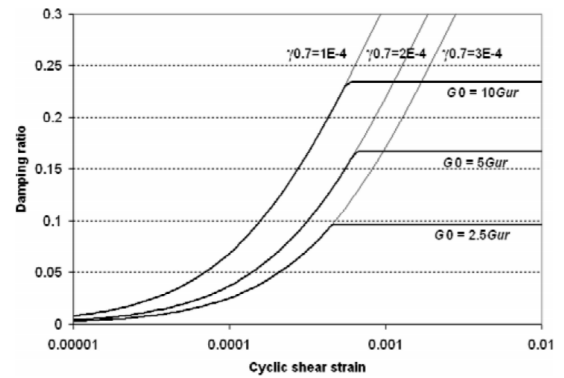


Figure 2.48: Damping ratio with cyclic shear strain (Brinkgreve et al., 2007)

2.8. Literature summary

The overview of the literature study is divided by soil-, pile- and interface behaviour. The last part of this section is dedicated to the expected implications and their influence on design.

2.8.1. Soil behaviour

Within the literature study several freezing and thawing consequences related to the physical, mechanical and hydraulic behaviour are reviewed. Table 2.11 gives an overview of those consequences. A subdivision is made on the state of the soil (i.e. frozen, thawed, multiple cycles) and the grain size as in fine or coarse.

Table 2.11: Soil behaviour during freezing, thawing and multiple cycles

Frozen soil		Thawed soil		Freeze-thaw cycles	
Fine	Coarse	Fine	Coarse	Fine	Coarse
(+) Pore pressure		(+) Excess pore pressure		(-) Cohesion	
(+) Void ratio		(-) Cohesion		(+) Plastic strains	
Cryogenic suction		(-) Void ratio		(-) Soil stiffness	
(-) Hydraulic conductivity		(+) Micro fissures		(-) Soil strength	
(+) Soil stiffness		(-) Soil stiffness		(-) Volume*	
(+) Thermal conductivity		(-) Soil strength			
(-) Heat capacity		(-) <i>Volume</i> ¹			
(+) Soil strength					
(+) Volume*					

¹ Volume change is dependent on permeability. Expansion happens if ice growth goes faster than drainage of the soil.

2.8.2. Pile behaviour

Table 2.12 shows most relevant factors related the behaviour of a pile foundation exposed to freezing and thawing conditions. The pile considered is fixed at the top and its tip is placed in a stiff sand layer.

Table 2.12: Pile behaviour during freezing, thawing and multiple cycles for a constrained pile

Freezing	Thawing	Freeze-thaw cycles
Contraction	Expansion	Ratcheting
Decrease in stress at head/tip	Increase in stress head/tip	Redistribution of stresses
Frost heave		Fatigue damage in concrete
Broken chemical bonds in concrete		

2.8.3. Visualisation of characteristics during non-isothermal conditions

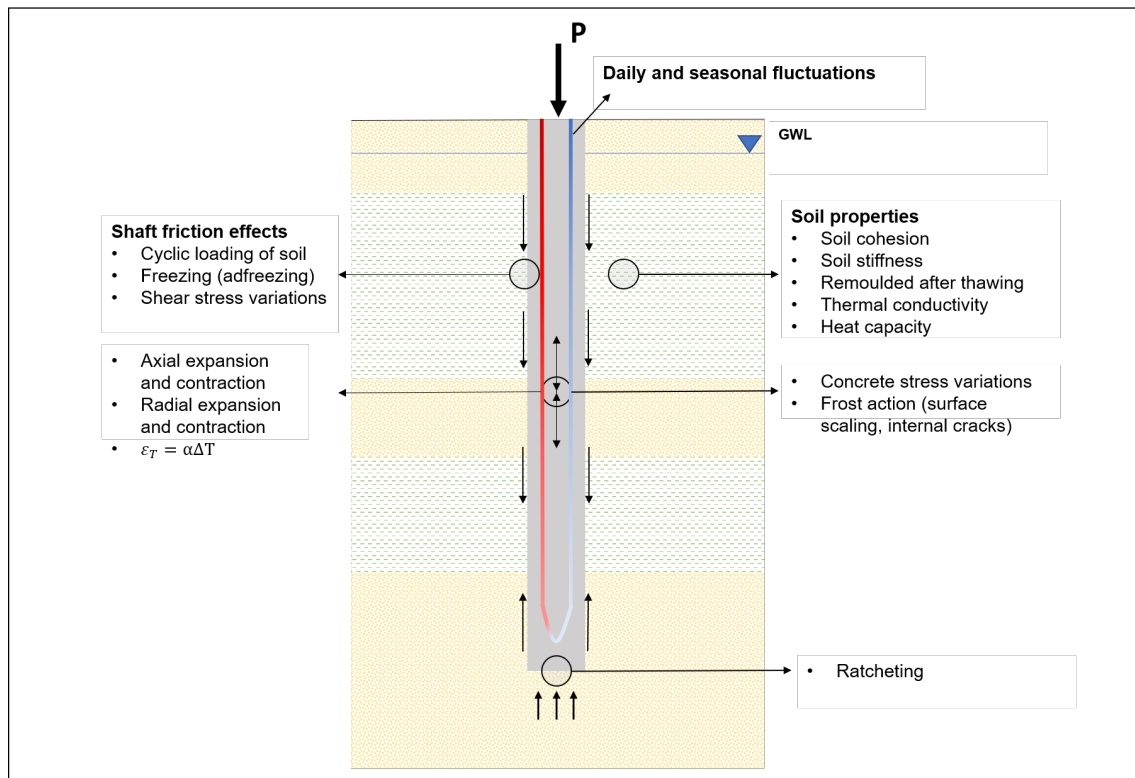


Figure 2.49: Visualisation of important pile and soil characteristics during non-isothermal conditions

2.8.4. Expected influence on settlements

During the operation of an energy pile many processes that affect the soil and pile take place due to its thermal variation. Understanding whether these affect the functioning of a pile positive or negative is important. So far the cyclic interactions are not fully understood and covered. In table 2.13 an overview is given of the effect of phenomena on the serviceability limit state (SLS). An example of freezing-thawing is the negative shaft resistance developed during thawing or the stresses developed by frost heaving forces during freezing. A check of the ultimate limit state (ULS) could be performed on the shaft behaviour, when fully mobilized the ultimate shaft resistance is reached. Furthermore, the ULS is reached when a settlement of $0.1D$ (10% pile diameter) occurs.

Table 2.13: Influence of freezing and thawing on the SLS

Phenomena	Potential result	Influence on SLS
Freezing		
Pile contraction	Tendency of downward movement	unfavourable
Ice formation	Increase in solid contact pressure	favourable
Increase in soil stiffness	Hardening of soil	favourable
Thawing		
Pile expansion	Upward movement	unfavourable
Thaw consolidation	Negative shaft resistance soft layers	unfavourable
Excess pore pressure	Decrease in effective stress	unfavourable
Freezing-thawing cycles		
Ratcheting	Permanent downward movement	unfavourable
Soil structure degradation	Softening of soil (remoulded character)	unfavourable
Decrease in soil cohesion	Loss of shear strength	unfavourable
Decrease in soil stiffness	Softening of soil	unfavourable

3

Thermal Analysis

An estimation of the amount of heat extraction until freezing around the pile is necessary for the geotechnical analysis of freezing-thawing soils. First an analytical solution is used to get an idea about the extraction. Hereafter, Comsol Multiphysics is used for the heat transfer in a pile group and around a single pile. This choice is based on the ease of implementing thermal boundaries in the model, the use of 3D analysis for pile groups and fluid pipes and the comparison of three methods to do temperature analyses, see appendix § C.3. The modules for heat transfer through porous media, heat transfer in pipes and Darcy's law are selected to simulate the physics, e.g. conduction and convection. It will not consider the mechanical and structural behaviour of the soil yet.

3.1. Analytical

The analytical solution in figure 3.1 could help to identify freezing at a certain distance of a thermal line source. The solution is evaluated for different initial soil temperatures and pile diameters. It does not account for freezing and thawing by means of latent heat. The result is based on a continuous extraction of 12 months and only conduction is considered. As is shown for the single piles used with a diameter of 0.4 m, temperatures below zero occur around 46 W/m continuous extraction for a year when considering an initial soil temperature T_0 of 12 °C.

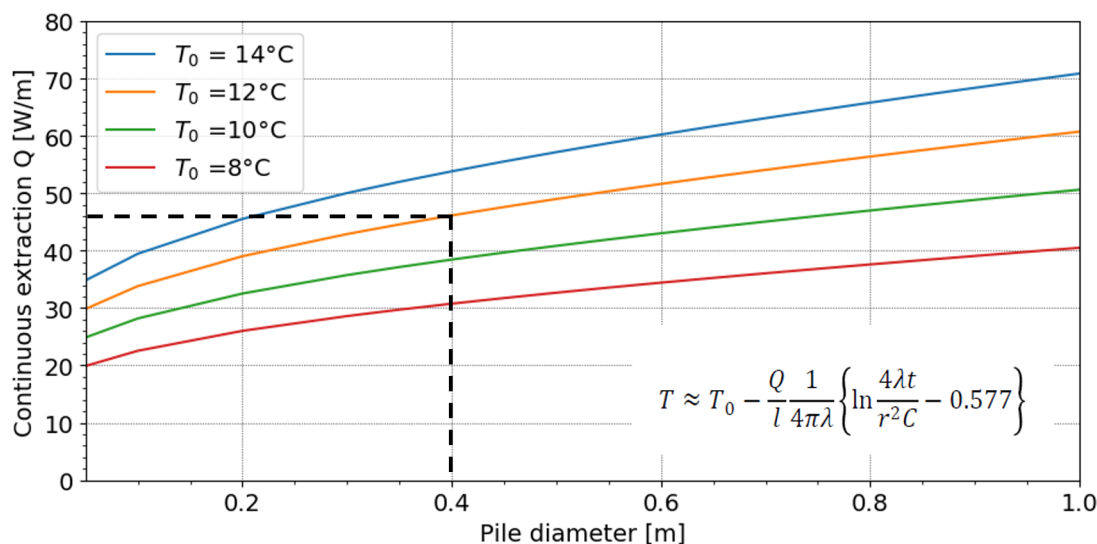


Figure 3.1: Freezing indication at the pile shaft based on 12 months of continuous extraction with $\lambda_{concrete} = 2.33$ W/(mK)

3.2. Pile group

The analytical indication did not include the group effect of thermal heat exchangers. A pile group model in Comsol can help to identify this difference. The heat transfer in porous media module is selected for the sand, clay and concrete domains. By setting a volume fraction of solids less than 1 it is possible to take the convection into account. The geometry and its top view based on the semidetached house in figure 3.5 is shown in figure 3.2. The domain size of the model is 60 m by 45 m with a depth of 22 m, which is considered large enough to ignore any boundary effects for the chosen time of extraction, see Appendix § C.3. The initial ground temperature is set at 12°C. The simplified soil stratigraphy is based on soil strata in the western part of the Netherlands with soft Holocene layers on top and a stiff Pleistocene sand layer as base. The piles are considered end-bearing at -16 m NAP in the so-called second sand layer.

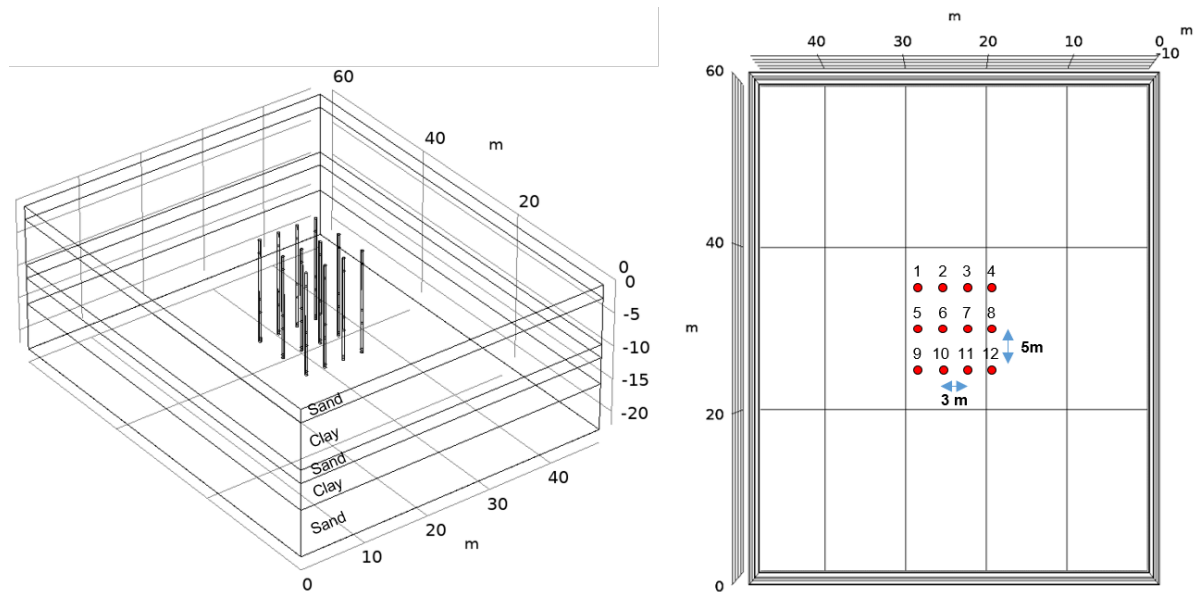


Figure 3.2: Geometry and top view Comsol pile group model

3.2.1. Boundary conditions

By setting a yearly temperature cycle at the top boundary the influence of the seasons is included, see figure 3.4. The other boundaries on the sides and bottom of the model are insulated, i.e. no heat flow across the boundary. The influence of this insulated condition and the corresponding domain size can be neglected as is shown in Appendix § C.3 in figure C.2 and C.3. All piles are activated as energy piles. The heat extraction by the fluid in the heat pipes is simplified by considering a heat flux on the surface of the piles, see figure 3.3.

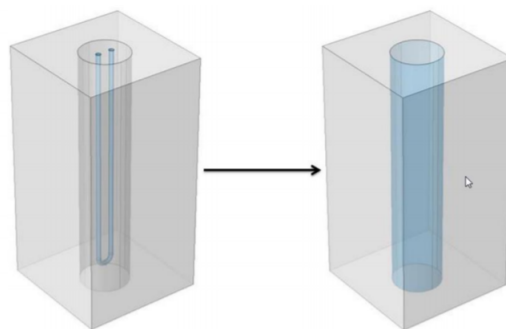


Figure 3.3: Simplified heat source Comsol 3D

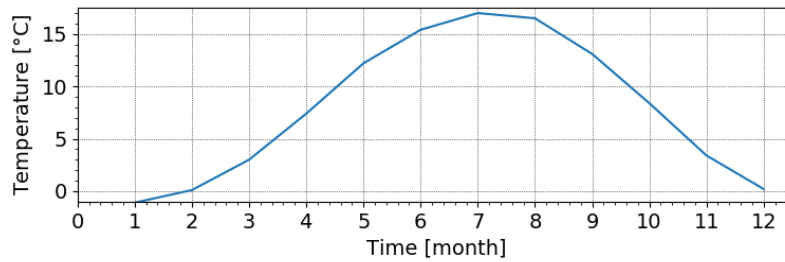


Figure 3.4: Thermal top boundary condition Comsol model

3.2.2. Heat demand

A realistic input can be acquired by taking the low temperature (35°C) heat demand of a household. The heat and cool demand data is provided by Witteveen+Bos and shows the characteristic values of half of the semidetached house shown in figure 3.5. The yearly low temperature heat demand is 20×10^3 MJ and cool demand is 2430 MJ. However, for the analysis the heat and cool demand are taken for the total semidetached house, i.e. 40×10^3 and 4860 MJ. The demand is divided over 12 months and in July and August only cooling takes place. The extraction distribution for half of the semidetached house based on a Dutch gas demand is depicted in figure 3.6 (CBS, 2016).

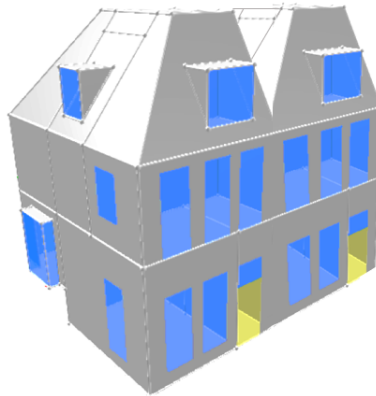


Figure 3.5: Semidetached house

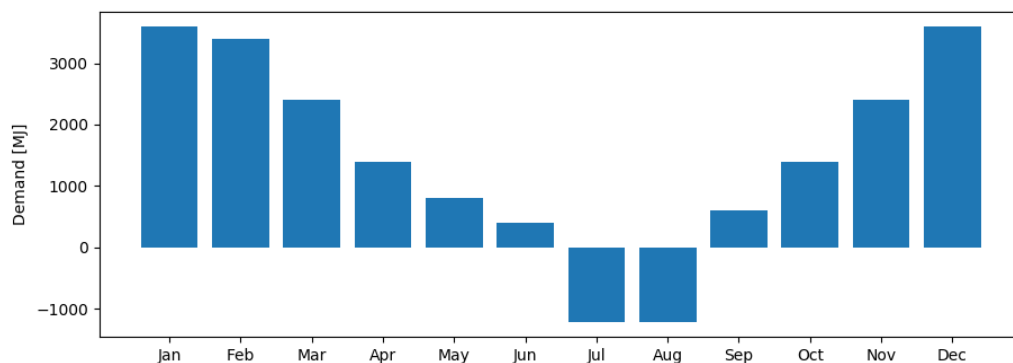


Figure 3.6: Monthly heat extraction based on gas demand (CBS, 2016)

3.2.3. Soil and pile properties

Table 3.1 gives an overview of the pile and soil properties used in the single pile model. It also indicates where the values are based on.

Table 3.1: Pile group parameters

Parameter	Value	Unit	Based on
Pile			
Foundation piles	12	-	Symmetric pile plan
Pile spacing x	3	m	Realistic spacing
Pile spacing y	5	m	Realistic spacing
Activated piles	10-12	-	Case 1 and 2
Diameter piles	0.4	m	Assumption on limit to fit in heat pipes
Length piles	16	m	1 m penetration in second sand layer
Soil			
Density sand	1900	kg/m^3	Table 2.b in (NEN, 2017)
Density clay	1750	kg/m^3	Table 2.b in (NEN, 2017)
Porosity sand	0.30	[-]	Assumption
Porosity clay	0.15	[-]	Assumption
Thermal conductivity sand	2.0	W/(mK)	Within range mentioned in Sanner et al. (2013)
Thermal conductivity clay	1.8	W/(mK)	Within range mentioned in Sanner et al. (2013)
Specific heat capacity sand c_p	800	J/(kgK)	Sanner et al. (2013)
Specific heat capacity clay c_p	875	J/(kgK)	Sanner et al. (2013)

3.2.4. Phase change

By enabling phase change in the soil domain the introduction of latent heat is possible around a specific freezing point. This will give a sort of extra capacity of the soil to transfer heat, but will also cause an abrupt change in specific heat. This will makes it hard to converge for the numerical model during the increase in energy by latent heat (334 kJ/kg). To overcome this sudden variation, the phase change is introduced over a temperature range, see figure 3.7. For the clay this range is larger (6°C) than for the sand (2°C) due to the freezing point depression for water in finer soils. Besides this difference the freezing point of clay is set at -3°C, while for sand it is -1°C. Important to mention that the freezing point in this figure has no specific physical meaning, it is just a point which helps to define the SFCC curve.

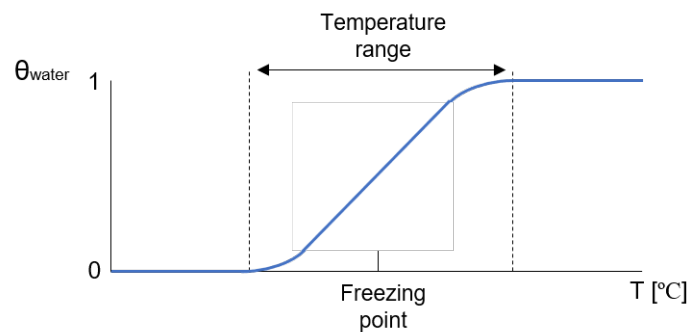


Figure 3.7: Smooth applied phase change of water

3.3. Results pile group

The model is able to determine the temperature evolution through the different types of soil. The most critical piles in the group are the two center piles, i.e. number 6 and 7. Figure 3.8 shows the temperature curves of the edges of pile 6 and 7 in the first clay layer. The computation comprises a seven years analysis. 1.0Q (7 W/m) stands for typical heat extraction from the model settings given in figure 3.6 and table 3.1. The increased heat demands are denoted by 1.5Q, 2.0Q and could contain a +sign to indicate that the model does not include

regeneration during the summer. Figure C.5 in Appendix § C.3 shows a 3D image to give the reader a better idea about the temperature state in the model after 7 years.

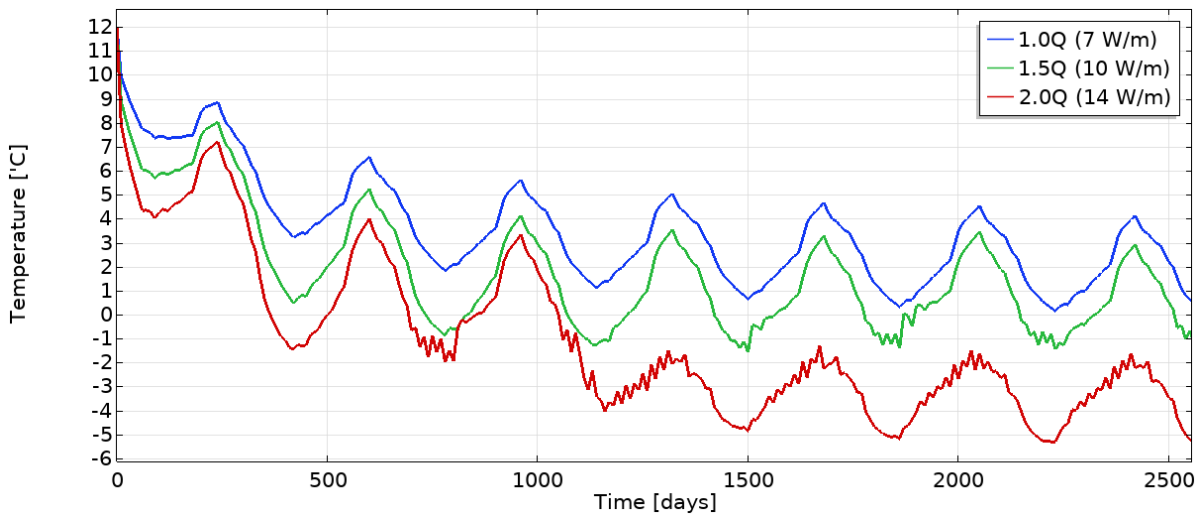


Figure 3.8: Average temperature at the pile edge of pile 6 in the first clay layer

The blue curve indicates that typical heat extraction in this pile group does not result in freezing circumstances at the center piles. Freezing conditions are reached at an increased extraction until an average of 10 W/m, i.e. 1.5Q. Although, the analytical approach for a simplified line solution gave a value of 46 W/m to reach freezing. This is mainly caused by the group influence and the more enhanced model. The introduction of latent heat in the clay layer when the temperatures are further reduced is visible by the fluctuations created by the numerical model. The cross section in figure 3.9 shows a slight reduction of the unfrozen water content around the pile at the clays layers.

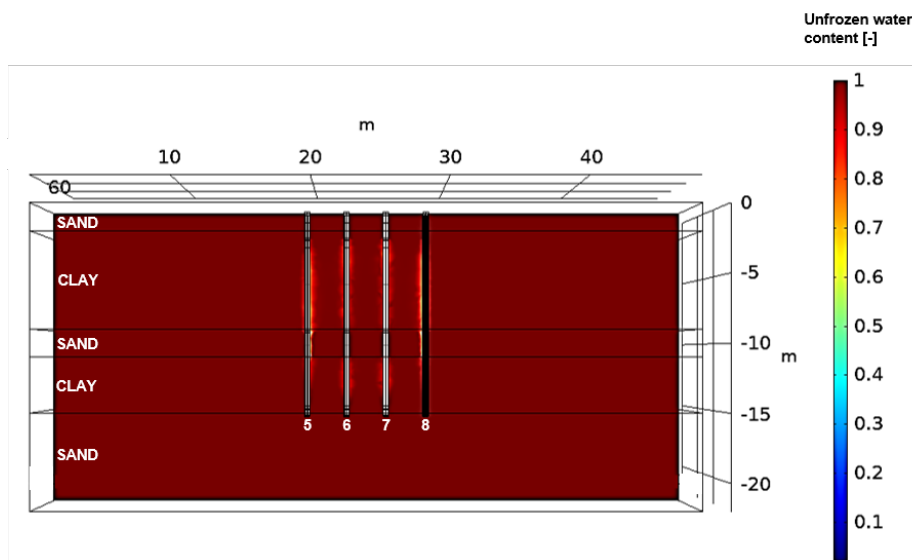


Figure 3.9: Phase indication with cross section through piles 5, 6, 7 and 8 at day 1850

3.4. Single pile

A single pile model is set up to get an idea about the temperature values for a single pile and if they correspond with the analytical solution. It will also give a better understanding about the thermal resistance of the concrete pile during the fluctuation of the fluid temperature. The soil stratigraphy, soil properties and boundary conditions are kept the same. However, in the pile group analysis the heat transfer pipe and concrete pile were considered as one cylindrical source with a heat flux on the surface, see figure 3.3 and in this single pile analysis the pipe with fluid flow is included.

3.4.1. Heat pipes

To be able to check the behaviour within the pile, a detailed analysis with a single pile is performed. As in equation 3.1 the energy exchange between the tubes and the surrounding concrete and soil can be calculated with extraction Q [W] as input and V_{fluid} as the volumetric flow rate [m^3/s].

$$T_{inlet} = T_{outlet} - \frac{Q}{\rho_{fluid} \times c_{fluid} \times V_{fluid}} \quad (3.1)$$

The amount of pipes, the location from the edge and the distance between the inlet and outlet pipe can be adjusted and are listed in table 3.2. See figure 3.10 with the embedded pipe and its temperature gradient between the inlet and outlet.

Table 3.2: Plastic pipe properties single pile analysis

Parameters	Value	Unit
Pipe length	15.5	m
Pipe diameter	30	mm
Pipe wall thickness	2	mm
Pipe separation	250	mm
Thermal conductivity	0.18	$W/(mK)$
Specific heat capacity	1470	$J/(kgK)$

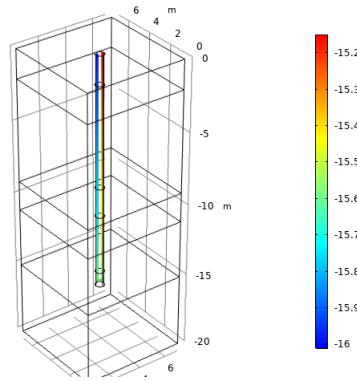


Figure 3.10: Temperature gradient within the fluid pipe

An anti-freeze solution is needed to prevent the freezing of the fluid in the pipe, but it should also have good thermal performance. The disadvantage is a increase in viscosity of the fluid, which is not in favor for the pumping power and thereby the overall systems efficiency. For the optimal heat transfer of the fluid in the pipes a low thermal resistivity between the fluid and the pipe surface is preferred. This is possible by making the flow between laminar and turbulent, i.e. transitional. Important to bear in mind that fluid flow within the pump should be laminar. For the transitional flow the Reynolds number Re has to be around 3500, it can be calculated according equation 3.2. In this case study a 35% monopropylene glycol solution is chosen with a freezing point at -15.5 °C. The parameters for a 35% monopropylene glycol solution are summarized in table

3.3. With the internal pipe diameter D equal to 26 mm this results in a average flow velocity v of 0.21 m/s and a flow rate of 0.11 l/s. Furthermore, ρ is the density of the fluid and μ is the dynamic viscosity.

$$Re = \frac{v \times D \times \rho}{\mu} \quad (3.2)$$

Table 3.3: Properties 35% monopropylene glycol solution at -10 °C

Parameters	Value	Unit
Density ρ	1043.9	kg/m^3
Dynamic viscosity μ	1.582×10^{-3}	$Pa \times s$
Thermal conductivity λ	0.398	$W/(m \times K)$
Heat capacity c	3713	$J/(kg \times K)$

3.4.2. Domain and mesh sensitivity

Three main domains are considered: the concrete pile, the embedded heat pipe as a single u-tube and the surrounding soil. The domain size influences the thermal results and its sensitivity is shown in figure 3.11a with the temperature results at the pile edge of four different domains after 1 year extraction of 30 W/m. The used soil properties are given in table 3.4.

Table 3.4: Soil properties sensitivity model

Properties	Unit	Concrete	Sand	Clay
Porosity	[-]	-	0.2	0.1
Specific heat capacity	[J/kgK]	800	850	700
Thermal conductivity	[W/mK]	2.33	2	1.8

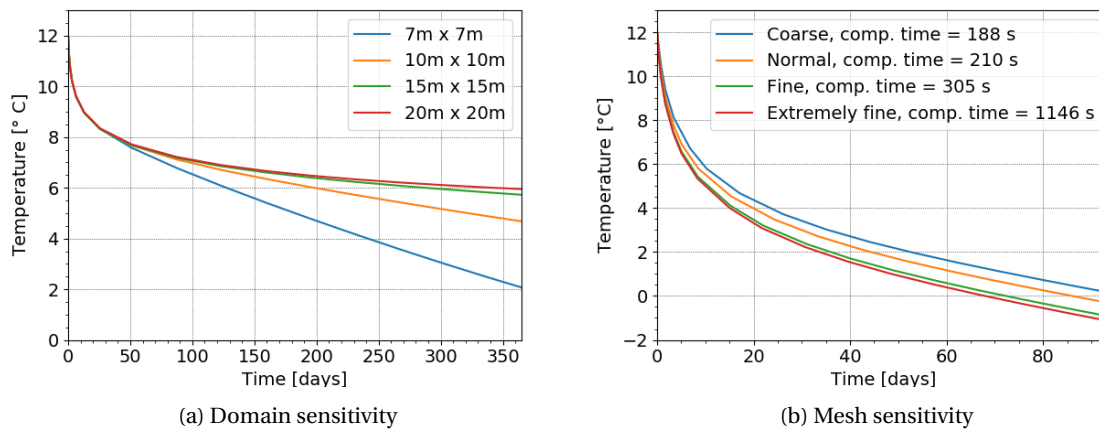


Figure 3.11: Temperature of pile edge

Also the mesh influences the results as is shown in figure 3.11b with in figure 3.12 the different meshes. The phase change is ignored and the heat extraction is constant at 60 W/m. The results are shown in terms of the average temperature at the pile shaft in the second layer and the amount time it took to compute. The curves indicate an equal temperature result. Although, the computing time for the coarse mesh (188 s) until the extremely fine mesh (1146 s) differs substantially. Based on these results and considering the increase in computation time for this simplified model, the fine mesh will be used in the single pile analysis.

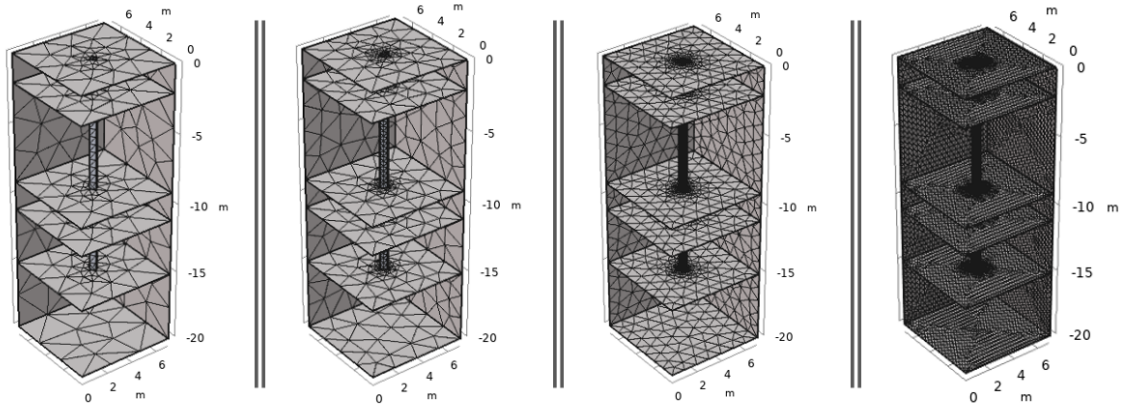


Figure 3.12: A coarse (4656 elements), normal (12669 elements), fine (106284 elements) and extremely fine (689454 elements) mesh

3.4.3. Heat demand

For the extraction values in the single pile analysis a daily cycle is introduced on the data by imposing a sinusoidal function on the average extraction with an amplitude of 4 W/m and a period of 24 hours. This will enable a more realistic fluctuation of the heat demand during the days as can be seen in the results below.

3.5. Results single pile

3.5.1. Fluid temperatures

The inlet fluid temperature and the difference between the inlet and the outlet is shown in figure 3.14 and 3.13. The difference between those curves is the energy that is extracted from the soil, which is similar as the heat demand at a specific hour. This can be checked with equation 3.1. In case of three times the heat extraction (21 W/m) subzero fluid temperatures of -4 are generated in the end of the year.

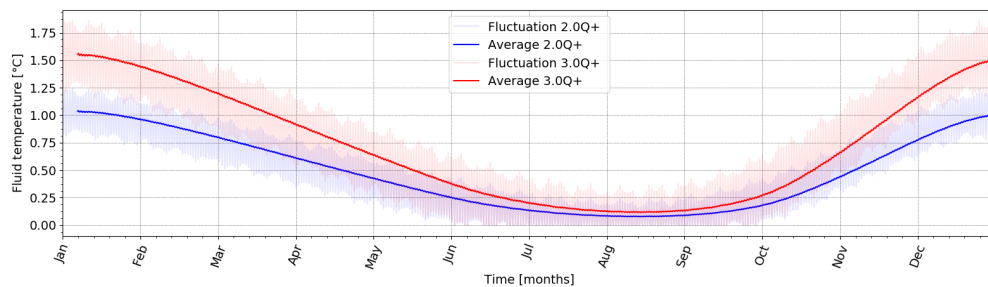


Figure 3.13: Fluid temperature difference outlet-inlet during typical heat extraction

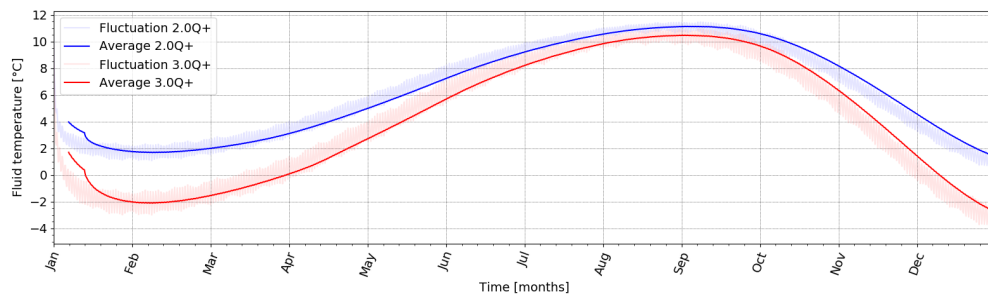


Figure 3.14: Fluid inlet temperature

3.5.2. Temperature of the pile

The results of 1 year two and three times typical extraction without regeneration (2.0Q+ and 3.0Q+) are shown below in figure 3.15 and 3.16. The daily and seasonal cycle are clearly visible in the temperatures. Thereby freezing conditions are not reached in both cases at the edge of the pile. This indicates the influence of a pile group compared with a single pile. Even with the temperature of the fluid reaching -4, the pile edges in the sand and remain unfrozen.

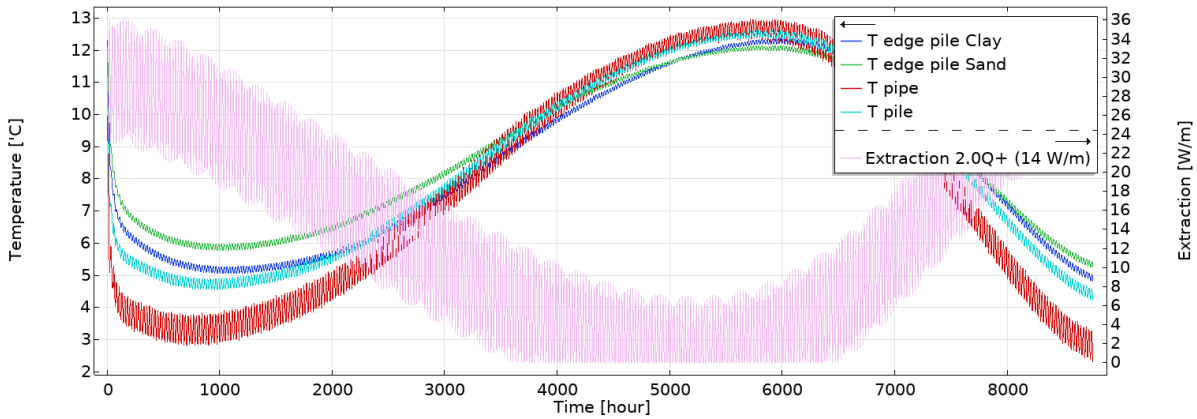


Figure 3.15: Temperature evolution at different parts of the single pile analysis during increased heat extraction

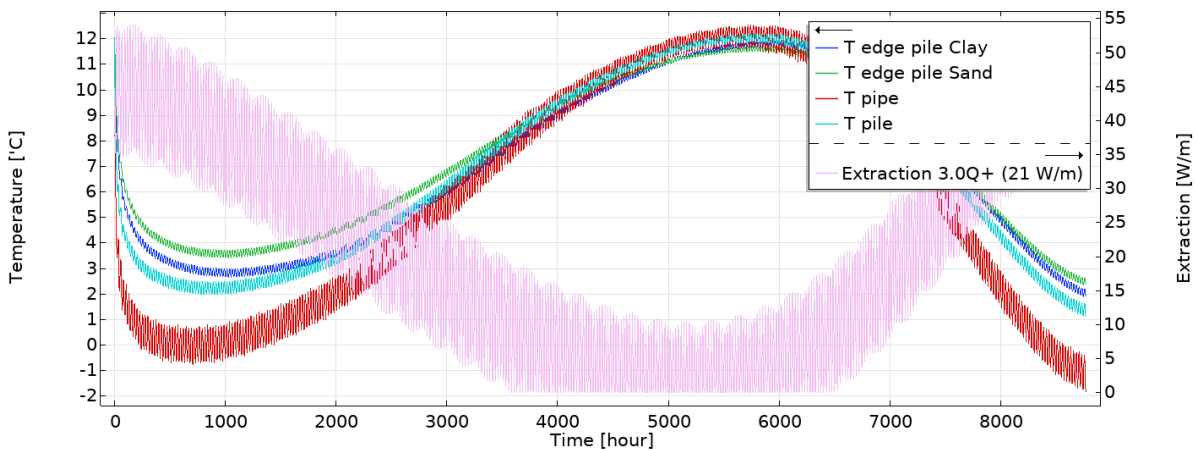


Figure 3.16: Temperature evolution at different parts of the single pile analysis during increased heat extraction

3.6. Discussion

The analytical solution gives an approximation for the extraction amounts necessary to reach 0 °C at a certain distance from a line source. However, only conduction and no latent heat of fusion is considered. For 1 year continuous extraction with a pile diameter of 0.4 m and an initial temperature of 12 °C a value of 46 W/m is found.

Freezing is allowed in the pile group analysis to take advantage of the extra capacity offered by the latent heat of fusion. The analysis resulted in a freezing situation along the most critical piles (6, 7) edge during an increased extraction of 1.5 times the typical extraction Q, i.e. 10 W/m. The value represents an average year extraction, so it includes the regeneration in the summer. The interaction between the piles is taken into account, but no quantification of this influence can be concluded from the results.

The more detailed single pile analysis with fluid pipes indicates the damping characteristic of the concrete by damping the temperature fluctuation of the fluid. A fluctuation of approximately 0.3 °C is found at the edge, while the pipe has a value of 1.5°C with this specific pipe configuration. The extraction until freezing does not take into account the group effect. The fluid temperature is also measured at the inlet and outlet of the pipe. The extraction of three times the typical extraction and no regeneration 3.0Q+ (21 W/m) results in

subzero fluid temperatures of $-4\text{ }^{\circ}\text{C}$. The maximum fluid temperature difference with this extraction is $1.75\text{ }^{\circ}\text{C}$. A change in temperature gradient at freezing point is visible as freezing occurs, explained by the introduction of latent heat. The heat extraction is not effected constant, which makes the phase transition beneficial.

4

Validation and understanding THM module

Ideally the thermal and geotechnical behaviour would be validated by comparing the temperatures and stresses with sensors around the specific energy pile. Unfortunately, this data is not available yet for a freezing-thawing situation. Therefore, the two case studies described in the literature study are selected to validate and understand the axisymmetric THM model in Plaxis without freezing. The soil layers differ in these two cases, which makes the London pile a floating pile, while the Lausanne pile is considered as an end-bearing pile. The heat pipes within the pile are not modelled, only a thermal boundary is applied at shaft of the concrete volume element.

4.1. London pile

The pile is subjected to a cooling and heating cycle. A static load of 1200 kN was applied at the top of the pile (Bourne-Webb et al., 2009). In figure 4.1 the imposed prescribed temperature scheme is shown and in figure 4.2a the axisymmetric model with a refined mesh around the pile is depicted. The initial temperature is 20 °C and the groundwater table is found at 3 m below ground level. The pile has a diameter of 550 mm and a length of 23 m.

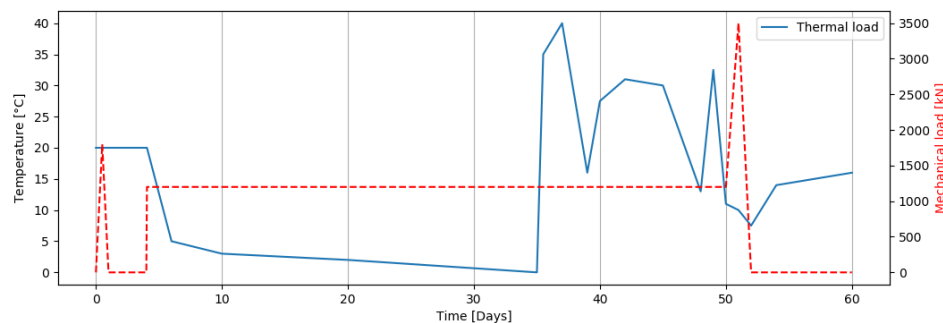


Figure 4.1: Thermal and mechanical loading scheme London pile

4.1.1. Model settings

The thermal line source is applied as temperature boundary at the pile surface. The axisymmetric boundary is closed for heat transfer, while a constant temperature of 20 °C is applied at the bottom, top and right boundary. The soil and concrete properties used in the numerical model can be found in Appendix § E.2. For the London clay an overconsolidation ratio (OCR) of 15 is used. The concrete pile is simulated as a linear-elastic material, the made ground as MC model, London clay and the terrace deposits as the HSS model. Furthermore, the interface reduction factor R_{inter} is set at 1 and 0.67 to cover a range of soil-pile interface behaviour.

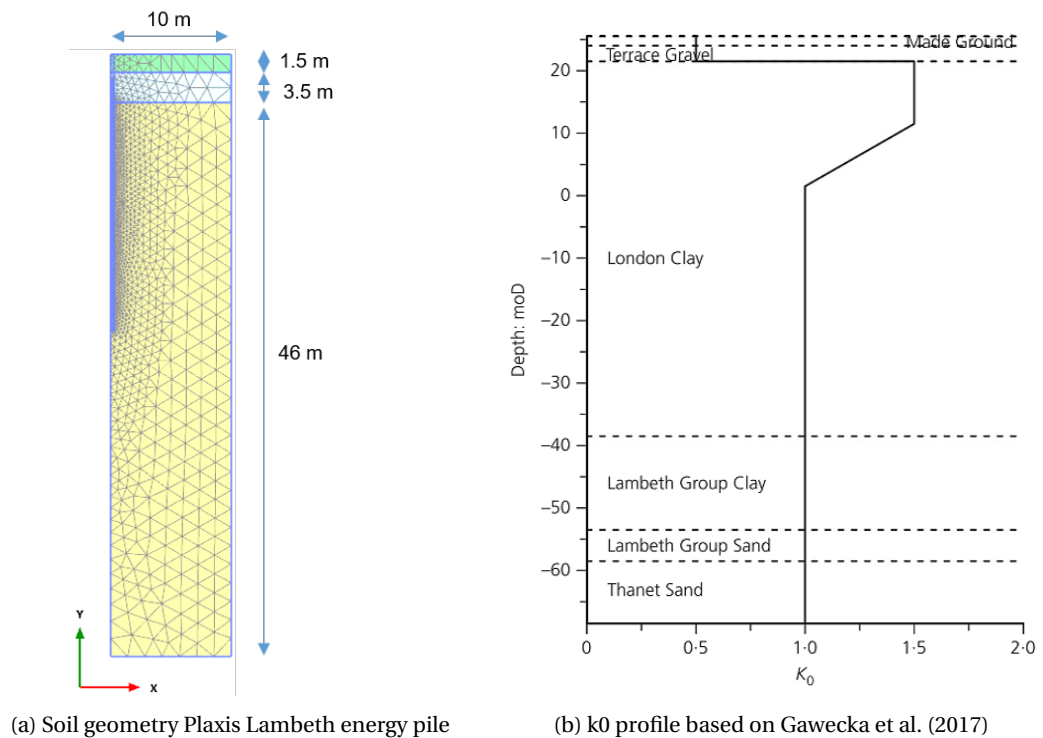


Figure 4.2: Characteristics model London energy pile

4.1.2. Construction phases

The following phases are considered:

1. Initial phase - k_0 procedure.
2. Pile washed in-place with soil temperature at 20 °C - plastic
3. Initial static load test 1800 kN - plastic
4. Unloading - plastic
5. Cooling with constant load 1200 kN at day 4 - fully coupled flow-deformation
6. Heating with constant load 1200 kN at day 35 - fully coupled flow-deformation
7. Variable cycle with constant load 1200 kN at day 46 - fully coupled flow-deformation
8. Load test 3500 kN - fully coupled flow-deformation
9. Heating until final day 62 without load - fully coupled flow-deformation

4.1.3. Results

The results are compared with the experimental outcome, see figure 4.3a and 4.3b. The first figure shows the vertical head displacement, which is mainly a result of pile deformation due to its expansion and contraction. The simulation is done for an interface reduction R_{inter} value between 0.67 and 1.0, for a bored pile a value of 0.67 is recommended by Plaxis. The results of the full-scale test and the numerical results agree over time, but a slight difference is found between day 30 and day 40. The sharp settlement of the test is the result of a steep cooling curve during these days. The pile in the Plaxis model behaves much stiffer during this cooling time compared with the full-scale test. In figure 4.3b the thermal distribution is evaluated at 0.5 m distance from the pile 9 m below ground level. The numerical result shows a similar trend, but still too much difference to validate the temperature distribution. This may be due to anisotropic soil properties, the ground water flow characteristic or another input problem. Also the use of a constant temperature boundary of 20 °C will have some impact.

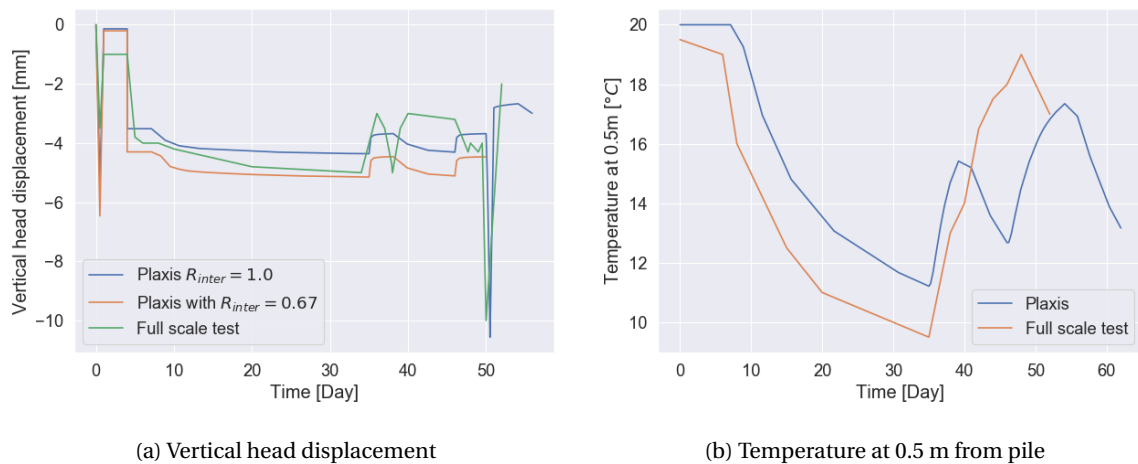


Figure 4.3: Results London pile

4.2. Lausanne pile

This end-bearing pile is subjected to the thermal load depicted in figure 4.4. In this case no mechanical load is applied on the pile, which allows the pile to change volume mainly in the upward direction. For more information about this in-situ test the reader is referred to Laloui et al. (2006), wherein also a numerical model is described.

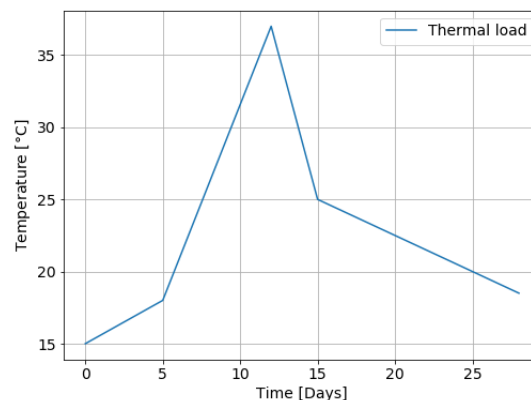


Figure 4.4: Thermal loading scheme Lausanne pile

4.2.1. Model settings

The geometry of the model is shown in figure 4.5a. The parameters of the pile and soil layers used in Plaxis are summarized in Appendix §E.2. The initial temperature is 15 °C and the groundwater level is set at the top. The thermal boundaries are closed except for the top boundary with a constant temperature of 15 °C and the thermal load, which is applied on the soil-pile interface. The bedrock is a sandstone, which is like the concrete pile modelled as a linear elastic material. The MC model is used for the other layers since these parameters are known and also used in the model of Laloui et al. (2006).

4.2.2. Construction phases

The following phases are considered:

1. Initial phase - k0 procedure.
2. Pile washed in-place - plastic
3. Thermal load - fully coupled flow-deformation

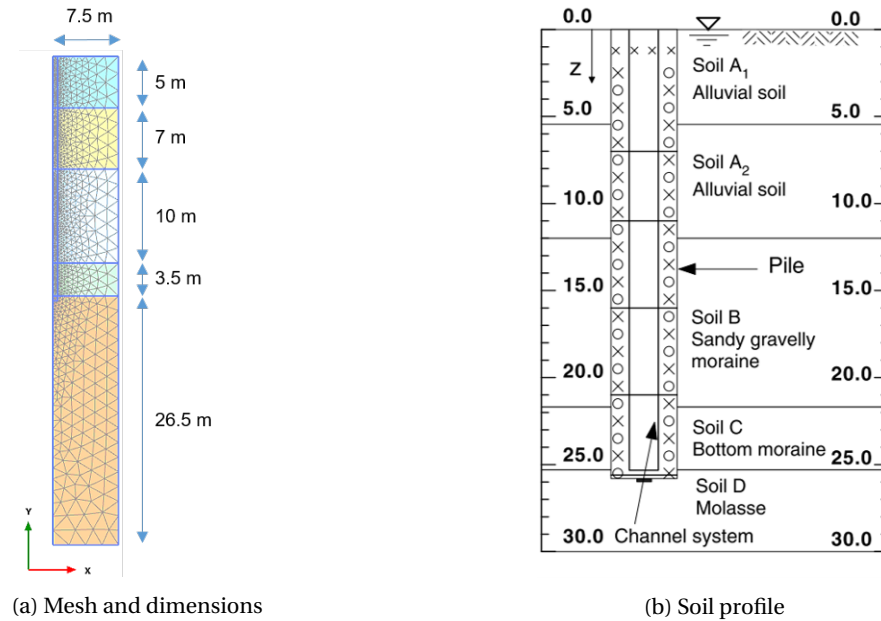
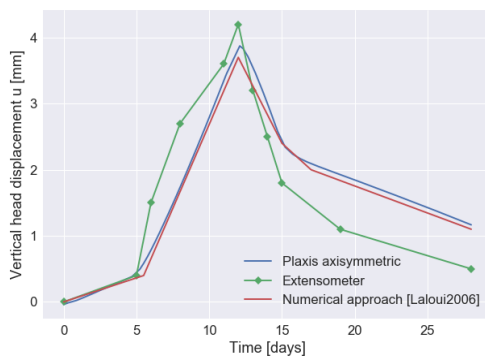


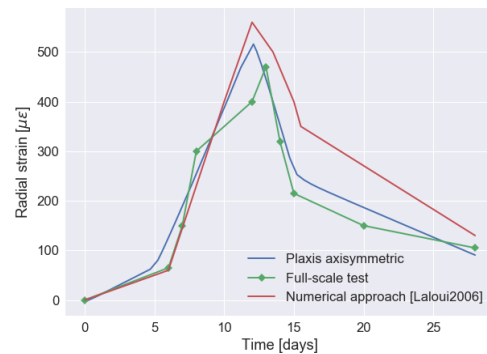
Figure 4.5: Characteristics Lausanne energy pile

4.2.3. Results

In figure 4.6a and 4.6b the results of the full scale test, the coupled multi-physical finite element approach of Laloui et al. (2006) and the Plaxis results are compared. No significant tip displacement is expected due to the stiff rock layer, but rather the pile deformation due to temperature change is computed. The first graph shows the vertical head displacement during the heating-cooling or expansion-contraction cycle. The other graph shown the expansion of the pile in radial direction, this also corresponds quite well with the measured values. The results almost coincide with each other, which confirms the working of the THM module in terms of volumetric changes of materials and their related stresses and strains.



(a) Vertical head displacement during thermal loading



(b) Change in radial strain at -16 m during thermal loading

4.3. Concluding remarks

The results of the floating pile (London) in a stiff clay layer and the end-bearing pile (Lausanne) are both simulated in an axisymmetric model with the THM module of Plaxis. Both piles show a similar trend in the vertical head displacement compared with their full scale measurement data. This displacement is mainly caused by the deformation of the piles during the thermal fluctuations. For the temperature distribution slightly different results were computed, which is probably caused by the assumptions for the thermal boundaries and the difference in thermal properties in the full-scale test compared with the input for the model. Freezing behaviour in the module is also not validated, but the trend in soil and pile behaviour during thermal variations is clarified.

5

Geotechnical THM analysis

Within this chapter the geotechnical behaviour of a pile during freezing-thawing cycles is analysed with the fully-coupled THM module together with the Hardening Soil with Small-Strain (HSS) model. This will help to understand the pile behaviour when exposed to thermal volume changes and resulting plastic deformations in a Dutch soil condition with an end-bearing pile. Two situations are distinguished: situation 1 with neutral plane at the top of the pile, i.e. all positive skin friction along the shaft, and situation 2 with neutral plane at the top of the first sand layer and above fully mobilized negative shaft resistance. The latter situation includes the negative skin friction as is mentioned in NEN (2017). In the results the changes in volumetric strains, excess pore pressures, vertical displacement of the pile head, shear stress along the shaft and axial stress in the pile are visualized during non-isothermal conditions. The thermal results until a freezing situation from chapter 3 are used to ensure that freezing-thawing situations along the edge of the pile occur.

5.1. Model settings

The model is axisymmetric with a radius of 15 m. The soil parameters are based on Dutch soil layers from the North-South metro line project in Amsterdam, see Appendix F with red marked layers. Furthermore, the groundwater level (GWL) is constant at -0.5 m NAP. The pile is simulated as a volume element, this replaces the soil with pile material, i.e. wished in-place. A service load is applied on top of the pile and its base is placed 1 m deep in a stiff sand layer. The displacement boundary conditions are set as follows: the symmetry axis and the right boundary are horizontally fixed, while the bottom is fully fixed and the top is free to move in all directions, see figure 5.1. The fluid pipes are simplified and modelled as a heat flux boundary at the soil-pile interface. This thermal boundary begins 0.1 m below surface level and ends 0.5 m above the tip of the pile. This choice is based on current pipe settings, but pipe might go deeper to increase heat extraction potential. The thermal boundary at the symmetry axis is closed, while at the bottom and right axis the boundary is set at a constant soil temperature of 12 °C. The thermal boundary at the top of the model simulates a yearly temperature cycle similar as in figure 3.4. The groundwater flow is closed at the symmetry axis and open for other boundaries. For the concrete pile a linear-elastic (LE) model is used. The drainage conditions of the pile are set as non-porous, for the sands drained and for the clays undrained. The mesh is made with 15 noded triangular elements and is refined as much as possible at the soil-pile interface to cope with the numerical instability in case of phase changing materials. A vertical line is introduced in the model at 0.3 m from the pile to have an extra refinement in the vicinity of the pile. The rest of the model is set at a course mesh size to reduce the computation time.

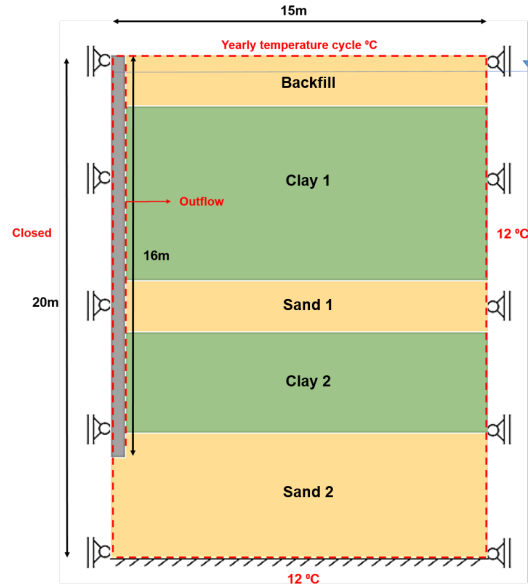


Figure 5.1: Modelling domain with thermal and displacement boundary conditions

5.1.1. Soil-pile interface

Interface elements are used to simulate the soil-pile behaviour by allowing relative displacements as slipping or gapping. The interface consist out of node pairs which interact as a linear elastic-perfectly plastic spring. The elastic and plastic state are given by equation 5.1 and 5.2.

$$|\tau| < -\sigma_n \times \tan(\phi_{interface}) + c_{interface} \quad (5.1)$$

$$|\tau| = -\sigma_n \times \tan(\phi_{interface}) + c_{interface} \quad (5.2)$$

It is defined by R_{inter} and relates the shear strength of the interface to the soil (Plaxis, 2019a). The value of R_{inter} lies between 1 and 0, respectively fully able to transfer shear stress and zero transfer of shear stress. Hence adjusting R_{inter} gives a reduced interface friction and cohesion. In this study a bored pile is considered and according to the Plaxis manual a value of 0.67 can be taken for R_{inter} .

5.1.2. Dilatancy cut-off parameters soil

The soil will reach its critical density due to unloading-reloading. Therefore it is necessary to include a dilatancy cut-off in the HSS model when the maximum void ratio is reached, see figure 5.2. The minimum, initial and maximum void ratio are asked as input for each material. In case of extreme dilation in the model during shearing a cut-off is activated at the decided value of the maximum void ratio. Otherwise the soil will continue dilation when shear deformations occur. The initial void ratio e_0 for the first and second sand layer are 0.5 and 0.4 respectively. It is further assumed that the minimum e_{min} value is 0.35 and maximum e_{max} is 0.9.

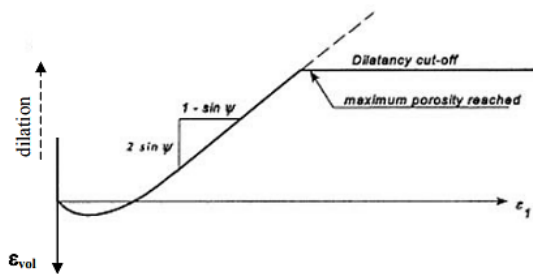


Figure 5.2: Dilatancy cut-off in drained triaxial test (Plaxis, 2019b)

5.1.3. Thermal properties

It is important to know if the thermal input considers the whole medium or only the solid parts. Plaxis uses geometric means over the soil, water and ice content to compute the overall thermal properties. The following thermal material properties are asked (Plaxis, 2019b):

Table 5.1: Thermal soil parameters asked in Plaxis

Property	Symbol	Unit	Explanation
Thermal conductivity	λ_s	W/mK	Thermal conductivity of a solid material
Specific heat capacity	c_s	J/kgK	Specific heat capacity of a solid material
Solid thermal expansion	$\alpha_{v,x,y,z}$	[-]	Total soil volume change either in all directions v or in an anisotropic direction x,y,z
Vapour diffusion coefficient	D_v	[-]	Controls the diffusion in a medium. When zero no mass flux of vapour will happen
Thermal diffusion enhancement factor	f_{Tv}	[-]	Influences of temperature on the heat flux of vapour.

Table 5.2 shows the thermal and hydraulic properties used in this study. The hydraulic conductivity is taken from the North-South line data in Appendix F) and the thermal parameters are taken within the ranges mentioned in literature. Important to mention that they are not the same as in the thermal analysis in chapter 3. The heat flux is a stepwise function from the thermal analysis and represents an excessive heat extraction to induce freezing-thawing, see figure 5.4. The extraction is considered negative. Figure 5.3 shows the two soil freezing characteristic curves (SFCC). This is an assumption and as described earlier dependent on many variables, e.g. pressure, salinity.

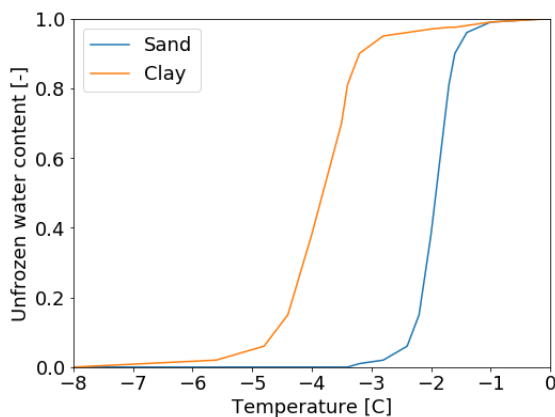


Figure 5.3: Soil freezing characteristic curve (SFCC) for sand and clay

Table 5.2: Thermal and hydraulic soil properties

Parameter	unit	Pile	Backfill	Clay 1	Clay 2	Sand 2	Sand 3
k_x	m/s	-	1.0×10^{-5}	1.0×10^{-4}	1.0×10^{-10}	1.5×10^{-4}	1.0×10^{-4}
k_y	m/s	-	1.0×10^{-5}	1.0×10^{-4}	1.0×10^{-10}	1.5×10^{-4}	1.0×10^{-4}
c_s	J/kgK	800	850	878	878	800	800
λ	W/mK	2.3	2.0	1.8	1.8	2.0	2.0
α_s	1/K	8.5×10^{-6}	1.7×10^{-5}	1.7×10^{-5}	1.7×10^{-5}	1.5×10^{-5}	1.5×10^{-5}

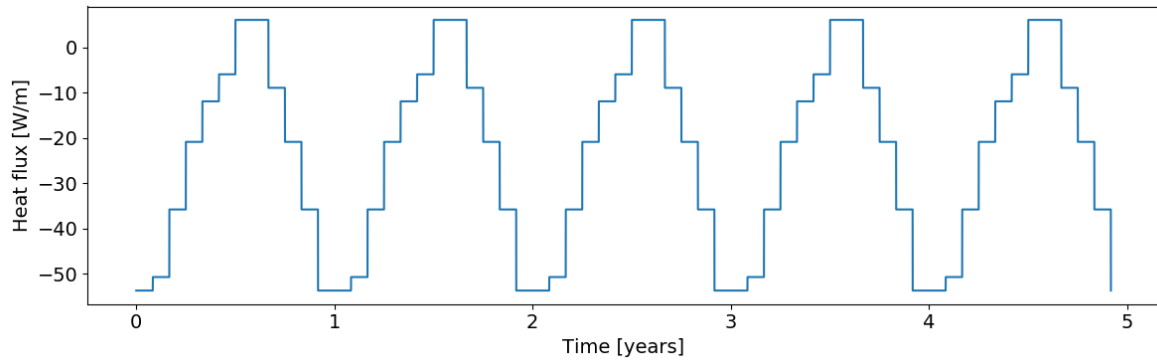


Figure 5.4: Heat flux boundary at edge of pile

5.1.4. Mechanical properties

Two types of material models are used, a linear-elastic (LE) model for the concrete pile and a more advanced HSS model for the soil layers. The HSS parameters in table 5.3 are based on the red marked soil layers of the North-South line project in appendix F and the small strain parameters are chosen within the range presented in table 2.10.

Table 5.3: Mechanical soil properties

Parameter	unit	Pile	Backfill	Clay 1	Clay 2	Sand 1	Sand 2
Model	-	LE	HSS	HSS	HSS	HSS	HSS
γ_{sat}	kN/m^3	24	18.4	16.9	18.5	20	20
E_{50}^{ref}	kN/m^2	-	20×10^3	10×10^3	8400	40×10^3	35×10^3
E_{oed}^{ref}	kN/m^2	-	20×10^3	5×10^3	3500	30×10^3	35×10^3
E_{ur}^{ref}	kN/m^2	-	60×10^3	25×10^3	36×10^3	200×10^3	190×10^3
m	-	-	0.8	0.8	0.8	0.5	0.5
G_0^{ref}	-	-	100×10^3	24×10^3	24×10^3	120×10^3	120×10^3
p^{ref}	kN/m^2	-	100	100	100	100	100
$\gamma_{0.7}$	-	-	1.0×10^{-4}				
E	kN/m^2	30×10^6	-	-	-	-	-
ν'	-	0.2	0.2	0.2	0.2	0.2	0.2
c_{ref}	kPa	-	0	6	0	0	0
ϕ_i	°	-	30	26	32	33	35
Ψ	°	-	2	0	0	3	5
ρ	kg/m^3	2500	2500	2500	2600	2600	2600

5.1.5. Service load

D-foundations is used to determine the bearing capacity of the pile before thermal loads are activated and to check if the values found in Plaxis are in the same order. In the first situation the top of the positive shaft friction and the bottom of the negative shaft friction are set at surface level, so no negative shaft friction is considered. For the second situation the top of the positive shaft friction and the bottom of the negative shaft friction are set at -9 m. D-foundations gives the tip, the positive and negative shaft resistance for the two situations, see table 5.4. Furthermore, two load-displacement curves are computed in Plaxis to check how the pile behaves with the interface reduction, see figure 5.5 and 5.6. These results can then be used to choose a realistic service load, which is kept on top of the pile during thermal variations. The ultimate bearing capacity read from the curve is around 900 kN for the first situation and 1250 kN for the second situation. The difference is found in the negative shaft resistance that can be mobilized and create extra positive shaft resistance. In Appendix B the negative shaft resistance of all layers above the end-bearing layer is calculated. For the service load in the model a value of 600 kN on the pile is chosen.

Table 5.4: Bearing capacity result in D-foundations

Situation	Base [kN]	Positive shaft [kN]	Negative shaft [kN]	Total [kN]
1	1174	1105	0	2279
2	1174	674	75	1773

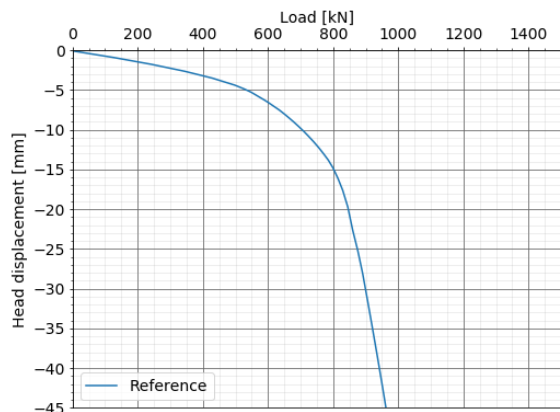


Figure 5.5: Load-displacement curve situation 1 in Plaxis

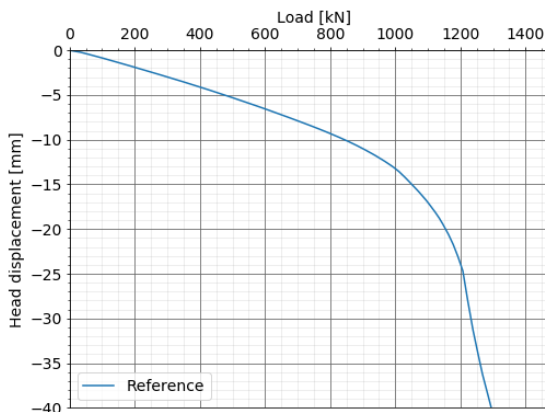


Figure 5.6: Load-displacement curve situation 2 in Plaxis

5.1.6. Calculation phases

The different steps in energy pile modelling are defined as construction stages in Plaxis. A difference between the approaches occurs after the initial loading stage until SLS. The pile with the neutral plane on top is directly thermally loaded via b (situation 1), while for the other model a surface load on the soil beside the pile is placed such that negative shaft resistance of the Holocene layers is considered (situation 2). The following stages are used for the two model situations:

1. Initial phase

This phase introduces the start of the model wherein the weight of the soil and the state of stress are established. Since the soil layers are horizontal the K_0 procedure is chosen as calculation type. The pore pressures are calculated according to the phreatic level of -0.5 m NAP.

2. Pile wished in-place - plastic calculation

In this phase the pile is activated as a volume element (wished in-place) with the interfaces R_{inter} 0.67 at the side and bottom of the pile. The installation effects of the pile are not considered here.

3. Loading pile until SLS - plastic calculation

By resetting the deformations of the previous phase the pile loading phase can start. By loading it until ULS the load-deformation curve is generated. A parallel calculation is performed of a pile loaded until SLS. This load is also kept on the pile during the thermal analysis such that only thermal effects are evaluated.

(a) Surface loading - plastic calculation

To move the neutral plane towards the top of the first sand layer a surcharge on the soil is applied of 25 kN. The difference is visible in figure 5.7 with on the left the shear stress of the model without surface load and on the right with surface load.

(b) No surcharge

4. Thermal operational phase - fully THM coupled 5 years

The loading on the pile is kept constant and the water flow and thermal boundaries are activated. This analysis is time-dependent and results in freezing-thawing situations along the pile shaft.

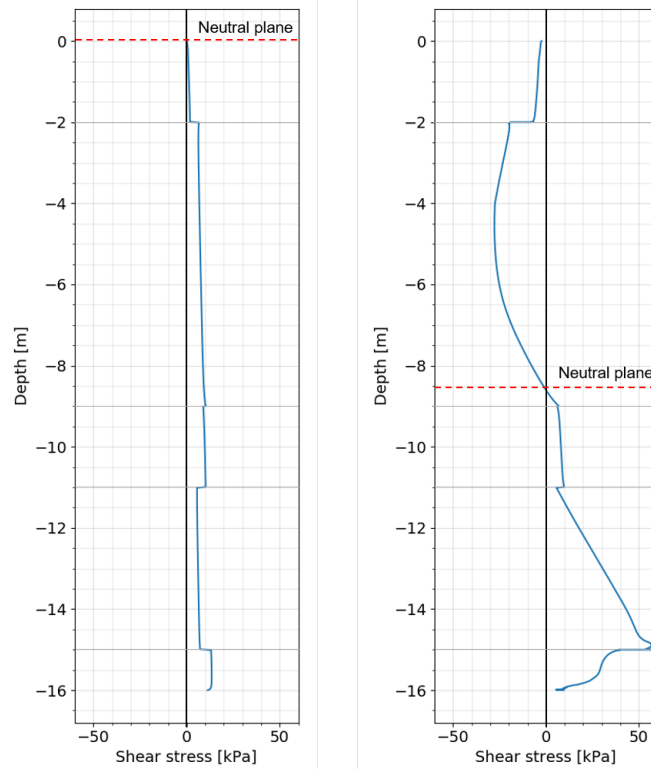


Figure 5.7: Neutral plane position for situation 1 on the left and position after surface load for situation 2 on the right

5.1.7. Expectation of results

The seasonal variation will be visible throughout the domain with each year one cooling (two parts) and one heating cycle. Thermal loads will probably result in reversible volume changes of the pile and soil. Due to shearing of and phase expansion in the soil plastic strains might develop as well. These strains result in a new stress distribution dependent on the load applied to the pile and shear resistance at the shaft. Furthermore, an increase in excess pore water pressure is expected in the low permeable layers if freezing occurs. This will reduce the effective stress and thereby the shear stress on the pile. Considering the dynamic load characteristics of this thermal load variation a slight ratcheting behaviour might be visible due to shear induced settlements over the years. The unloading-reloading principle of the soil along the pile during pile expansion and contraction is visualized in figure 5.8.

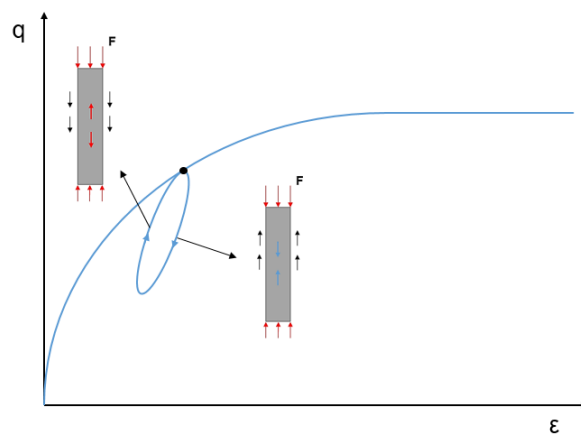


Figure 5.8: Schematic loading-unloading-reloading behaviour of the pile due to expansion and contraction

5.2. Results THM temperature distribution

To get an idea about the changes in the model during thermal operation of the energy pile 4 months based on the seasonal variation are picked from each year. The months are April, July, October and December. Furthermore, specific nodes and stress points along the pile are picked to be able to determine the changes in behaviour, see figure 5.9.

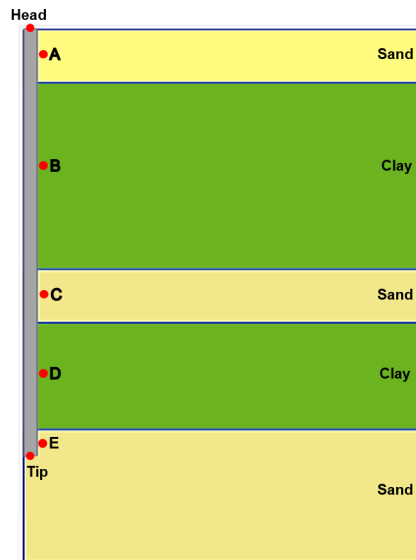


Figure 5.9: Specific measurement locations in the domain

Figure 5.10 gives an idea about the temperature distribution of the four months in year 3. In Appendix G figure G.1 the distribution is shown for all months within the five computed years. The energy pile is visible on the left side of the model and the thin white line represents the freezing front. Within the first months of all years, so during the cooling stage, most of the interfaces along the pile are frozen. It begins with the edge in the upper clay layer and continuous with the second clay and first sand layer as is expected according to its SFCC and its position nearby the subsurface, i.e. lower pressure. The temperature curves over time of points A, B, C, D and E along the shaft are shown in figure 5.11. It indicates that the soil domain is partly regenerated during the heating stages in the summer months, but there is a slight reduction of temperature over the years. The peak of point A in the backfill layer is the result of the imposed surface temperature boundary and the initial condition of the model set at 12 °C.

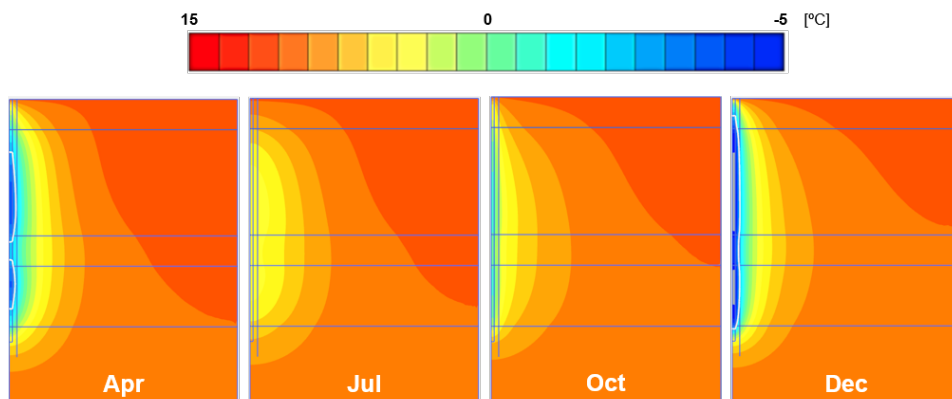


Figure 5.10: Year 3 of operation

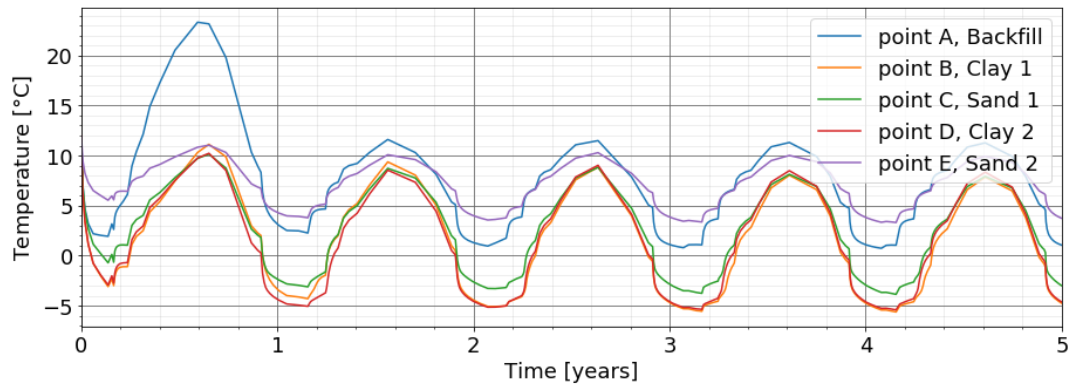


Figure 5.11: Temperature along the shaft at measurement locations

5.3. Situation 1: results THM module without surcharge

This section describes the influence on the pile with positive shaft friction along all edges of the pile, i.e. neutral plane on top. The working of the THM model was evaluated for non-freezing situations in the previous chapter. To evaluate an extension of the THM module with freezing and thawing the volumetric strains and pore pressures are computed in the chosen points along the shaft.

5.3.1. Volumetric strains

Figure 5.12 presents the strain increments by the freezing of pore water. This is the result of the increase in ice saturation which correlates with the stepwise increase of the volumetric strain. The plastic failure points created by the expansion are shown in figure 5.13. The freezing in the two clay layers results also in more volumetric strain in the specific point compared with freezing in the sand layers, but the plastic strains in the sand spread at more distance from the pile due to its low freezing temperature in the SFCC. For the thawing moments the volumetric strain just slightly drops, but is not clearly visible in the graph. Plastic deformations are expected when ice forms in the soil (frost heave), some deformation will not be recovered completely in a thawing state (figure 2.21). However, the amount and the accumulative character is remarkable and shows that the previous expansion has no influence on the future freezing cycles. Freezing in the bearing layer, point E, does not occur in this case and is probably caused by the absence of the thermal boundary at these depths.

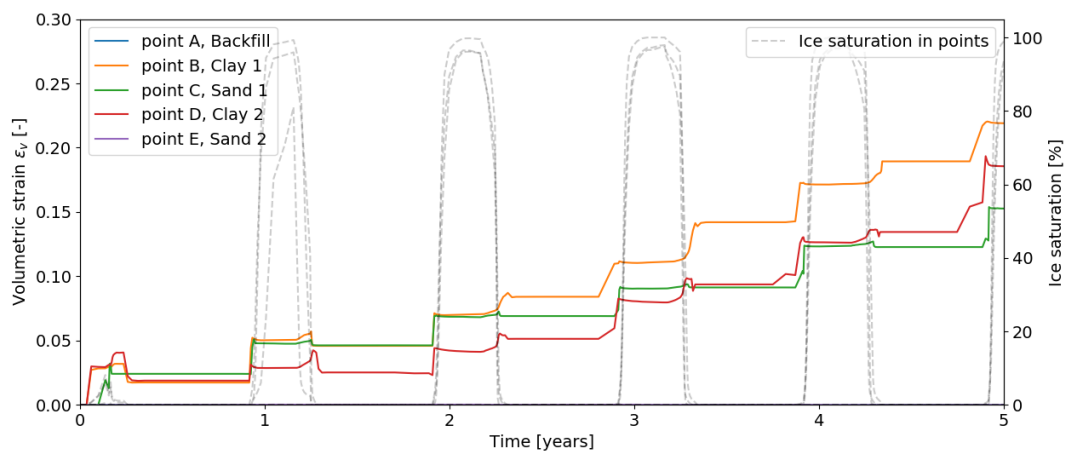


Figure 5.12: Volumetric strains and ice saturation in the case without surcharge situation 1

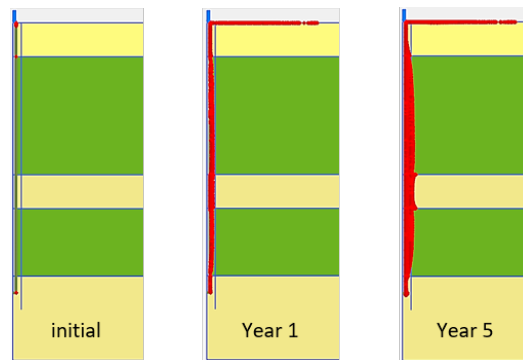


Figure 5.13: Plastic points before thermal, after the first year and after the fifth year situation 1

5.3.2. Pore pressure distribution

The excess pore pressure in figure 5.14 shows a negligible fluctuation during ice formation and thawing in the soil. The increase in excess pore pressure during the thermal loading cycles is the result of expansion and contraction due to ice formation and low hydraulic conductivity. The increase in pressure in the clay layer is therefore also prospected. The other layers show a more drained behaviour like in point C or are not freezing as in the upper layer, point A and E. The induced pore pressures are also really low and will not make a substantial difference in the pile behavior. Especially when considering that the fluctuation of the groundwater level will give a much bigger value in clayey soils. However, it indicates the formation of ice in the THM module of Plaxis. Important to bear in mind that the cryosuction is not included in this THM analysis.

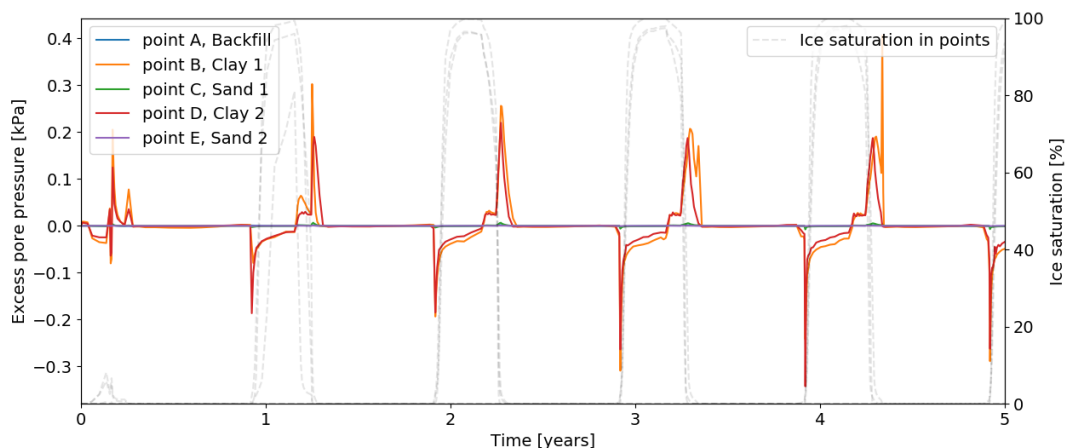


Figure 5.14: Excess pore pressure along the pile shaft situation 1

5.3.3. Pile deformation and displacement

A node at the head and tip of the pile are analysed over time, see figure 5.15. The figure shows the varying settlement of the pile during heating-cooling cycles and the initial settlement caused by the mechanical service load of 600 kN. The pile deforms by expanding and contracting over the seasons and causes the tip to go up and head to go down in a cooling situation and vice versa in a heating stage. The varying settlement gives a clear view on the settlement that can be expected over the seasons. The thermal expansion and contraction of the pile can be determined and also the extra settlement after each cycle is visible. The pile displacement increases over the years, which is called the ratcheting and it is the result of degradation of shaft friction. The displacement over 5 years is 11 mm for situation 1 with the neutral plane on top of the pile.

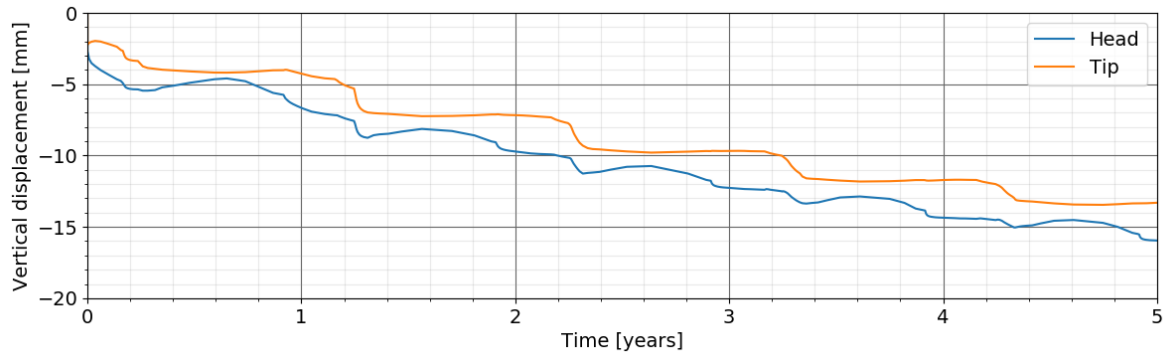


Figure 5.15: Vertical displacement of the head and tip of the pile during 5 years of operation with neutral plane at stop situation 1

5.3.4. Mobilized shear stress

In figure 5.16 the shear stress along the pile is depicted. During the thermal variations and freezing volumetric strains occur along the pile. In December of year three the substantial amount of frozen water in the sand layer increases the effective stress and in that way the shear stress on the pile. Since the expansion is symmetric the upper part of the sand 1 layer moves upwards, while the lower part downwards. This results in a decrease in positive shaft mobilization at the bottom and an increase in the top of the layer.

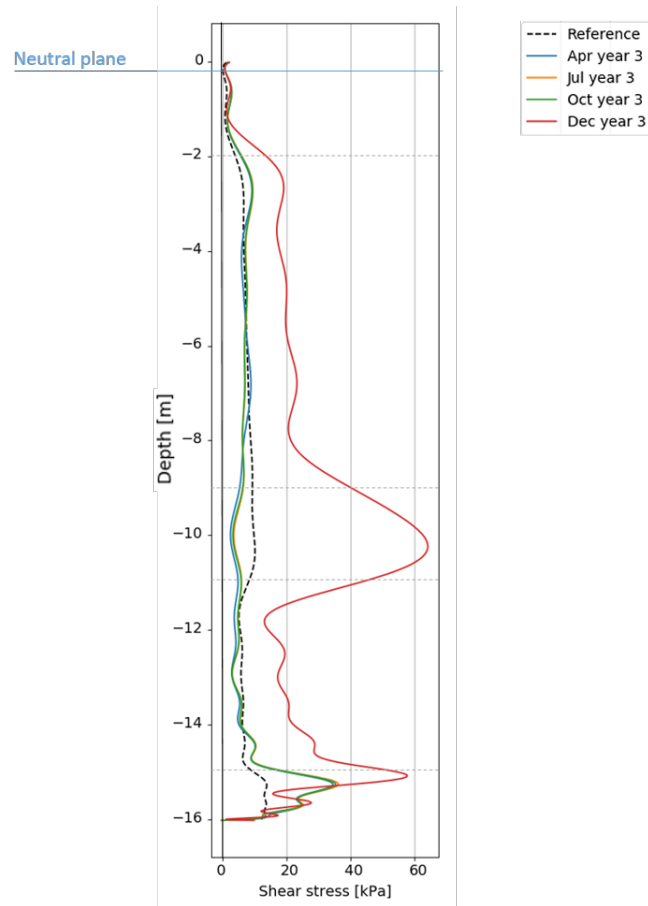


Figure 5.16: Shear stress along the pile situation 1

5.4. Situation 2: results THM module with surcharge

This section describes the influence of thermal cycles on a pile in situation 2 with the neutral plane on top of the first sand layer and above the neutral plane negative skin friction.

5.4.1. Volumetric strains

The expansion and contraction of the soils due thermal variations and freezing inside the pores is shown in figure 5.17 by the volumetric strain in the different points along the pile edge. It indicates again a continuous expansion due to ice forming, but does not show a notable reduction in the thawing phase. Remarkable is the difference in the steep expansion of clay in year 3, which is not in line with the freezing.

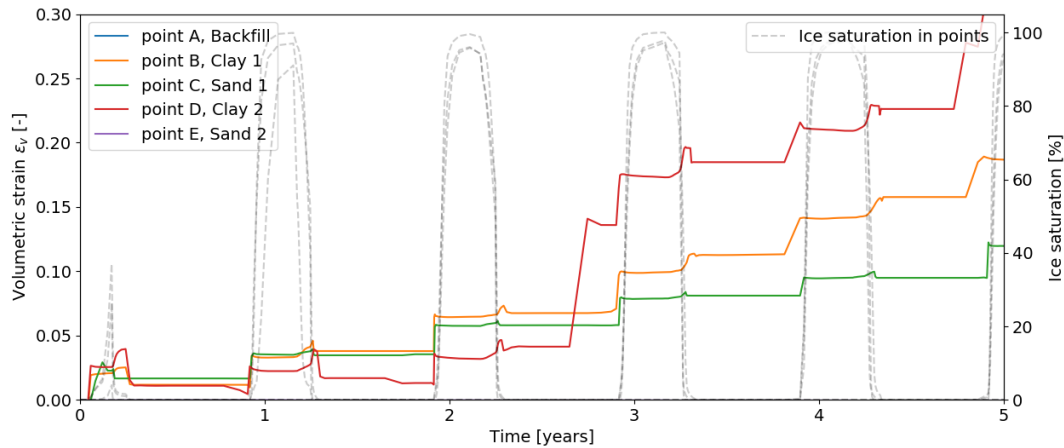


Figure 5.17: Volumetric strains plus ice saturation situation 2

5.4.2. Pore pressure distribution

Figure 5.18 represent the excess pore pressure with the ice saturation in the different layers. It shows a similar trend as in the previous situation.

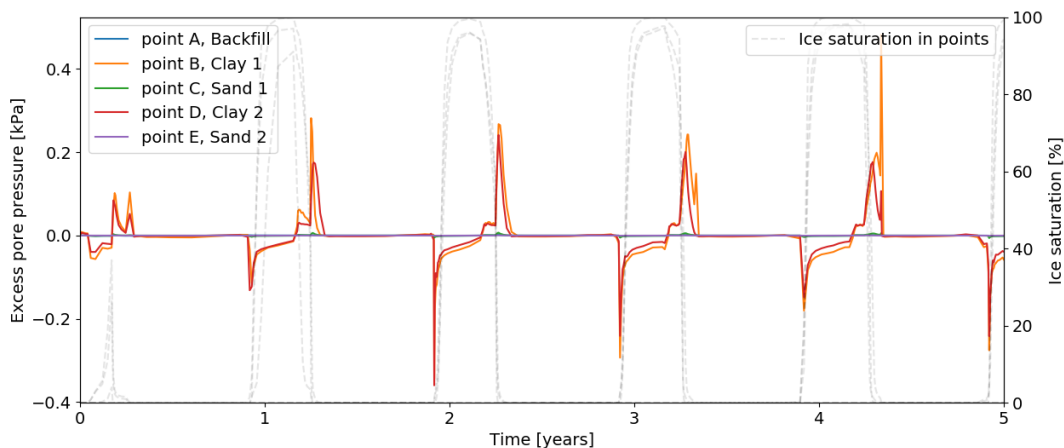


Figure 5.18: Excess pore pressure in the soil along the pile shaft situation 2

5.4.3. Pile deformation and displacement

The displacement and deformation of the pile is also in this situation measured by a node on the head and tip of the pile. The initial settlement is larger due to the surface load in combination with the service load applied in this case. The surface load on the soil pulls the pile downwards and creates at the same time some negative shaft resistance. The influence of the thermal cycles on the displacement of the pile is much smaller compared with the previous case. This is expected as the soil around the pile is more compacted due to the surcharge and the

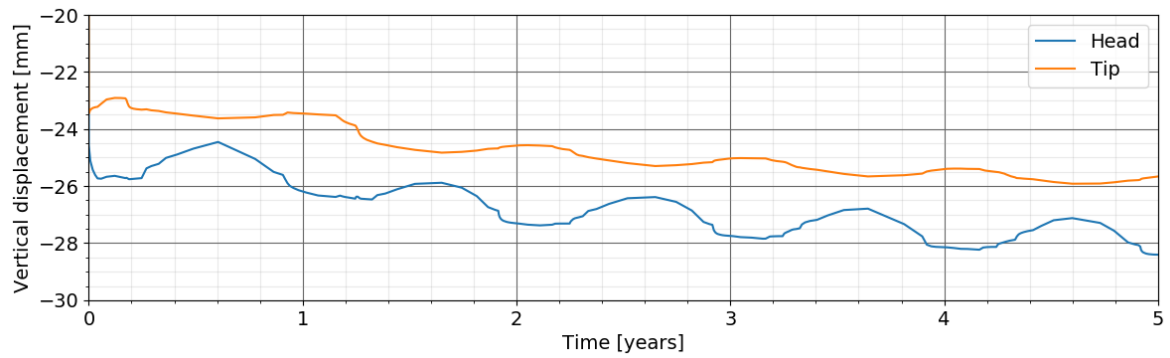


Figure 5.19: Vertical displacement of the head and tip of the pile during 5 years of operation with neutral plane at second sand layer situation 2

5.4.4. Mobilized shear stress

The stresses in the pile are continuously changing during temperature variations. The expansion and contraction of the pile are causing a big part of it, but the soil volume change at the shaft also influences the distribution of the stresses. Figure 5.20 shows the shear stress along the pile depth in year 3.

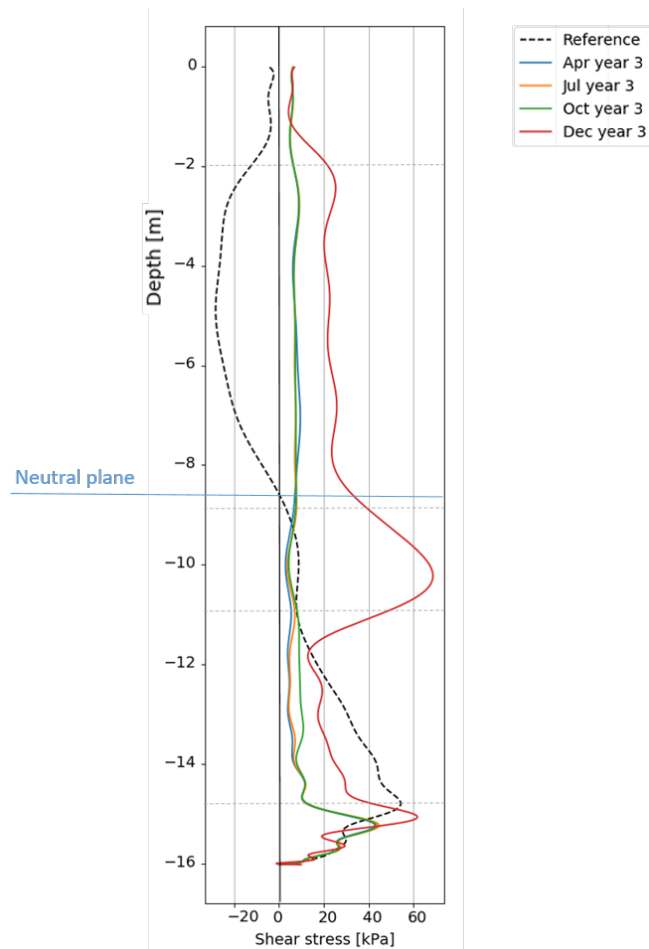


Figure 5.20: Shear stress at the shaft of the pile situation 2

The shear stress above the neutral plane changes from negative to positive due to the increase in effective stress on the soil as result of volumetric strains. The behaviour in the sand is again a bit strange as it shows that no shear or even negative shear resistance is mobilized in that layer. The reason behind is also explained

in situation 1 and is probably caused by the symmetric expansion that causes a upward displacement at the top of the sand layer. Thus more mobilization, and a downwards displacement at the bottom of this layer, so less mobilization. This difference is clearly visible as the layer keeps expanding over the years. The shaft resistance can be determined by multiplying the shear stress values with the periphery of the pile.

5.5. Discussion

The THM module without a special unfrozen-frozen model of Plaxis is in some extent able to show freezing-thawing in different soil types. The seasonal cycles are visible and the change in pore pressure together with the change volumetric strain indicates that phase expansion due to freezing took place. However, a significant accumulative strain development over the years is visible, which is remarkably high and constant during each freezing and thawing cycle. Plastic deformations during freezing in the pores will indeed result in some strains, but according to literature and reality this will have a certain influence on the strain development of future cycles. In this way also the shear along the pile keeps increasing due to the volumetric strain increase and becomes dependent on the amount of frozen water content in the soils. It seems that plastic volumetric strain is generated in the form of expansion. This can be explained by the reduction in effective stress due to the increase in pore pressure. When the soil shears again the yield surface is reached earlier and thus plastic volumetric strain in the form of expansion will occur. This is a limitation of choosing a constitutive model that is not able to simulate temperature dependent strength, stiffness and the remoulded character of thawed soft soils. A more advanced model that could take into account these effects would improve the reliability of the results.

6

The impact of change in soil cohesion and stiffness due to freezing-thawing

The previous chapter used a fully-coupled THM model in which soil strength and stiffness variations during freezing-thawing cycles were not captured. However, these changes will probably have an effect on the pile bearing capacity. Within this chapter the most favourable and unfavourable conditions in terms of soil cohesion and stiffness are imposed along the shaft. This analysis uses the same soil stratigraphy and boundary conditions. The soil parameters are also taken from the North-South Line data presented in Appendix F in which the chosen layers are marked with red. Two methods are distinguished, the first one represents a pile behaviour with the shaft resistance positive along the whole shaft. The second method approaches the behaviour of the pile with considering negative shaft resistance as is shown in figure 5.7. Both situations and their approach in the Plaxis model are visualized in figure 6.1 below.

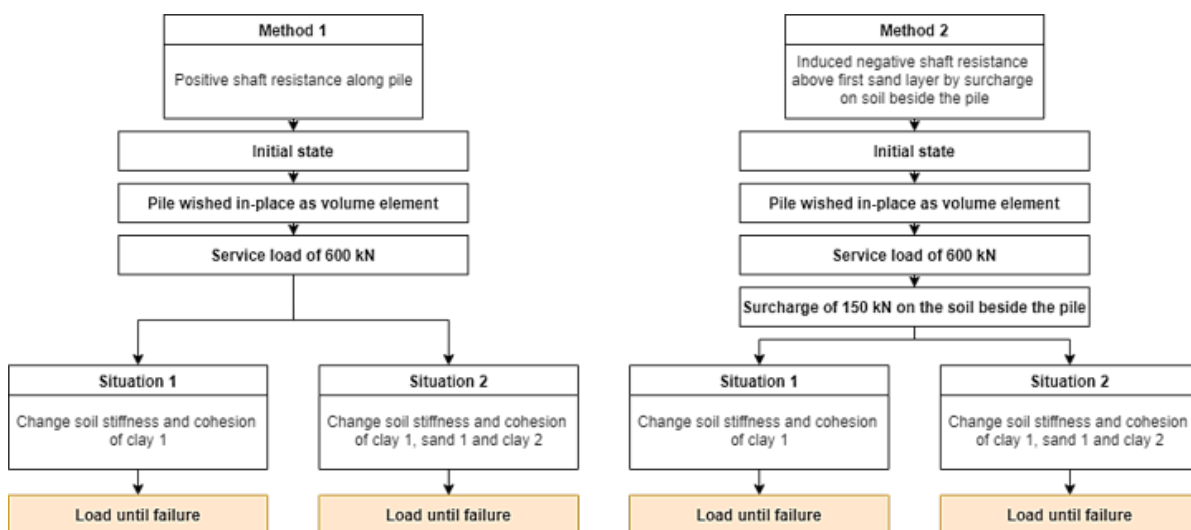


Figure 6.1: Plaxis approach for impact on soil strength and stiffness variation

The soil strength and stiffness are manually adjusted in an extra construction phase by changing the soil material around the edge of the pile, see figure 6.2. The first analysis is done for the situation where only the upper clay layer is frozen and thawed. According to the thermal analysis and the literature study it is the first place where freezing will occur. The second analysis will freeze and thaw both clay layers and the first sand layer along the shaft. The thickness of the soil material that is changed along the edge is based on a simplified geometry and the earlier results in the thermal analysis. Therefore a rectangular layer with a thickness of 20 mm is taken around the pile in clay 1, sand 1 and clay 2. Furthermore, a vertical service load of 600 kN is applied on top of the pile. Situation 2 with negative resistance in the soft Holocene layers is simulated by a surcharge of 25 kN which is placed on top of the soil beside the pile.

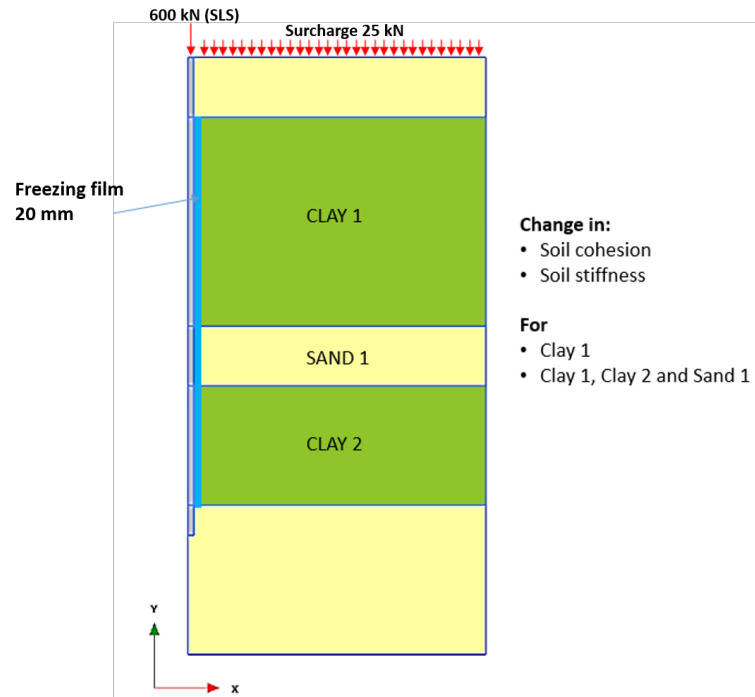


Figure 6.2: Locations with manually changed sections along the shaft

The values are varied separately and based on the parameters mentioned in table 6.2. For all parameters three phases are considered: initial, frozen and thawed. By comparing the resulting load-displacement curves with the reference curve that did not experience any freezing-thawing changes the stiffness behaviour of the pile is found, see figure 5.5 and 5.6 for the first and second method. The settlements are summarised in the end for each method.

6.1. Soil stiffness and cohesion variation

The change in Young's modulus E during temperature variations for frozen soils are measured in Morgenstern et al. (1975). The following relations for sand (equation 6.1), silt (equation 6.2) and clay (equation 6.3) are found. Important to mention that these relations are only valid until -5°C for silt and clay and -10°C for sand. Furthermore, the reference stiffness are 400 and 500 MPa. The significant increase is caused by the presence of ice and its high Young's modulus, i.e. at 0°C approximately 9 GPa. The importance of the unfrozen water content is visible in the relation as the values 4.2, 3.5 and 0.46, since for a clay more will stay unfrozen at a certain freezing temperature. For the soil stiffness in the thawed state a reduction could occur for soft layers. As in figure 2.19 the stiffness of a highly frost susceptible clay became half of the initial stiffness. To be conservative this reduction is also used in this analysis for the two clay layers in case of thawing.

$$E = 500(1 + 4.2|T|) \quad (6.1)$$

$$E = 400(1 + 3.5|T|) \quad (6.2)$$

$$E = 500(1 + 0.46|T|) \quad (6.3)$$

The relation 6.4 mentioned in Plaxis (2015) between E , E_{oed} and ν is used to transform the Young's modulus to E_{oed} . From there the E_{50} and E_{ref} for the HSS model are determined. For the Poisson's ratio ν in frozen soil the value of ice is used, which is equal to 0.31 (Wu et al., 2010).

$$E_{oed} = \frac{E(1 - \nu)}{(1 + \nu)(1 - 2\nu)} \quad (6.4)$$

The change of cohesion is based on frost heave results of Wu et al. (2010) in table 6.1 and on figure 2.17 described in the literature study.

Table 6.1: Mechanical soil parameters at freezing temperatures (Wu et al., 2010)

Soil type	Mechanical parameters	-20 °C	-10 °C	-5 °C	-2 °C	0 °C	20 °C
Clay in active layer	Density (kg/m ³)	1920	1920	1920	1920	1920	1920
	Elastic modulus (Mpa)	200	100	50	23.4	6	6
	Poisson's ratio (Mpa)	0.32	0.32	0.32	0.32	0.35	0.35
	Cohesion (Mpa)	0.6	0.6	0.6	0.57	0.15	0.15
	Angle of internal friction (degree)	26	26	26	26	24	24
Clay in permafrost layer	Density (kg/m ³)	1834	1834	1834	1834	1834	1834
	Elastic modulus (Mpa)	500	300	100	70	3	3
	Poisson's ratio (Mpa)	0.15	0.15	0.15	0.15	0.2	0.2
	Cohesion (Mpa)	1.3	1.3	1.3	1.3	0.1	0.2
	Angle of internal friction (degree)	20	20	20	20	18	18

6.1.1. Volumetric strain

For the expansion of pure water to ice a value of 9% is often mentioned. Assuming a saturated soil with an average void ratio e of 0.5 for all layers, the porosity n used to determine the volumetric expansion of the soil volume is 0.33. By multiplying the increase in volume of water 9% with the water present and comparing it with the initial condition, it results in a volumetric increase of 3%. To simulate this expansion the freezing clay volume expands with 1% volumetric strain for the reduction until -2°C and 2% for the reduction until -4°C. During contraction, i.e. thawed state, this expansion is reversed by a prescribed volumetric strain of -3%. For the sand layer no change is applied by considering that the drainage capability of the layer is high and therefore less pressure is build up within the pores.

6.1.2. Soil parameters

To simulate a freezing-thawing cycle three stages are considered. The first stage is the reference state in which no thermal effects are considered. The second stage simulates a frozen pile edge with a temperature of -4°C. The last stage changes the parameters of the soil towards a thawed state. But before the change of parameters a service load is applied to both situations and a extra vertical load is placed on the soil in the negative resistance situations. The parameters used in the different stages are shown in table 6.2 below.

Table 6.2: Change in soil strength and stiffness

Parameter	unit	Pile	Backfill	Clay 1	Sand 1	Clay 2	Sand 2
T>0 °C reference							
E	kN/m^2	30×10^6	-	-	-	-	-
E_{50}^{ref}	kN/m^2	-	20×10^3	10×10^3	40×10^3	8.4×10^3	35×10^3
E_{oed}^{ref}	kN/m^2	-	20×10^3	4×10^3	30×10^3	3.5×10^3	35×10^3
E_{ur}^{ref}	kN/m^2	-	60×10^3	25×10^3	200×10^3	35×10^3	190×10^3
m	-	-	0.8	0.8	0.5	0.8	0.5
v'	-	0.20	0.15	0.15	0.20	0.15	0.2
c_{ref}	kPa	-	0	6	0	0	0
ϕ'	°	-	30	26	33	32	35
T=-4°C frozen							
E	kN/m^2	-	-	67×10^3	481×10^3	59×10^3	-
E_{50}^{ref}	kN/m^2	-	-	187×10^3	666×10^3	164×10^3	-
E_{oed}^{ref}	kN/m^2	-	-	93×10^3	666×10^3	82×10^3	-
E_{ur}^{ref}	kN/m^2	-	-	561×10^3	1998×10^3	491×10^3	-
m	-	-	-	0.8	0.5	0.8	-
v'	-	-	-	0.31	0.31	0.31	-
c_{ref}	kPa	-	-	570	300	300	-
ϕ'	°	-	-	26	33	32	-
T>0°C thawed							
E	kN/m^2	-	-	2×10^3	27×10^3	3×10^3	-
E_{50}^{ref}	kN/m^2	-	-	4×10^3	30×10^3	3.5×10^3	-
E_{oed}^{ref}	kN/m^2	-	-	2×10^3	30×10^3	2×10^3	-
E_{ur}^{ref}	kN/m^2	-	-	12×10^3	90×10^3	10.5×10^3	-
m	-	-	-	0.8	0.5	0.8	-
v'	-	-	-	0.15	0.20	0.15	-
c_{ref}	kPa	-	-	0	0	0	-
ϕ'	°	-	-	26	33	32	-

6.2. Situation 1: positive shaft resistance over all layers

The shaft resistance acts at all layers in this first situation. The load-displacement over the pile is compared for the three stages or reference (initial), frozen and thawed. The impact of the different stages are distinguished below for the influence of the change in soil cohesion, soil stiffness and the location of the freezing.

6.2.1. The influence of soil cohesion

The soil cohesion increases during ice formation in a soil. Two cases are considered in which only the first clay layer is frozen or both clay layers plus the first sand layer is frozen. To simulate a remoulded clay without any cohesion after thawing the value is set at zero, see table 6.3. Figure 6.3 of clay 1 shows an extra settlement of 6 mm in a thawed state when considering a service load of 600 kN. In case of frozen soil no significant reduction in the prospected settlement compared with the reference is found. For the influence of all layers figure 6.4 indicates a settlement of 10 mm compared with the reference curve. The frozen state gives a reduction of 1.5 mm in settlement compared with the reference curve.

Table 6.3: Cohesion of frozen and thawed states

State	Clay 1	Sand 1	Clay 2
Frozen T=-4°C	570	300	300
Thawed	0	0	0

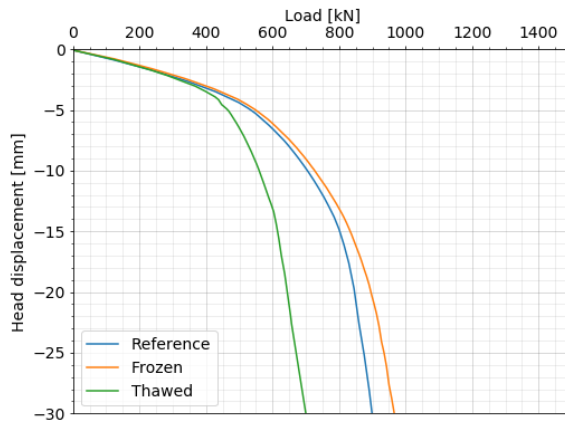


Figure 6.3: Influence of cohesion of clay layer 1

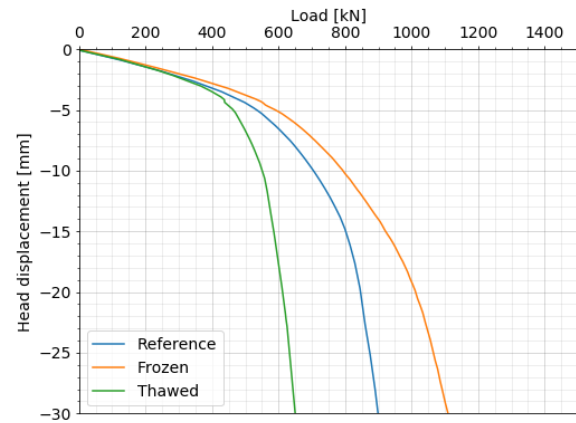


Figure 6.4: Influence of cohesion of all layers

6.2.2. The influence of soil stiffness

For the soil stiffness the same approach is used. Table 6.4 shows the values used in the analysis. The stiffness for the clay layers is reduced with 50% to capture the worst case scenario for the stiffness after one cycle as mentioned in (Steiner et al., 2018). The curves for the thawed state in figure 6.5 and figure 6.6 indicate an increase in the settlements of 3 and 1 mm respectively. In case of all edges frozen along the pile an reduction of 2 mm is expected at the service load of 600 kN.

Table 6.4: Stiffness of frozen and thawed states

State	Clay 1	Sand 1	Clay 2
Frozen T=-4°C			
E_{50} [MPa]	187	666	164
E_{oed} [MPa]	93	666	82
E_{ur} [MPa]	561	1998	491
Thawed			
E_{50} [MPa]	4	40	4
E_{oed} [MPa]	2	30	2
E_{ur} [MPa]	12	200	18

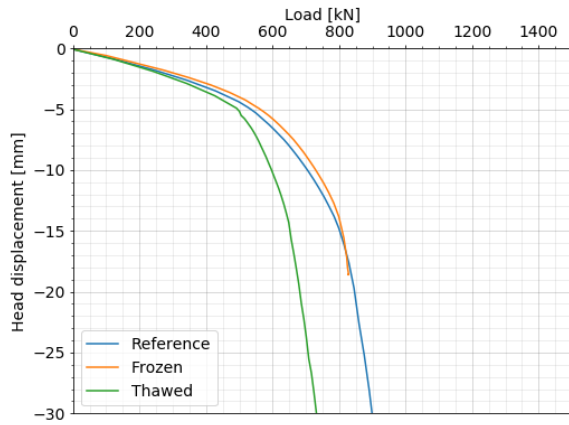


Figure 6.5: Influence of stiffness of clay layer 1

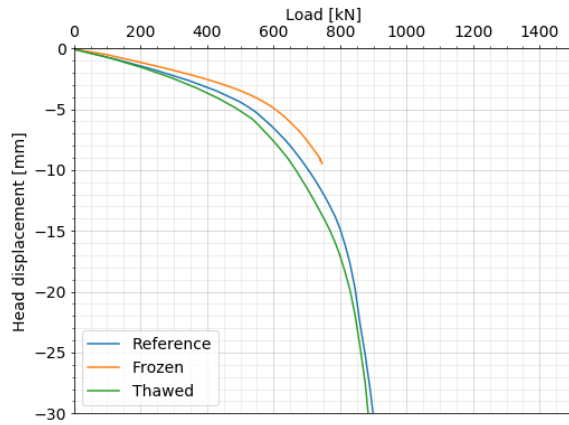


Figure 6.6: Influence of stiffness of all layers

6.2.3. The influence of soil stiffness and cohesion

In this section the previous results are combined for the two cases. The sensitivity is determined of the location that is affected. Figure 6.7 and 6.8 show the load-displacement results for freezing in clay 1 and freezing in all three layers respectively. In the first situation a settlement difference with the reference curve is in the range of 1 mm at 600 kN and the second situation wherein all layers are involved a range of 2 mm is visible.

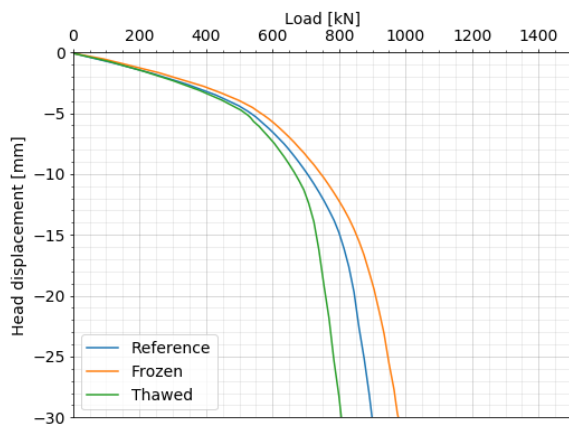


Figure 6.7: Influence of cohesion and stiffness of clay layer 1

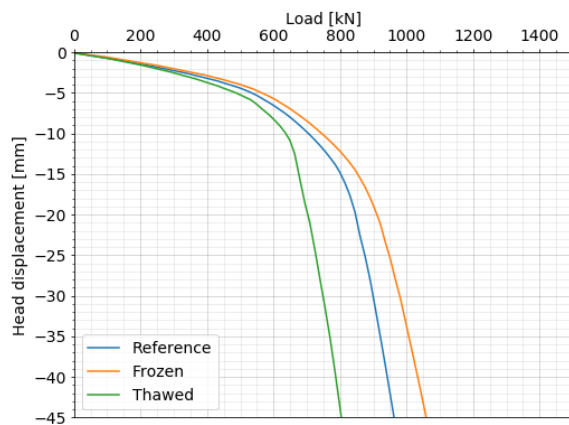


Figure 6.8: Influence of cohesion and stiffness of all layers

6.2.4. Overview

The impact of the change in cohesion, stiffness and location is evaluated and below an overview of the expected settlements is given for only clay 1 as affected layer (table 6.5) and for clay 1, clay 2 and sand 1 as affected layers (table 6.6)

Table 6.5: Pile displacement when clay 1 is affected

State	Cohesion	Stiffness	Cohesion and stiffness
Reference	7.0 mm	7.0 mm	7.0 mm
Frozen	6.5 mm	6.0 mm	5.5 mm
Thawed	14.0 mm	10.0 mm	7.5 mm

Table 6.6: pile displacement when clay 1, clay 2 and sand 1 are affected

State	Cohesion	Stiffness	Cohesion and stiffness
Reference	7.0 mm	7.0 mm	7.0 mm
Frozen	5.0 mm	5.0 mm	6.0 mm
Thawed	17.0 mm	7.5 mm	8.0 mm

6.3. Situation 2: negative shaft resistance in Holocene layers

The shaft resistance is set negative in the layers above the first sand layer by a surcharge load on the soil beside the pile. This will also drag the pile downwards. The new reference situation and thereby the displacements are measured from this state. Furthermore, the axial stress over the pile is also computed for the three situations to evaluate a change in load transfer through the soil via the shaft. The cohesion and stiffness parameters are varied as mentioned in the table 6.2 of the previous section.

6.3.1. The influence of soil cohesion

In figure 6.9 and 6.4 the influence of cohesion is shown for the second situation. The curves indicate that more shaft resistance can be mobilized and less displacement is expected for the same service load. The reduction in cohesion in the negative shaft resistance does not influence the load-displacement curve. For the change in cohesion for the second clay layer however, the increase in cohesion leads to more shaft resistance. The linear part of the graph shows a stiffer behaviour than the reference curve.

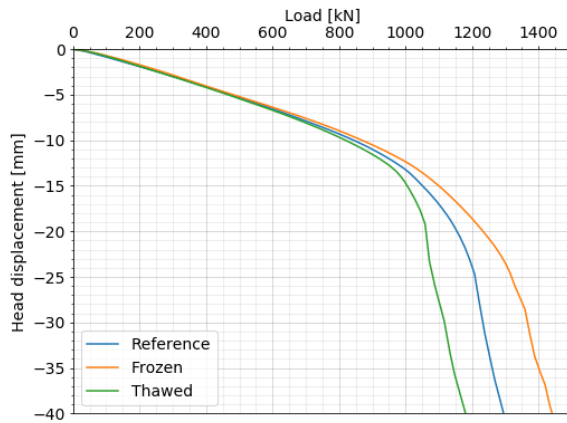


Figure 6.9: Influence of cohesion of clay layer 1

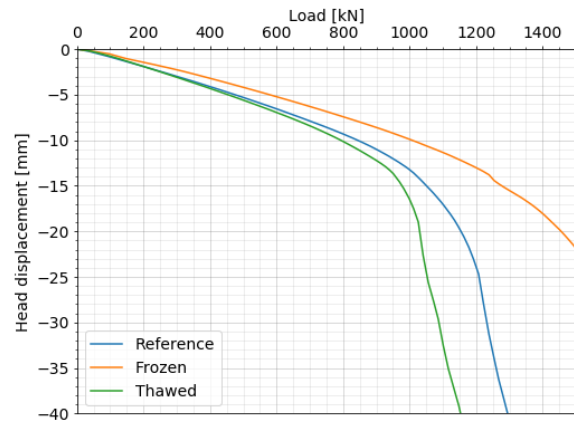


Figure 6.10: Influence of cohesion of all layers

6.3.2. The influence of soil stiffness

When only the stiffness in the first clay layer is affected no substantial change in load-displacement occurs as visible in figure 6.11. However, when all layers are affected the pile displacement acts stiffer again as visible by the less steep curve in figure 6.12 for frozen state.

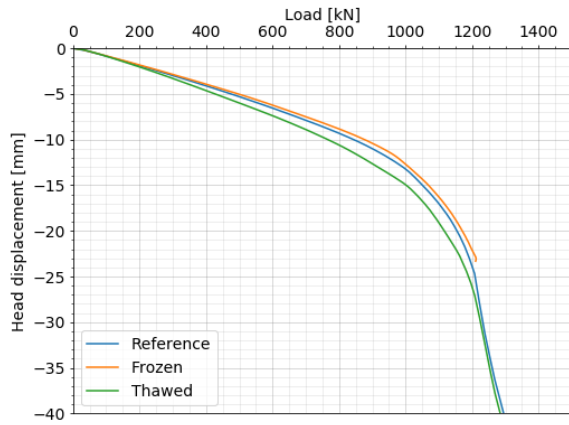


Figure 6.11: Influence of stiffness of clay layer 1

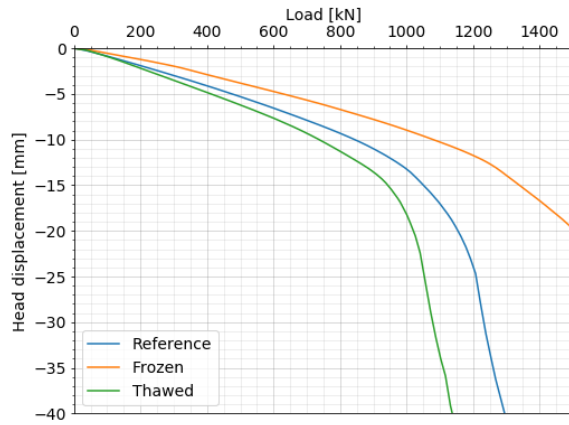


Figure 6.12: Influence of stiffness of all layers

6.3.3. The influence of soil stiffness and cohesion

Figure 6.13 and 6.14 show the results of changing both parameters in only clay 1 or in all the layers. It is actually summation of the two graphs for clay 1 above and also for all layers above. In the first graph not much difference is found compared with the graph where only soil cohesion changed, see figure 6.9.

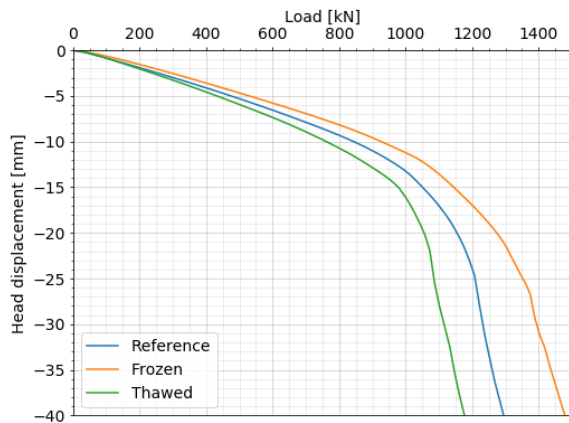


Figure 6.13: Influence of cohesion and stiffness of clay layer 1

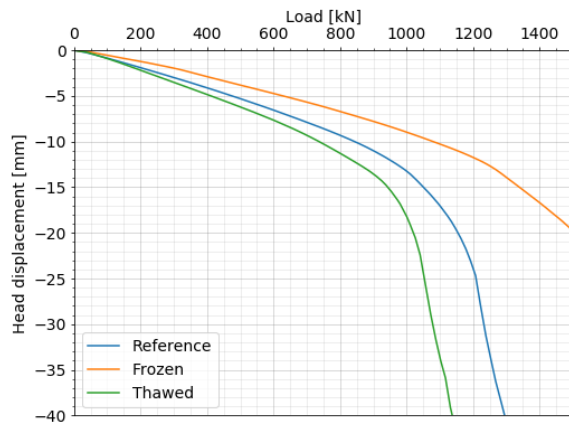


Figure 6.14: Influence of cohesion and stiffness of all layers

6.3.4. Overview

The impact of the change in cohesion, stiffness and location is evaluated and below an overview of the expected settlements is given for only clay 1 as affected layer (table 6.7) and for clay 1, clay 2 and sand 1 as affected layers (table 6.8)

Table 6.7: Pile displacement when clay 1 is affected

State	Cohesion	Stiffness	Cohesion and stiffness
Reference	6.5 mm	6.5 mm	6.5 mm
Frozen	6.5 mm	6.0 mm	5.5 mm
Thawed	6.5 mm	7.5 mm	7.5 mm

Table 6.8: pile displacement when clay 1, clay 2 and sand 1 are affected

State	Cohesion	Stiffness	Cohesion and stiffness
Reference	6.5 mm	6.5 mm	6.5 mm
Frozen	5.0 mm	4.5 mm	4.5 mm
Thawed	7.0 mm	8.0 mm	8.0 mm

6.3.5. Influence on shear stress

The shear stress is computed after one freezing-thawing cycle along the edge of the pile, so in its thawed state. Important to mention that negative indicates positive shear stress in Plaxis and vice versa. The left graph is the impact of change in soil stiffness or soil cohesion at clay 1, the middle graph shows the impact at all the layers and the right graph compares the two when the soil stiffness and the soil cohesion are changed. This latter variant shows the influence of the location of freezing. First of all, the soil cohesion reduction in clay 1 visible in the first graph shows an increase in shear stress due to the negative shaft resistance which is converted into positive due to the settlement of the pile as result of cohesion. In this case more shaft resistance is mobilized.

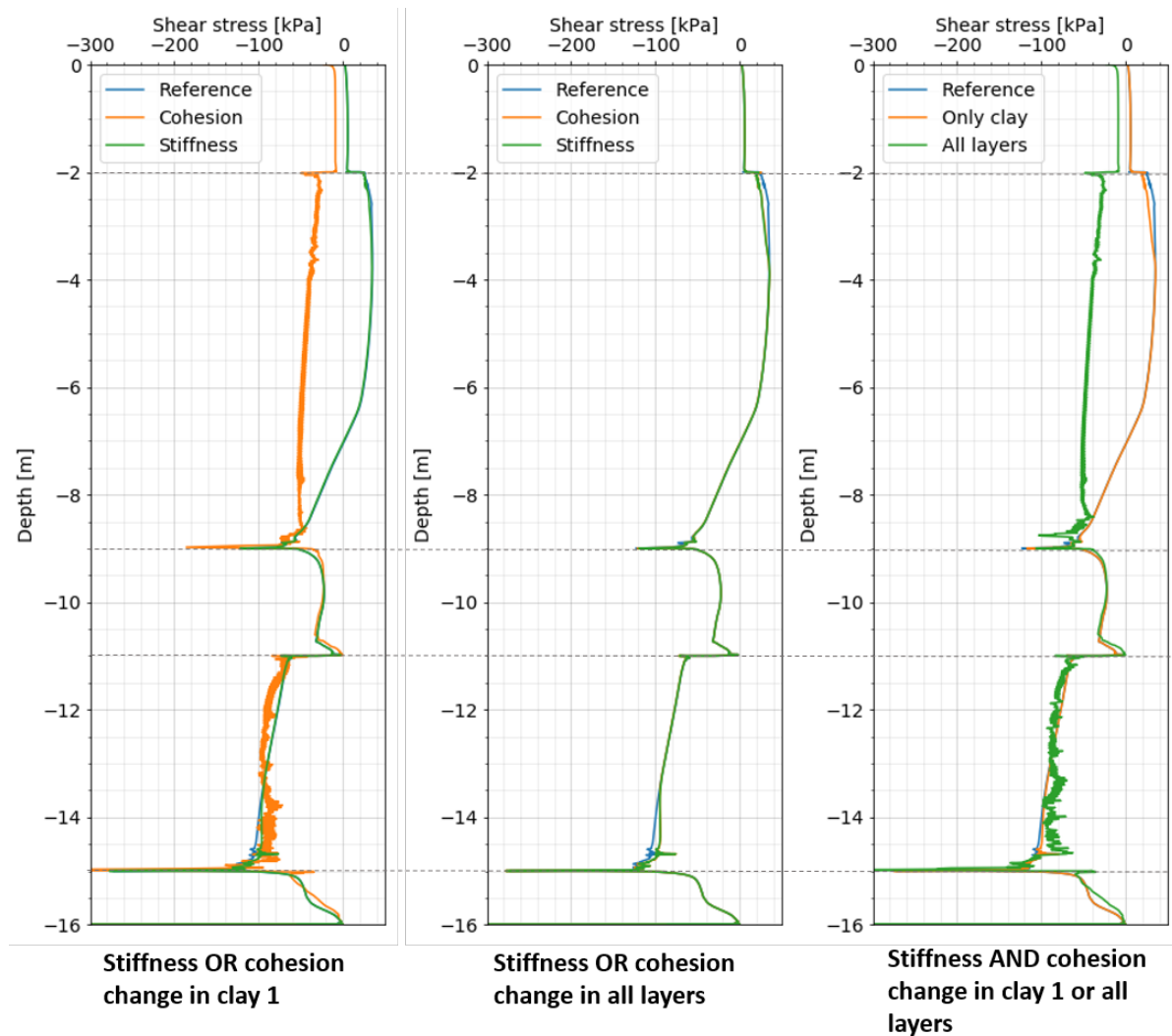


Figure 6.15: Shear stress along pile in situation 2 in its thawed state

6.4. Discussion

Comparing both situations it seems that the cohesion of the first clay layer has more affect on the stiff behaviour of the pile in situation 1. This can be explained by the initial negative shaft resistance in situation 2

at this layer, which is in case of zero cohesion actually disappearing. In the first situation positive shaft resistance was mobilized in this layer and by reducing the cohesion it also reduced the positive resistance. In this way the pile settles more. The stiffness shows more impact than the cohesion on the linear part of the load-displacement in situation 2.

Conclusions and recommendations

This chapter describes the conclusions of the three different aspects of this thesis and gives recommendations for field of practice and further research. First the main research question is answered and hereafter the sub questions formulated in the introduction are covered.

7.1. Conclusions

The behaviour of an energy pile during temperature variations with phase changing circumstances is analysed. The freezing-thawing effect on the concrete material is assessed by a literature study. Furthermore, a thermal analysis in Comsol and a geotechnical analysis in Plaxis are done. which is as follows:

What is the influence of freezing-thawing cycles on the geotechnical performance of an end-bearing energy pile?

The results presented in this thesis and the literature review are computed and written for specific conditions, e.g. soil stratigraphy and thermal loads. Considering the design approach in the Netherlands and in particular for an end-bearing pile, the freezing-thawing around the interface has no significant effect on the bearing capacity of the pile. The piles are mostly designed on the tip resistance. Furthermore, the negative shaft resistance which might be induced in the soft layers is either already added as extra load on the pile or subtracted from the determined bearing capacity. In addition, freezing in the sandy end-bearing layer is a will not result in any loss in cohesion. Thereby, the loss of cohesion along the top layers might even cause a decrease in negative shaft friction, which would increase the safety factor if the negative shaft friction is initially subtracted from the bearing capacity.

7.1.1. Frost resistance of concrete

For the impact on concrete and the influence of its characteristics the following sub question arised in the introduction:

What is the influence of freezing-thawing on the concrete material?

This is dependent on the mixture of the concrete material and the temperature ranges it is exposed to. The most harmful consequences are internal cracking and surface scaling. These phenomena could be prevented by using a proper mixture of concrete. A high water-cement ratio is the main cause of the increase in frost-susceptibility. Air entrainment agents could help to reduce this susceptibility by lowering the capillary forces with air voids. These voids also help to release pressure in case freezing occurs, so no tensile stress in the concrete can occur and thereby no internal cracks.

7.1.2. Thermal analysis

The thermal analysis is done in Comsol Multiphysics to answer the sub question below. The study is based on assumption of a pile plan for a semi-detached house.

What is the likelihood of freezing around an energy pile?

The thermal analysis within Comsol indicated that no freezing occurred at the shaft of the pile with this specific soil stratigraphy and heat demand. Freezing occurred in the situation with long-term excessive heat extraction, which was reached at two times the typical heat extraction. Furthermore, the clay layers are more frost-susceptible, but a sharp decrease in unfrozen water content is expected in the sand during subzero temperature conditions.

7.1.3. Geotechnical analysis

The following questions below were formulated for the geotechnical analysis.

- *How can freezing-thawing processes be quantified in terms of change in geotechnical pile behaviour?*
- *To what range is it possible to incorporate these quantifications in the pile design approach or to give an indication for limiting situations?*

Most of the freezing-thawing takes place along the shaft of the pile and it mainly affects the cohesion of the soft layers after thawing. This will reduce the amount of shaft resistance and will move more load to the tip. However, in case of more settlement along the shaft due to freezing and thawing and a design approach without including full mobilization of the negative shaft resistance in the soft layers there is a chance that layers that were first not considered as negative resistance will in a new situation induce an extra load on the pile for which is not designed for in the initial case. This effect can be ignored if the design already took all the soft layers as negative shaft in the design of the pile. To refer back to the first question asked, the potential negative shaft friction due to thawing could be used as quantification of the effect on the pile loads.

7.2. Recommendations

This chapter addresses the recommendations following from this thesis for further scientific research and for the application of end-bearing energy piles.

7.2.1. Recommendations for further research

First of all, it can be stated that in this report specific assumptions are made that have to be validated by further research. It would be interesting to find a more generic thermal and geotechnical approach to determine the effects of freezing-thawing around energy piles.

Frost resistance of concrete

Laboratory experiments could be performed to check the frost-resistance of concrete with different concrete mixtures and with freezing-thawing from the inside. Hereafter the optimal concrete mixture in terms of frost resistance and thermal conductivity can be established.

To quantify potential damage within the concrete it is recommended to check the effect of the amount of cycles on the strength of the concrete material. The equation proposed in the literature study for the dynamic modulus as damage variable could be used to describe its changed state after freezing-thawing.

Thermal analysis

This report investigates one type of pile group and household. A study into the effect of pile group configuration, i.e. separation and number of activated piles, will help to understand the group influence on freezing situations. From there a generalized solution for common pile groups in the Netherlands will help the construction industry to decide on the use of energy piles and fluid temperature ranges.

In this study the groundwater flow and groundwater salinity has been ignored. The frost susceptibility of the soil will decrease due to the regeneration by the inflow of water. Furthermore, the groundwater salinity will bring down the freezing point. More research will help to quantify the influence of groundwater flow and salinity on thermal evolution and thereby also frost-susceptibility around an energy pile at a specific location.

Besides, the fluid solution in the pipe increases in viscosity with percentage of anti-freeze. It would be interesting to see what the effect is of using the increased viscous anti-freeze on the efficiency of the heat exchange and the pump.

Geotechnical analysis

First of all, important phenomena are ignored in the THM analysis without a proper unfrozen-frozen soil model such as cryosuction, strength reduction and stiffness variations. For further research it is recommended to incorporate these phenomena.

Secondly, this report discusses the result of change in soil strength and stiffness within a single freezing-thawing cycle. The change in parameters is based on limited data from literature and the expansion and contraction of the pile and soil material is also not included in the analysis. Further research is required to establish the validity of the changing pile volume and soil parameters.

Additionally, the thesis focused on one specific pile and subsoil, but it is recommended to perform the same analysis for different piles to generate a generic solution. For example a different approach would be needed for floating piles compared with the investigated end-bearing pile within this thesis. Also the effect of installation of the pile on future frost-susceptibility along the shaft is not assessed and might be valuable if the installation type could reduce this susceptibility.

7.2.2. Recommendations for field of practice

For the three aspects assessed in this thesis certain practical recommendations can be given for the design of end-bearing energy piles in case of potential freezing-thawing situations.

Concrete mixture

The mixture should be chosen based on appropriate thermal conductivity and its frost resistance. Air entrainment agents and a low W/C ratio can definitely help to prevent deterioration effects such as internal cracking and surface scaling.

Thermal settings

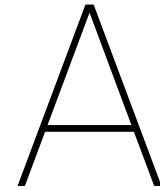
For end-bearing energy piles with the tip in clean sands it is recommended to place the heat pipes over the full length of the pile to optimize the extraction potential since freezing will not effect the bearing layer according to the literature study.

Geotechnical settings

It is recommended to design an end-bearing energy pile with freezing potential of full mobilization of negative shaft resistance at the layers above the end-bearing layer. Preloading of subsoil besides the pile could help to reduce future settlements along the pile in soft compressible soils and in that way solve the negative shaft development.

I

Appendices



Literature

This appendix supports the literature study in chapter 2.

Frost susceptibility ^a	Frost group	Kind of soil	Amount finer than 0.02 mm (wt %)	Typical soil type under USCS ^b
Negligible to low	NFS ^c	a. Gravels	0–1.5	GW, GP
		b. Sands	0–3	SW, SP
Possibly	PFS ^d	a. Gravels	1.5–3	GW, GP
		b. Sands	3–10	SW, SP
Low to medium	S1	Gravels	3–6	GW, GP, GW-GM, GP-GM
Very low to high	S2	Sands	3–6	SW, SP, SW-SM, SP-SM
Very low to high	F1	Gravels	6–10	GM, GW-GM, GP-GM
Medium to high	F2	a. Gravels	10–20	GM, GM-GC, GW-GM, GP-GM
		b. Sands	6–15	SM, SW-SM, SP-SM
Medium to high	F3	a. Gravels	>20	GM, GC
Low to high		b. Sands except very fine silty sands	>15	SM, SC
Very low to very high	F4	c. Clays, $I_p > 12$	—	CL, CH
Low to very high		a. All silts	—	ML, MH
Very low to high		b. Very fine silty sands	>15	SM
Low to very high	F4	c. Clays, $I_p > 12$	—	CL, CL-ML
Very low to very high		d. Varved clays and other fine-grained banded sediments	—	CL and ML; CL, ML, and SM; CL, CH, and ML; CL, CH, ML, and SM

^a Based on laboratory frost-heave tests.

^b G, gravel; S, sand; M, silt; C, clay; W, well graded; H, high plasticity; L, low plasticity.

^c Non-frost susceptible

^d Requires laboratory frost-heave test to determine frost susceptibility.

Figure A.1: Frost design soil classification of U.S. Corps of Engineers (Andersland and Ladanyi, 1994)

B

Negative skin friction Eurocode

The negative skin friction is calculated below according to Eurocode 7. The calculation is based on the soil stratigraphy used in this thesis with the pile resting on the second stiff sand layer. In the norm the layers above this sand layers are taken as compressible layers, which all contribute to the negative skin friction. $h_{1;2;3;4}$ is the thickness of the compressible layers, $K_0 = 1 - \sin(\phi)$ is at rest natural ground pressure, σ'_v is the effective pressure at the bottom of the layer, $\delta = \phi'$ is friction angle between non-displacement pile and soil and O_s is the circumference of the pile. The values used are summarized in table B.1.

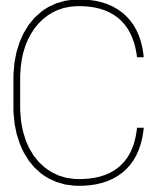
$$\begin{aligned}
 F_{s;nk;k} = & \left(\frac{1}{2} \times K_{0;1} \times \sigma'_{v;1} (\delta_1) \right. \\
 & + h_2 \times K_{0;2} \times \frac{(\sigma'_{v;1} + \sigma'_{v;2})}{2} (\delta_2) \\
 & + h_3 \times K_{0;3} \times \frac{(\sigma'_{v;2} + \sigma'_{v;3})}{2} \times \tan(\delta_3) \\
 & \left. + h_4 \times K_{0;4} \times \frac{(\sigma'_{v;3} + \sigma'_{v;4})}{2} \times \tan(\delta_4) \right) \times O_s
 \end{aligned} \tag{B.1}$$

layer	Soil type	thickness h [m]	ϕ and δ	K_0	σ'_v [kPa]	$F_{s;nk;k}$ [kN]
Layer 1	backfill	2	30	0.50	18.38	5.30
Layer 2	Clay	7	26	0.56	68.71	83.25
Layer 3	Sand	2	33	0.46	89.09	47.14
Layer 3	Clay	4	32	0.47	123.85	125.08

Table B.1: Negative skin friction for conceptual model

With $O_s = 1.26$ m, this results in $F_{s;nk;k} = 1.26 \times (5.30 + 83.25 + 47.14 + 125.08) = 328$ kN From there the design value for negative skin friction of a single pile is calculated as below with $\gamma_{f;nk} = 1.0$, which of course does not change the result.

$$F_{nk;d} = F_{s;nk;k} \times \gamma_{f;nk} \tag{B.2}$$



Comsol Multiphysics

Extra information and additional results are presented here to support the thermal analysis in chapter 3. The first part with thermal verification supports part of the choice of Comsol. The second section indicates that the chosen model domain has no influence on the temperature results for the extraction duration of 7 years.

C.1. Thermal verification

The temperature distribution of a simplified model is determined with three different methods: (i) An analytical solution, (ii) a model in Comsol and (iii) a Plaxis simulation. The geometry and soil stratigraphy of the model is simplified by choosing one homogeneous layer such that many parameters are held constant in the different methods. Like in Plaxis, the energy pile is simplified by seeing it as a cylindrical heat sink (axisymmetric) and implemented as a line source. In all performed simulations the model has the following input parameters:

Length line source [m]	$T_{initial}$ [K]	ρ [kg/m^3]	λ [W/(m K)]	c [J/(kg K)]	Q [W]	Time [days]
10	285.15	1900	2.8	1800	500	730

Table C.1: Input parameters temperature verification model

Equation C.1 shows the analytical solution for a continuous operation of extraction. The solution for the first days is manually changed to $T_{initial}$, since for low t the equation will increase the temperature even when energy is extracted. After a certain time the reduction in temperature at a distance r is calculated again.

$$T \approx T_{initial} - \frac{Q}{L} \frac{1}{4\pi\lambda} \left\{ \ln \frac{4\lambda t}{r^2 C} - 0.577 \right\} \quad (C.1)$$

The curves below show the numerical and analytical approach of temperature evolution around an energy pile. The three results show that the numerical solutions overlap, while the analytical solution shows a higher reduction of temperature.

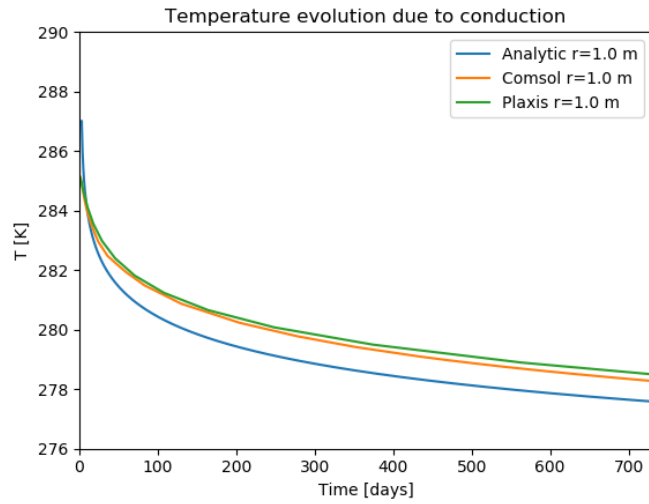


Figure C.1: Temperature evolution at 1 m

C.2. Domain influence

The influence of the domain size is evaluated with two models depicted in figure C.2. Figure C.3 indicates that the influence of the insulated boundary conditions can be neglected.

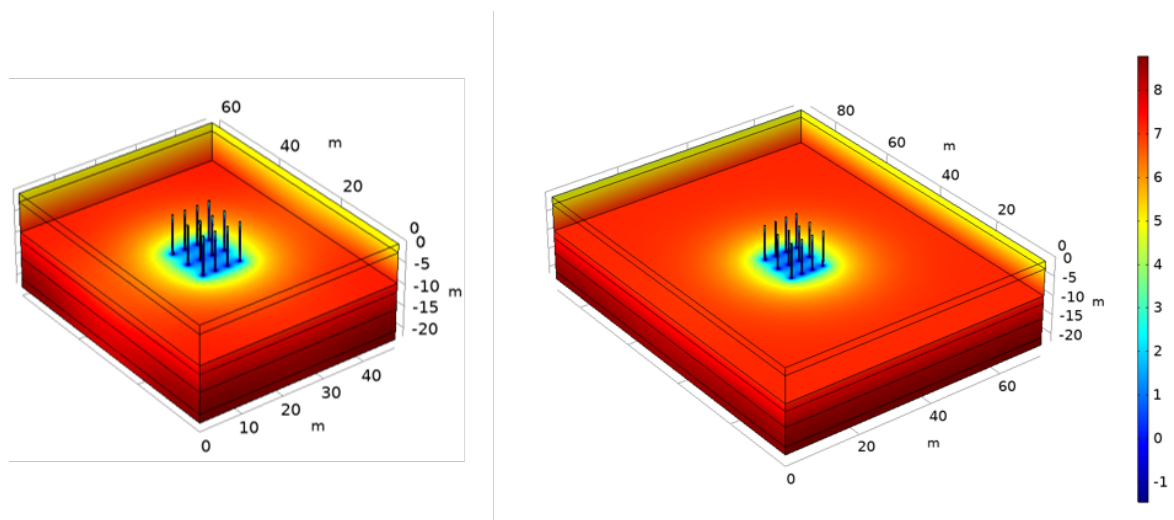


Figure C.2: Normal and enlarged domain size pile group model

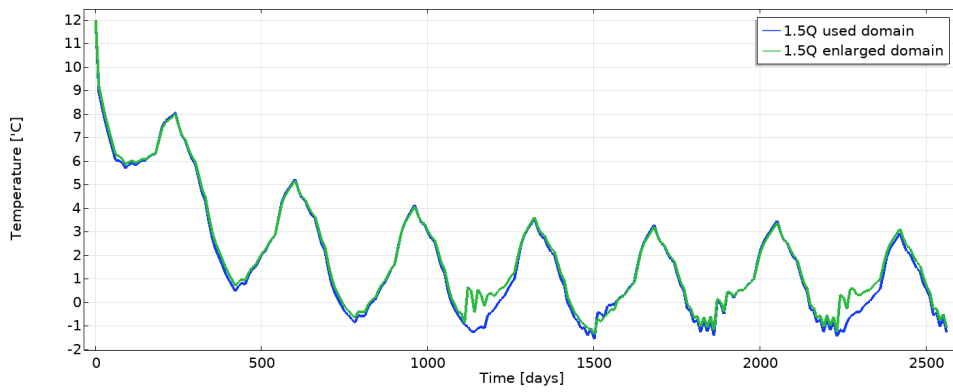


Figure C.3: Sensitivity of domain size pile group model

C.3. Extra results

In figure C.4 below the average shaft temperature of the center piles of the group is checked with an analysis of 10 year. In figure C.5 the distribution for typical extraction 1Q and increase extraction of 2Q is shown.

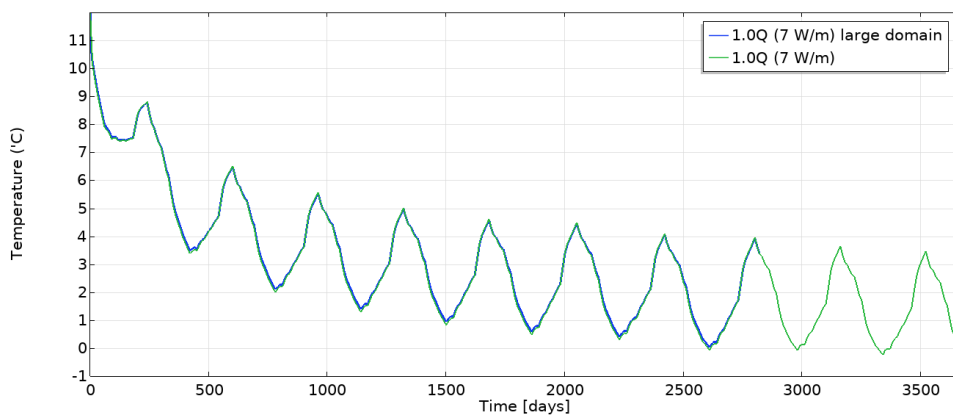


Figure C.4: 10 years heat extraction

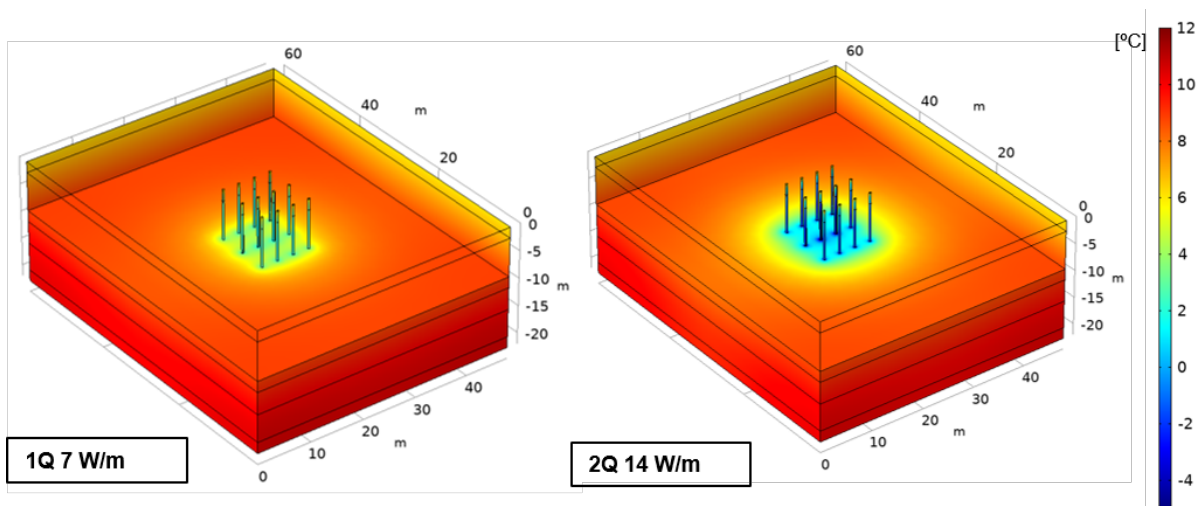


Figure C.5: 3D temperature evolution at t = 2560 days (7 years)



Thermo-hydro-mechanical in Plaxis

This appendix shortly assesses certain aspects of THM Plaxis and describes the input.

D.1. solving sequence

In freezing a volume increase is expected, but due to the limited pore size this volume change is resisted. The result is an increase in excess pore pressures and a reduction of permeability. Due to an increase in pore pressure the effective mean stress decreases. This general behaviour is described by the THM module. Important to bear in mind that this is not dependent on the constitutive model. The constitutive model determines how the effective stress changes with deformation or vice versa.

Within the fully-coupled THM module three equations have to be solved for pore water pressure ΔP , displacement ΔU and temperature ΔT . The coupling means that the three are linked to each other, which is more realistic, but also makes things more difficult and time consuming. The solution of the equations is estimated by solving all three in a loop. For the change in temperature the energy balance is also necessary, which checks that the change in temperature corresponds well with the flux that is pulled-out.

D.2. Thermal settings

D.2.1. Temperature dependent properties

By enabling the temperature-dependent fluid parameters in the project properties window of Plaxis, the density, thermal conductivity, specific heat capacity and the dynamic viscosity of the fluid are changing during thermal temperature variations. Another important adjustment is the water temperature that flows into the model, the default value is 20 °C, but can be changed to any other value.

D.2.2. Thermal expansion and contraction

The thermal expansion of water and ice are defined in the project properties window. The coefficients for the other materials should be changed in the material input.

D.2.3. Latent heat

The introduction of latent heat in the model is possible such that a phase change unfrozen water in the pores to ice is simulated. The bold part in equations below represents this latent heat term. The equations for specific heat capacity ρC and thermal conductivity λ change to equation D.1 and D.2 (Plaxis, 2015):

$$\rho C = (1 - n)\rho_s + nS\rho_w(C_w + \mathbf{l}\frac{dw_u}{dT}) + n(1 - S)\rho_v C_v \quad (D.1)$$

$$\lambda = (1 - n)\lambda_s + nS[\mathbf{w}_u\lambda_w + (1 - \mathbf{w}_u)\lambda_i] + n(1 - S)\lambda_g \quad (D.2)$$

D.2.4. Melting point depression

In Aukenthaler et al. (2016) a relation for the SFCC is described between the particle size distribution and the void ratio, see equation D.5, D.4 and D.3. The specific surface area (SSA) is here a measure of the area of all the grains per unit mass and is calculated with an empirical function based on the mean of particle diameters d_{grains} . In a permeable coarse soil such as a sand, the water will freeze significant faster than in a clay.

$$\theta_{uw} = \frac{\rho_{water}}{\rho_{soil}} \exp(0.2618 + 0.5519 \times \ln(SSA) - 1.4495(SSA)^{-0.2640} \times \ln(T_{freezing} - T)) \quad (D.3)$$

$$SSA = 3.89 \times d_{grains}^{-0.905} \quad (D.4)$$

$$d_{grains} = \exp(m_{clay} \ln d_{clay} + m_{silt} \ln d_{silt} + m_{sand} \ln d_{sand}) \quad (D.5)$$

where:

$m_{clay,silt,sand}$ = are the mass fractions (%) of the clay silt and sand

$d_{clay,silt,sand}$ = are the grain size limits of the fractions.

Important to keep in mind that this produces a rather steep curve, which could result in significant computing time and sometimes not converging solutions. By introducing a smooth curve this is prevented.

D.2.5. Thermal influence on load-displacement

Different temperatures are imposed to a simple pile model to understand the influence of expansion and contraction of the pile and soil constituents on the load-displacement behaviour. Freezing is disabled, so only the soil particles and pore water change in volume due to temperature changes. The load-displacement curves are shown in figure D.1. As the pile and soil constituents expand the effective stress increases at the interface, this results in an increase in the shear strength and thereby an increase in the shaft resistance.

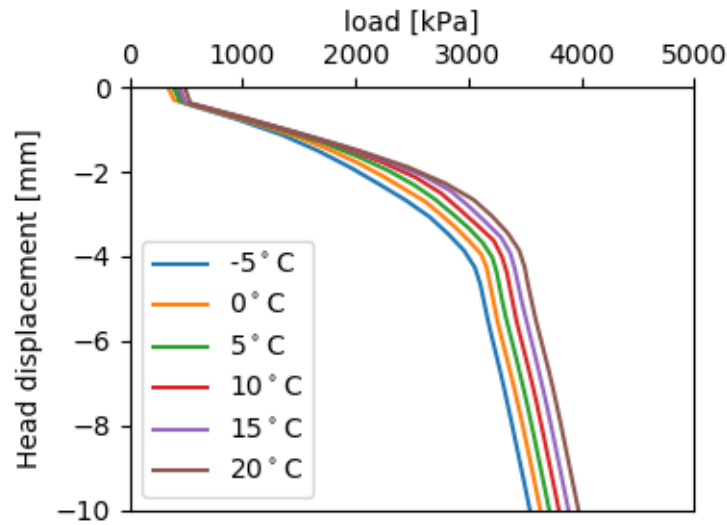
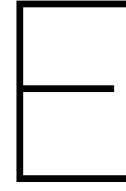


Figure D.1: Load displacement curves with different temperatures at the interface



Parameters Validation

E.1. London

Table E.1: Soil properties London pile model in Plaxis (Bourne-Webb et al., 2009; Gawecka et al., 2017)

Parameter	unit	Pile	Made Ground	Terrace Deposits	London Clay
Model	-	LE	MC	HSS	HSS
γ_{sat}	kN/m^3	24	18	20	20
E_{50}^{ref}	kN/m^2	-	-	20×10^3	35×10^3
E_{oed}^{ref}	kN/m^2	-	-	20×10^3	20×10^3
E_{ur}^{ref}	kN/m^2	-	-	60×10^3	75×10^3
power(m)	-	-	-	1.0	0.75
G_0^{ref}	-	-	-	42×10^3	52×10^3
p^{ref}	kN/m^2	-	-	100	360
$\gamma_{0.7}$	-	-	-	-	3.0×10^{-4}
E'	kN/m^2	40×10^6	10×10^3	-	-
ν'	-	0.3	0.2	0.2	0.2
c_{ref}	kPa	-	0	0	5
ϕ'	°	-	30	35	25
Ψ	°	-	0	17.5	12.5
k_x	m/s	-	1.0×10^{-5}	1.0×10^{-4}	1.0×10^{-10}
k_y	m/s	-	1.0×10^{-5}	1.0×10^{-4}	1.0×10^{-10}
c_s	J/kg/K	800	863	890	900
λ	W/m/K	2333	1400	1400	1790
ρ	kg/m^3	2500	2780	2500	2600
α_s	1/K	8.5×10^{-6}	1.7×10^{-5}	1.7×10^{-5}	1.7×10^{-5}

E.2. Lausanne

Table E.2: Soil properties Lausanne pile model in Plaxis (Bui et al., 2019)

Parameter	unit	Concrete Pile	Soil A1	Soil A2	Soil B	Soil C	Soil D
γ_{sat}	kN/m^3	25.0	26.0	25.35	21.27	22.18	25.5
E'	kN/m^2	2.92×10^7	2.6×10^5	2.6×10^5	8.4×10^4	9.04×10^4	2.6×10^6
ν'	-	0.1769	0.1461	0.1461	0.4	0.4	0.1517
c_{ref}	kPa	-	5	3	6	20	-
ϕ'	°	-	30	27	23	27	-
Ψ	°	-	7.5	7.5	7.5	7.5	-
k_x	m/s	-	2.0×10^{-6}	7.0×10^{-7}	1.0×10^{-5}	2.0×10^{-10}	-
k_y	m/s	-	2.0×10^{-6}	7.0×10^{-7}	1.0×10^{-5}	2.0×10^{-10}	-
c_s	J/kg/K	800	863	863	890	890	784
λ_s	W/m/K	2.1	1.8	1.8	4.45	4.17	1.1
ρ_s	kg/m^3	2500	2780	2780	2735	2740	2550
α_s	1/K	1.0×10^{-5}	1.0×10^{-5}	1.0×10^{-4}	1.0×10^{-4}	1.0×10^{-4}	1.0×10^{-6}

F

Parameters North-South metro line Amsterdam

Tracé		Noord tot en met Europaplein		Parameters ter behoeve van Eindig Elementen Model berekeningen		Massa		Sterkte		Doortlatendheid		Additioneel		Hardening Soil model				
nr.	grondlaag	Omschrijving	γ_m [kN/m ³]	γ_{nat} [kN/m ³]	γ_m [kPa]	c' [kPa]	ϕ' [°]	ψ [°]	k_v [m/s]	v [-]	K_0 [-]	POP [kPa]	OCR [-]	γ_m [-]	Préf [kPa]	$E'_{SO,ref}$ [kPa]	Soed,ref [kPa]	Eurref [m]
01	Aanvulling	Aanvullend materiaal, puin, klei, veen en zand	1.0	15.0	1.2	18	22	18	1.0E-05	0.15		1.3		1.3	6600	4600	10200	
01A	Ophooglaag, zand	Ophoogmateriaal zand	1.0	15.0	1.2	23	27	18	1.0E-04	0.15		1.3		1.3	17134	11500	36500	
01	Geulopvulling veen met kleilagen	Geulopvulling veen met kleilagen	1.0	12.1	1.2	9	20	18	1.0E-07	0.15	0.50	1.0		1.0	2000	1000	5000	0.8
07	Geulopvulling slappe klei	KLEI, met zandlaagjes	1.0	16.9	1.2	26	26	26	1.0E-05			1.0		1.3	3000	1000	17000	
07A	Geulopvulling slappe klei	KLEI, met zandlaagjes	1.0	13.9	1.2	17	20	17	1.0E-07			1.0		1.3	3300	800	18000	
08	Hollandveen	VEEN (bruin)	1.0	10.5	1.2	5	20	18	1.0E-07			1.0		1.3	2000	1000	7000	0.8
09	Oude zeekei	KLEI (matig zand), grils	1.0	16.9	1.2	22	26	26	1.0E-09			1.0		1.3	2800	1600	16900	
10	Wadczelling, zandhoudend	ZAND (matig fijn), sterk kleihoudend/ KLEI, grils,	1.0	17.9	1.2	27	27	23	1.0E-06			1.0		1.3	7700	3100	92000	
10B	Wadczelling, zandhoudend	ZAND (matig fijn), sterk kleihoudend/ KLEI, grils,	1.0	17.9	1.2	23	35	35	1.0E-07	0.20	0.40	1.0		1.3	10000	4000	25000	0.5
11	Wadczelling, hydrobia klei	KLEI (grils), sterk zandig	1.0	15.2	1.2	27	27	23	1.0E-08			1.0		1.3	18200	7800	52000	
12	Basisveen	VEEN (bruin), met enkele kleilaagjes	1.0	11.7	1.2	6	21	18	1.0E-07			1.0		1.3	2000	1000	7000	0.8
13	Eerste zandlaag	ZAND (grils), matig fm, zwak siltig	1.0	19.3	1.2	28	28	28	1.5E-03	0.20	0.40	1.0		1.3	26900	15400	109000	0.5

- 1) De onder- en bovengrens van de vervormingsberekeningen mtd het Hardening soil model, zijn afgeleid uit verschillende typen onderzoek.
- 2) Dilatatiehoek is gedefinieerd als: $\psi = \phi' - 30^\circ$
- 3) Laag 01, aanvulling is door de verschillende soorten materiaal (hout, puin, grind, klei, veen, zand) zeer divers van samenstelling.
- 4) De hoek van inwendige wrijving (ψ) is gebaseerd op een rek niveau van 15%, dat wil zeggen na bezwijken.
- 5) De "engineering judgement" van het "nolboeien is grotendeels gebaseerd op archief gegevens van Omegam.
- 6) De dwarscontractiecoëfficiënt (ν) is afgeleid uit literatuuronderzoek.
- 7) De K0 waarde is gebaseerd op de heek van inwendige wrijving bij bezwijken voor zand en op de Ip waarde voor klei.
- 8) De verticale doortlatendheid is gelijk aan de horizontale doortlatendheid, behalve voor laag 04, 08 en 12. Voor deze lagen is de horizontale doortlatendheid 2x zo groot.

registratie	projeccoe	status	Definitief
D3	01270L		
autorisatie	naam	paraaf	datum
opgemaakt	HERJ		00-04-07
goedgekeurd	TEUE		
vrijgegeven	GRAF		

Noord tot en met Europaplein
Parameters ten behoeve van Eendig Elementen Model berekeningen

Tracé		grondlaag		Omschrijving		Massa		Sterkte		Doortendheid		Additioneel		Hardening Soil model		
nr.		γ_m [-]	γ_{rel} [kN/m ³]	γ_m [-]	c' [kPa]	ϕ' [°]	k_v [m/s]	v [-]	K_0 [-]	PCP [kPa]	OCR [-]	γ_m [-]	Pref [kPa]	E ⁵⁰ rel [kPa]	E _{ur} ref [kPa]	m
14	Allerod	1.0	18.5	1.2	23	23	3.0E-04	0.20	0.40	100	1.3	1500	5400	23100		
			18.5		28	28	3.0E-04					15000	7000	30000		
			18.5		33	33	3.0E-05					17000	13000	45000	0.5	
			18.5		35	35	3.0E-06					19000	20000	60000		
			18.5		42	42	3.0E-06					24700	26000	78000		
15	Gauwling klei met zandlagen	1.0	17.8	1.2	23	23	3.0E-08	0.15	0.50	100	1.3	6500	1900	19200		
			17.8		27	27	1.0E-06					8400	2800	35600		
			17.8		32	32	1.0E-03					8400	3800	35000	0.8	
			17.8		36	36	1.0E-10					8400	4800	42000		
			17.8		43	43	1.0E-10					6900	5900	54600		
16	ZAND (maltig fijn, met Heilaagjes, schelpen)	1.0	18.5	1.2	23	23	1.0E-04	0.15	0.47	100	1.3	6500	3100	19200		
			18.5		27	27	1.0E-04					8400	4000	25000		
			18.5		33	33	1.0E-05					8400	5000	35000	0.8	
			18.5		38	38	1.0E-06					8400	6000	42000		
			18.5		46	46	1.0E-06					10800	7800	54600		
17	Tweeste zandlaag	1.0	19.3	1.2	28	28	1.0E-03	0.20	0.40	100	1.3	24600	19200	61900		
			19.3		33	33	1.0E-03					32000	25000	60000		
			19.3		35	35	1.0E-04					35000	35000	100000	0.5	
			19.3		39	39	1.0E-05					38000	45000	200000		
			19.3		47	47	1.0E-05					64600	83600	314000		
17A	Mariene siltig Eenzand	1.0	18.4	1.2	23	23	2.4E-05	0.20	0.40	100	1.3	20800	1500	6200		
			18.4		27	27	2.4E-05					27000	5000	60000		
			18.4		33	33	2.4E-06					30000	20000	120000	0.5	
			18.4		35	35	2.4E-07					33000	25000	160000		
			18.4		42	42	2.4E-07					42900	32500	165000		
18	Overschraaglaag	1.0	18.0	1.2	23	23	1.0E-07	0.46		100	1.3	58000	2300	28800		
			18.0		27	27	1.0E-07	0.46				7300	3000	59000		
			18.0		34	34	1.0E-08	3.15	0.48	100	1.3	9600	4000	64000	0.8	
			18.0		34	34	1.0E-09	0.53				11000	5000	60000		
			18.0		41	41	1.0E-09	0.53				14300	6900	104000		
19	Mariene Eenklei (zone 1)	1.0	17.9	1.2	10	24	2.0E-08	0.58		100	1.3	6200	2300	23100		
			17.9		10	29	2.0E-08	0.58				8000	3000	30000		
			17.9		20	32	2.0E-09	3.15	0.88	100	1.3	11000	4000	50000	0.8	
			17.9		30	34	2.0E-10	0.76				14000	5000	65000		
			17.9		15	41	2.0E-10	0.76				18200	6500	84500		
19A	Mariene Eenklei (zone 2)	1.0	17.1	1.2	10	24	2.0E-08	0.55		100	1.3	6800	2700	28900		
			17.1		10	29	2.0E-08	0.55				9000	3500	35000		
			17.1		20	34	2.0E-09	3.15	0.35	100	1.3	12000	4500	55000	0.8	
			17.1		30	35	2.0E-10	0.74				16000	5900	70000		
			17.1		15	42	2.0E-10	0.74				18500	7200	91000		
193	Mariene Eenklei (zone 3)	1.0	17.2	1.2	10	23	2.0E-08	0.31		100	1.3	5400	1900	21500		
			17.2		10	28	2.0E-08	0.31				7000	2500	28000		
			17.2		20	30	2.0E-09	3.15	0.71	100	1.3	9000	3000	45000	0.8	
			17.2		30	32	2.0E-10	0.79				11000	3500	60000		
			17.2		15	38	2.0E-10	0.79				14300	4800	78000		
19C	Mariene Eenklei (zone 4)	1.0	16.6	1.2	10	23	2.0E-08	0.31		100	1.3	4600	1900	21500		
			16.6		10	28	2.0E-08	0.31				6000	2500	29000		
			16.6		20	30	2.0E-09	3.15	0.71	100	1.3	8000	3000	40000	0.8	
			16.6		30	32	2.0E-10	0.79				10000	3500	55000		
			16.6		15	38	2.0E-10	0.79				13000	4600	71600		
20	Laag van Haring	1.0	14.5	1.2	22	22	6.0E-08	0.58		100	1.3	5400	1200	19200		
			14.5		26	26	6.0E-08	0.58				7000	1500	25000		
			14.5		10	28	6.0E-09	3.15	0.54	100	1.3	10000	2000	46000	0.8	
			14.5		30	30	6.0E-10	0.73				13000	2500	60000		
			14.5		15	36	6.0E-10	0.73				16900	3300	78000		

1) De onder- en bovengrens van de vervormingsberekeningen mbt. het Hardening soil model, zijn afgeleid uit verschillende typen onderzoek.
2) Diilatatiehoek is gedefinieerd als: $v = \phi' - 3\theta'$

- Laag 01, aanvulling is door de verschillende soorten materiaal (hout, puin, grind, klei, veen, zand) zeer divers van samenstelling.
- De hoek van inwendige wrijving (ϕ) is gebaseerd op een rek niveau van 15% dat wil zeggen na bezwijken
- De "engineering judgement" van het holoceen is groterdoelen gebaseerd op archief gegevens van Omegam.
- De dwarsontactcoëfficiënt (v) is afgeleid uit literatuuronderzoek.
- De K_0 waarde is gebaseerd op de hoek van inwendig bezwijken bij bezwijken voor zand en op de ϕ waarde voor klei.
- De verticale doortendheid is gelijk aan de horizontale doortendheid, behalve voor laag 04, 06 en 12. Voor deze lagen is de horizontale doortendheid 2x zo groot.
- γd'roog is gelijk aan γnat

registratie	projectcode	status
D3	01270L	Definitief
autorisatie	naam	paraaf
	HERJ	00-04-07
oorgenaakt	TEJE	
goedgekeurd	GRAF	
vrijgegeven		

G

THM analysis

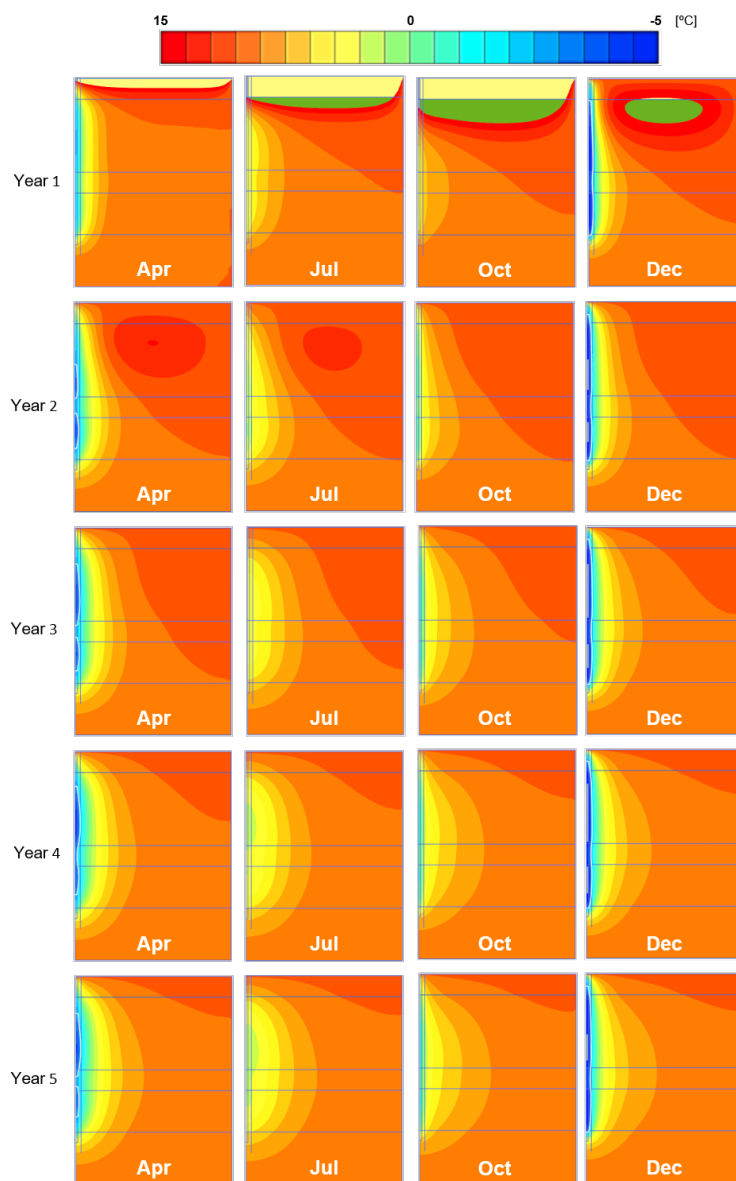


Figure G.1: Temperature distribution over five years

Bibliography

- Central Bureau for Statistics (CBS)., 2016. URL <https://opendata.cbs.nl/statline/#/CBS/nl/dataset/81528NED/table?dl=5A22>.
- A. Abdulghader and T. Mohammad. Adfreeze Strength and Creep Behavior of Pile Foundations in Warming Permafrost. 2018.
- M Alberdi-Pagola. *Aalborg Universitet Design and performance of energy pile foundations Precast quadratic pile heat exchangers for shallow geothermal energy systems*. PhD thesis, Aalborg University Denmark, 2018.
- B.L. Amatya, K. Soga, P.J. Bourne-webb, T. Amis, and L. Laloui. Thermo-mechanical behaviour of energy piles. *Géotechnique*, 62(6):503–519, 6 2012. ISSN 0016-8505. doi: 10.1680/geot.10.P.116. URL <http://www.icevirtuallibrary.com/doi/10.1680/geot.10.P.116>.
- G. Amiri, G. Grimstad, and M. Aukenthaler. The Frozen and Unfrozen Soil Model. Technical report, Plaxis bv, 2016.
- O.B. Andersland and B. Ladanyi. *An Introduction to Frozen Ground Engineering*. Springer US, 1994. ISBN 978-1-4757-2292-5. doi: 10.1007/978-1-4757-2290-1. URL <http://link.springer.com/10.1007/978-1-4757-2290-1>.
- L. U. Arenson, S. M. Springman, and D. C. Segó. The rheology of frozen soils. *Applied Rheology*, 17(1), 2006. doi: 10.3933/ApplRheol-17-12147.
- L. U. Arenson, D. C. Segó, and T. F. Azmatch. A new hypothesis on ice lens formation in frost-susceptible soils. 2008.
- M. M. Arzanfudi and R. Al-Khoury. Freezing-thawing of porous media: An extended finite element approach for soil freezing and thawing. 2018.
- M. Aukenthaler, R. B. J. Brinkgreve, and A. Haxaire. A practical approach to obtain the soil freezing characteristic curve and the freezing/melting point of a soil-water system. In *GeoVancouver 2016: the 69th Canadian Geotechnical Conference*, pages 1–8, Vancouver, Canada, 2016.
- D. Banks. *An Introduction to Thermogeology: Ground Source Heating and Cooling*. Wiley-Blackwell, Oxford, UK, 7 2012. ISBN 9781118447512. doi: 10.1002/9781118447512. URL <http://doi.wiley.com/10.1002/9781118447512>.
- O. Boënnec. Piling on the energy. *Geo drilling International*, pages 25–28, 2009. ISSN 09693769.
- P. J. Bourne-Webb and T. M. Bodas Freitas. Thermally-activated piles and pile groups under monotonic and cyclic thermal loading—A review. *Renewable Energy*, 2018. ISSN 18790682. doi: 10.1016/j.renene.2018.11.025.
- P. J. Bourne-Webb, B. Amatya, K. Soga, T. Amis, C. Davidson, and P. Payne. Energy pile test at Lambeth College, London: geotechnical and thermodynamic aspects of pile response to heat cycles. *Géotechnique*, 59(3):237–248, 4 2009. ISSN 0016-8505. doi: 10.1680/geot.2009.59.3.237. URL <http://www.icevirtuallibrary.com/doi/10.1680/geot.2009.59.3.237>.
- P.J. Bourne-Webb, B. Amatya, and K. Soga. A framework for understanding energy pile behaviour. In *Proceedings of the Institution of Civil Engineers - Geotechnical Engineering*, volume 166, pages 170–177, 4 2013. doi: 10.1680/geng.10.00098. URL <http://www.icevirtuallibrary.com/doi/10.1680/geng.10.00098>.
- H. Brandl. Energy piles and diaphragm walls for heat transfer from and into the ground. *Deep Foundations on Bored and Auger Piles - Bap Iii*, 1998.

- H. Brandl. Energy foundations and other thermo-active ground structures. *Géotechnique*, 56(2):81–122, 3 2006. ISSN 0016-8505. doi: 10.1680/geot.2006.56.2.81. URL <http://www.icevirtuallibrary.com/doi/10.1680/geot.2006.56.2.81>.
- J Briaud. *Geotechnical Engineering*. John Wiley & Sons, Inc., Hoboken, NJ, USA, 2013. ISBN 9781118686195. doi: 10.1002/9781118686195. URL <http://doi.wiley.com/10.1002/9781118686195>.
- R. B. J. Brinkgreve, S. Kumarswamy, and F. Foria. PLAXIS Material Models Manual. pages 81–92, 2017.
- R.B.J. Brinkgreve, P. G. Bonnier, and M. H. Kappert. Hysteretic damping in a small-strain stiffness model. In *Numerical Models in Geomechanics*, pages 737–742. Taylor & Francis, 2007. doi: 10.1201/NOE0415440271.ch106. URL <http://www.crcnetbase.com/doi/10.1201/NOE0415440271.ch106>.
- T.A. Bui, A. Casarella, A. Di Donna, and R. B. J. Brinkgreve. Advanced Thermo-Hydro-Mechanical modelling features for practical applications in energy geotechnics. *Proceedings of the XVII ECSMGE-2019 Geotechnical Engineering foundation of the future*, 2019. doi: 10.32075/17ECSMGE-2019-0499.
- T. P. Burt and P. J. Williams. Hydraulic conductivity in frozen soils. *Earth Surface Processes*, 1(4):349–360, 10 1976. ISSN 03601269. doi: 10.1002/esp.3290010404. URL <http://doi.wiley.com/10.1002/esp.3290010404>.
- R. Campanella and J. Mitchell. Influence of Temperature Variations on Soil Behavior. *Journal of the Soil Mechanics and Foundations Division*, pages 609–734, 1968.
- E. J. Chamberlain and A. J. Gow. Effect of Freezing and Thawing on the Permeability and Structure of Soils. In *Developments in Geotechnical Engineering*, volume 26, pages 73–92. 1979. doi: 10.1016/B978-0-444-41782-4.50012-9. URL <https://linkinghub.elsevier.com/retrieve/pii/B9780444417824500129>.
- O. Copuroglu. *The characterisation, improvement and modelling aspects of Frost Salt Scaling of Cement-Based Materials with a High Slag Content*. Delft, 1 edition, 2006. ISBN 978-90-9020622-6.
- Daryl F Dagesse. Cyclic Freezing and Thawing Effects on Atterberg Limits of Clay Soils. *68e Conférence Canadienne de Géotechnique et 7e Conférence Canadienne sur le Pergélisol, 20 au 23 septembre 2015, Québec, Québec.*, (October), 2015.
- N. Davis. *Permafrost: A Guide to Frozen Ground in Transition*, volume 34. Fairbanks, Alaska, USA., 2 2002. doi: 10.2307/1552516. URL <https://www.jstor.org/stable/1552516?origin=crossref>.
- N. J. D’Cunha, D. Misra, and A. M. Thompson. Experimental investigation of the applications of natural freezing and curdlan biopolymer for permeability modification to remediate DNAPL contaminated aquifers in Alaska. *Cold Regions Science and Technology*, 59(1):42–50, 10 2009. ISSN 0165232X. doi: 10.1016/j.coldregions.2009.05.005. URL <https://linkinghub.elsevier.com/retrieve/pii/S0165232X09000913>.
- P Eslami-nejad and M Bernier. Freezing of geothermal borehole surroundings: A numerical and experimental assessment with applications. *Applied Energy*, 98:333–345, 2012. ISSN 03062619. doi: 10.1016/j.apenergy.2012.03.047. URL <http://dx.doi.org/10.1016/j.apenergy.2012.03.047>.
- K. A. Gawecka, D. M. G. Tabora, D. M. Potts, W. Cui, L. Zdravković, and M. S. Haji Kasri. Numerical modelling of thermo-active piles in London Clay. *Proceedings of the Institution of Civil Engineers - Geotechnical Engineering*, 170(3):201–219, 6 2017. ISSN 1353-2618. doi: 10.1680/jgeen.16.00096. URL <http://www.icevirtuallibrary.com/doi/10.1680/jgeen.16.00096>.
- C.P.J.M Geelen and H.J.L Witte. *ISSO-Publicatie 73: Ontwerp en uitvoering van verticale bodemwarmtewisselaars*. ISSO, 2017. ISBN 978-90-5044-308-1.
- (TNO-MEP) Geelen, C., (TNO-MEP) Krosse, L., (KODI) Sterrenburg, P., (ECN) Bakker, E.J., and (ECN) Sijpheer, N. TNO-rapport: Handboek Energiepalen, 2003.
- I. Ghaaowd, A. Takai, T. Katsumi, and J. S. McCartney. Pore water pressure prediction for undrained heating of soils. *Environmental Geotechnics*, 4(2):70–78, 4 2015. ISSN 2051-803X. doi: 10.1680/jenge.15.00041. URL <http://www.icevirtuallibrary.com/doi/10.1680/jenge.15.00041>.

- S. A. Ghoreishian Amiri, G. Grimstad, M. Kadivar, and S. Nordal. Constitutive model for rate-independent behavior of saturated frozen soils. *Canadian Geotechnical Journal*, 53(10):1646–1657, 10 2016. ISSN 0008-3674. doi: 10.1139/cgj-2015-0467. URL <http://www.nrcresearchpress.com/doi/10.1139/cgj-2015-0467>.
- A. Golchin, P. J. Vardon, M. A. Hicks, I. A. Pantev, and M. M. Arzanfudi. Energy-piles in the Netherlands : geotechnical behaviour. 2019.
- GSHP Association. Thermal pile design, installation and materials standards, 2012. URL <https://www.nhbcfoundation.org/wp-content/uploads/2016/05/NF21>.
- J. Habert, H. Mroueh, J. Josifovski, W. Bogusz, D. Sterpi, and K. Georgiadis. Synthesis of a benchmark exercise for geotechnical analysis of a thermoactive pile. *Environmental Geotechnics*, pages 1–12, 3 2019. ISSN 2051-803X. doi: 10.1680/jenge.18.00054. URL <https://www.icevirtuallibrary.com/doi/10.1680/jenge.18.00054>.
- J. S. Harris. *Ground freezing in practice*. Thomas Telford Ltd, London, 1 edition, 1 1995. ISBN 0 7277 1995 5. doi: 10.1016/S0165-232X(96)00008-0. URL <https://linkinghub.elsevier.com/retrieve/pii/S0165232X96000080>.
- K. S. Henry. A Review of the Thermodynamics of Frost Heave. Technical report, US Army Corps of Engineers, 2000.
- T. Hueckel, B. François, and L. Laloui. Explaining thermal failure in saturated clays. *Géotechnique*, 59(3):197–212, 4 2009. ISSN 0016-8505. doi: 10.1680/geot.2009.59.3.197. URL <http://www.icevirtuallibrary.com/doi/10.1680/geot.2009.59.3.197>.
- R. Katzenbach, F. Clauss, and S. Rochée. Analysis of the freeze thaw performance of geothermal heat exchanger borehole grout materials. In *International Conference on Soil Mechanics and Geotechnical Engineering*, Paris, 2013.
- (RVO) Kleefkens, O. Status rapportage warmtepompen technologie en markt in Nederland, 2014. URL https://www.rvo.nl/sites/default/files/2014/11/Definitief_StatusrapportageWarmtepompen.pdf.
- C. Knellwolf, H. Peron, and L. Laloui. Geotechnical Analysis of Heat Exchanger Piles. *Journal of Geotechnical and Geoenvironmental Engineering*, 137(10):890–902, 2011. ISSN 1090-0241. doi: 10.1061/(asce)gt.1943-5606.0000513.
- L. Laloui, M. Nuth, and L. Vulliet. Experimental and numerical investigations of the behaviour of a heat exchanger pile. *International Journal for Numerical and Analytical Methods in Geomechanics*, 30(8):763–781, 7 2006. ISSN 0363-9061. doi: 10.1002/nag.499. URL <http://doi.wiley.com/10.1002/nag.499>.
- Guoyu Li, Wei Ma, Shuping Zhao, Yuncheng Mao, and Yanhu Mu. Effect of Freeze-Thaw Cycles on Mechanical Behavior of Compacted Fine-Grained Soil. (August):72–81, 2012. doi: 10.1061/9780784412473.008.
- H. Li and W. N. Lu. Dynamic Behavior of Pile Foundation in Frozen and Thawing Soil. *Applied Mechanics and Materials*, 105-107:1391–1399, 2011. doi: 10.4028/www.scientific.net/amm.105-107.1391.
- Y.-C. Li, H. R. Thomas, P. Cleall, C. Harris, and M. Kern-Luetschg. Modelling of cryogenic processes in permafrost and seasonally frozen soils. *Géotechnique*, 59(3):173–184, 2009. ISSN 0016-8505. doi: 10.1680/geot.2009.59.3.173.
- F. Loveridge and W. Powrie. Pile heat exchangers: thermal behaviour and interactions. *Proceedings of the Institution of Civil Engineers - Geotechnical Engineering*, 166(2):178–196, 2012. ISSN 1353-2618. doi: 10.1680/geng.11.00042.
- F. Loveridge, W. Powrie, and P. Smith. A review of the design and construction aspects for bored thermal piles. *Ground Engineering*, pages 2011–2014, 2013. ISSN 01932306. doi: 10.1016/S0193-2306(04)10005-7.

- N. R. Morgenstern, N. A. Tsytoich, and G. K. Swinzow. The mechanics of frozen ground [book review]. *American Journal of Science*, 276(7):921–922, 9 1975. ISSN 0002-9599. doi: 10.2475/ajs.276.7.921. URL <https://linkinghub.elsevier.com/retrieve/pii/0148906276907476><http://www.ajsonline.org/cgi/doi/10.2475/ajs.276.7.921>.
- Haskoning Nederland B V Mw. Nen 9997-1. (december 2011), 2012.
- R. M. Nagare, R. A. Schincariol, W. L. Quinton, and M. Hayashi. Effects of freezing on soil temperature, freezing front propagation and moisture redistribution in peat: laboratory investigations. *Hydrology and Earth System Sciences*, 16(2):501–515, 2 2012. ISSN 1607-7938. doi: 10.5194/hess-16-501-2012. URL <https://www.hydrol-earth-syst-sci.net/16/501/2012/>.
- NEN. NEN 9997-1 + C2 Geotechnisch ontwerp van constructies. (november 2017), 2017.
- C. W. W. Ng and C. Zhou. Plastic Deformations of Unsaturated Fine-Grained Soils Under Cyclic Thermo-Mechanical Loads. In *Springer Series in Geomechanics and Geoengineering (2017)*, pages 14–28, 2017. doi: 10.1007/978-3-319-52773-4_{_}2. URL http://link.springer.com/10.1007/978-3-319-52773-4_2.
- C. W. W. Ng, C. Shi, A. Gunawan, and L. Laloui. Centrifuge modelling of energy piles subjected to heating and cooling cycles in clay. *Géotechnique Letters*, 4(4):310–316, 2014a. doi: 10.1680/geolett.14.00063.
- C.W.W. Ng, C. Shi, A. Gunawan, L. Laloui, and H.L. Liu. Centrifuge modelling of heating effects on energy pile performance in saturated sand. *Canadian Geotechnical Journal*, 52(8):1045–1057, 2014b. ISSN 0008-3674. doi: 10.1139/cgj-2014-0301.
- J. F. Nixon and N. R. Morgenstern. The Residual Stress in Thawing Soils. *Canadian Geotechnical Journal*, 10(4):571–580, 11 1973. ISSN 0008-3674. doi: 10.1139/t73-053. URL <http://www.nrcresearchpress.com/doi/10.1139/t73-053>.
- C. G. Olgun, T. Y. Ozudogru, and C. F. Arson. Thermo-mechanical radial expansion of heat exchanger piles and possible effects on contact pressures at pile–soil interface. *Geotechnique Letters*, 4(july-september): 170–178, 2014. ISSN 20452543. doi: 10.1680/geolett.14.00018.
- C. Guney Olgun, Tolga Y. Ozudogru, Sherif L. Abdelaziz, and Aykut Senol. Long-term performance of heat exchanger piles. *Acta Geotechnica*, 10(5):553–569, 2015. ISSN 18611133. doi: 10.1007/s11440-014-0334-z.
- Plaxis. Thermal and coupled THM analysis. *Essential for Geotechnical Professionals*, 2015.
- Plaxis. PLAXIS Scientific Manual 2019. 2019a.
- Plaxis. Plaxis 2D Reference Manual 2019. pages 87–100, 2019b.
- J. Qi, P.A. Vermeer, and G. Cheng. A review of the influence of freeze-thaw cycles on soil geotechnical properties. *Permafrost and Periglacial Processes*, 17(3):245–252, 7 2006. ISSN 1045-6740. doi: 10.1002/ppp.559. URL <http://doi.wiley.com/10.1002/ppp.559>.
- A.M.I. Raouf, M.I.N. Raouf, H. Abuel-Naga, and A.G. Nasser. Energy piles: current state of knowledge and design challenges. *Environmental Geotechnics*, 2(4):195–210, 8 2015. ISSN 2051-803X. doi: 10.1680/envgeo.13.00019. URL <http://www.icevirtuallibrary.com/content/article/10.1680/envgeo.13.00019>.
- S. W. Rees, M. H. Adjali, Z. Zhou, M. Davies, and H. R. Thomas. Ground heat transfer effects on the thermal performance of earth-contact structures. *Renewable & sustainable energy reviews*, 4(3):213–265, 2000. ISSN 13640321. doi: 10.1016/S1364-0321(99)00018-0.
- J. Ren, S.K. Vanapalli, and Z. Han. Soil freezing process and different expressions for the soil-freezing characteristic curve. *Sciences in Cold and Arid Regions*, 9(3):221–228, 2017. doi: 10.3724/SPJ.1226.2017.00221. URL http://www.scar.ac.cn/hhkxen/ch/reader/create_pdf.aspx?file_no=20170306&year_id=2017&quarter_id=3&falg=1.
- L. T. Roman, V. P. Merzlyakov, and A. N. Maleeva. Thermal deformation of frozen soils: Role of water and gas saturation. *Earth's Cryosphere*, 21(3):24–31, 2017. ISSN 15607496. doi: 10.21782/KZ1560-7496-2017-3(24-31).

- A.F. Rotta Loria. Performance-based Design of Energy Pile Foundations. *DFI Journal - The Journal of the Deep Foundations Institute*, 12(2):94–107, 5 2018. ISSN 1937-5247. doi: 10.1080/19375247.2018.1562600. URL <https://www.tandfonline.com/doi/full/10.1080/19375247.2018.1562600>.
- R. Şahin, M. A. Taşdemir, G. Rüstem, and C. Çelik. Optimization study and damage evaluation in concrete mixtures exposed to slow freeze-thaw cycles. *Journal of Materials in Civil Engineering*, 19(7):609–615, 2007. ISSN 08991561. doi: 10.1061/(ASCE)0899-1561(2007)19:7(609).
- A. K. Sani, R. M. Singh, T. Amis, and I. Cavarretta. A review on the performance of geothermal energy pile foundation, its design process and applications. *Renewable and Sustainable Energy Reviews*, 106(March): 54–78, 5 2019. ISSN 13640321. doi: 10.1016/j.rser.2019.02.008. URL <https://doi.org/10.1016/j.rser.2019.02.008> <https://linkinghub.elsevier.com/retrieve/pii/S1364032119301017>.
- B. Sanner. Ground Source Heat Pumps – history , development , current status , and future prospects. *12th IEA Heat Pump Conference 2017*, 2017.
- B. Sanner, M. Reuss, and E. Konstantinidou. VDI 4640 – a German guideline for shallow geothermal energy use. In *European Geothermal Congress 2013*, 2013.
- I. Sass, D. Brehm, W.G. Coldewey, J. Dietrich, R. Klein, and T. Kellner. *Shallow Geothermal Systems - Recommendations on Design, Construction, Operation and Monitoring*. Wiley-VCH Verlag GmbH & Co. KGaA, Weinheim, Germany, 5 2016. ISBN 9783433606674. doi: 10.1002/9783433606674. URL <http://doi.wiley.com/10.1002/9783433606674>.
- P. Skels and K. Bondars. Applicability of Small Strain Stiffness Parameters for Pile Settlement Calculation. *Procedia Engineering*, 172:999–1006, 2017. ISSN 18777058. doi: 10.1016/j.proeng.2017.02.149. URL <http://dx.doi.org/10.1016/j.proeng.2017.02.149> <https://linkinghub.elsevier.com/retrieve/pii/S1877705817306550>.
- A. Steiner, P.J. Vardon, and W. Broere. The influence of freeze–thaw cycles on the shear strength of illite clay. *Proceedings of the Institution of Civil Engineers - Geotechnical Engineering*, 171(1):16–27, 2 2018. ISSN 1353-2618. doi: 10.1680/jgeen.16.00101. URL <http://www.icevirtuallibrary.com/doi/10.1680/jgeen.16.00101>.
- M. E. Suryatriyastuti, H. Mroueh, and S. Burlon. A load transfer approach for studying the cyclic behavior of thermo-active piles. *Computers and Geotechnics*, 55:378–391, 2014. ISSN 0266352X. doi: 10.1016/j.compgeo.2013.09.021. URL <http://dx.doi.org/10.1016/j.compgeo.2013.09.021>.
- M. Sutman, C.G. Olgun, and L. Laloui. Cyclic Load–Transfer Approach for the Analysis of Energy Piles. *Journal of Geotechnical and Geoenvironmental Engineering*, 145(1):04018101, 1 2019. ISSN 1090-0241. doi: 10.1061/(ASCE)GT.1943-5606.0001992. URL <http://ascelibrary.org/doi/10.1061/%28ASCE%29GT.1943-5606.0001992>.
- H. Tian, C. Wei, H. Wei, and J. Zhou. Freezing and thawing characteristics of frozen soils: Bound water content and hysteresis phenomenon. *Cold Regions Science and Technology*, 103:74–81, 2014. ISSN 0165232X. doi: 10.1016/j.coldregions.2014.03.007. URL <http://dx.doi.org/10.1016/j.coldregions.2014.03.007>.
- TNO. Lithostratigrafische Nomenclator van de Ondiepe Ondergrond, versie 2013., 2013. URL <https://www.dinoloket.nl/nomenclator-ondiep>.
- A Verruijt. *Grondmechanica*. Delfse Uitgevers Maatschappij b.v., Delft, 1990. ISBN 90-6562-045-1.
- J. S. Weaver and N. R. Morgenstern. Pile design in permafrost. *Canadian Geotechnical Journal*, 18(3):357–370, 1981. ISSN 0008-3674. doi: 10.1139/t81-043.
- J.S. Wettlaufer and M. Grae Worster. PREMELTING DYNAMICS. *Annual Review of Fluid Mechanics*, 38(1):427–452, 1 2006. ISSN 0066-4189. doi: 10.1146/annurev.fluid.37.061903.175758. URL <http://www.annualreviews.org/doi/10.1146/annurev.fluid.37.061903.175758>.
- L. M. Wotherspoon, S. Sritharan, and M. J. Pender. Modelling the response of cyclically loaded bridge columns embedded in warm and seasonally frozen soils. *Engineering Structures*, 32(4):933–943, 2010. ISSN 01410296. doi: 10.1016/j.engstruct.2009.12.019. URL <http://dx.doi.org/10.1016/j.engstruct.2009.12.019>.

- Y. Wu, Y. Sheng, Y. Wang, H. Jin, and W. Chen. Stresses and deformations in a buried oil pipeline subject to differential frost heave in permafrost regions. *Cold Regions Science and Technology*, 2010. ISSN 0165232X. doi: 10.1016/j.coldregions.2010.07.004.
- S. Xiao, M. T. Suleiman, R. Elzeiny, C. Naito, S. Neti, and M. Al-Khawaja. Effect of Temperature and Radial Displacement Cycles on Soil–Concrete Interface Properties Using Modified Thermal Borehole Shear Test. *Journal of Geotechnical and Geoenvironmental Engineering*, 144(7):04018036, 7 2018. ISSN 1090-0241. doi: 10.1061/(ASCE)GT.1943-5606.0001892. URL <http://ascelibrary.org/doi/10.1061/%28ASCE%29GT.1943-5606.0001892>.
- H. Yu, H. Ma, and K. Yan. An equation for determining freeze-thaw fatigue damage in concrete and a model for predicting the service life. *Construction and Building Materials*, 137:104–116, 2017. ISSN 09500618. doi: 10.1016/j.conbuildmat.2017.01.042. URL <http://dx.doi.org/10.1016/j.conbuildmat.2017.01.042>.
- L. Yuanming, Y. Yugui, C. Xiaoxiao, and L. Shuangyang. Strength criterion and Elastoplastic constitutive model of frozen silt in generalized plastic mechanics. *International Journal of Plasticity*, 2010. ISSN 07496419. doi: 10.1016/j.ijplas.2010.01.007.
- Y Zhang. *Thermal-Hydro-Mechanical Model for Freezing and Thawing of Soils*. PhD thesis, University of Michigan, 2014. URL <https://deepblue.lib.umich.edu/handle/2027.42/108828>.
- Y. Zhang and R.L. Michalowski. Thermal-hydro-mechanical modeling of frost action in frost-susceptible soils. *Geotechnical Special Publication*, (236 GSP):735–744, 2014. ISSN 08950563. doi: 10.1061/9780784413388.077.